THE ROLE OF HYDROGEN AS A TEMPORARY ALLOYING ELEMENT DURING THE MANUFACTURING STAGES OF TI-6Al-4V BY THE POWDER METALLURGY ROUTE

CENTRE FOR MATERIALS ENGINEERING

MASTERS DISSERTATION

Student: Marie Mellisa Sandy Mariaye

Supervisor: Prof. R.D Knutsen

Abstract

The aim of this research was to investigate the effects of using hydrogen as a temporary alloying element in the manufacturing of titanium (Ti) and Ti-6Al-4V by the powder metallurgy (PM) route using commercially pure titanium (CP Ti), titanium hydride (TiH_2) and Ti-6Al-4V powders as starting materials. Several powder blends were selected and respective samples were pressed at compaction pressures ranging from 300-500MPa for green density and strength measurements. It was found that the higher the level of TiH_2 in the powder blend, the lower the green density and strength. However, powder blends containing more than 40wt% of TiH_2 did not result in considerable decrease in green strength and density. The selected powder blends underwent thermal decomposition analysis. The results show that hydrogen introduction is more beneficial in the form of a hydrogen atmosphere rather than using TiH_2. Samples of selected powder blend were pressed and sintered at 1050°C under argon and partial hydrogen atmospheres. While the general trend was that sintered densities improved with TiH_2 content as well as in the presence of hydrogen in the sintering atmosphere, there was an unexpected decrease from green to sintered density for the TiH_2-6Al-4V samples sintered in partial hydrogen at 1050°C. These results were supported by the microstructural analysis. Additional sintering trials for CP Ti-6Al-4V and TiH_2-6Al-4V for different sintering conditions were also conducted and their relative sintered densities were concurrent with the density results obtained in the current literature (>97%). Elemental mapping conducted proved that the diffusion of the MA particles were the same for both TiH_2-6Al-4V and CP Ti-6Al-4V. The decrease from green to sintered density in the TiH_2-6Al-4V samples was due to the formation and trapping of H_2O (g). At 1050°C the rate of H_2 and subsequent H_2O gas release is lower as compared to 1200°C. Hence, H_2O gas molecules are trapped for longer causing the formation of larger pores that are harder to shrink especially at 1050°C. In a negative pressure atmosphere like vacuum, the higher pressure gradient between sample and atmosphere will favour faster diffusion rate of H_2O gas which prevents big pore formation thus favouring faster densification. Sintering TiH_2 based compacts in a partial hydrogen atmosphere has not proven to be very beneficial in aiming to decrease the sintering temperature.

Acknowledgements

I would like to express my deepest appreciation to my supervisor, Professor Robert Knutsen for his guidance, help and insights during this project.

I would also like to thank the Council for Scientific and Industrial Research (CSIR) without whom this research would not have been possible.

I would also like to convey my sincere gratitude to Dr Deborah Blaine and Hendrick Bosman, from the University of Stellenbosch, for their help and assistance during this project.

I would also like to thank my peers at the Centre for Materials Engineering, UCT, for their motivation and support throughout this project.

Last but not least, I would like to thank my family for their encouragement.

Plagiarism declaration

I, Marie Mellisa Sandy Mariaye, know the meaning of plagiarism and declare that all the work in this document, except for those that are correctly acknowledged, is my own.

Signature: Signed by candidate

Date: 10th October 2018

MRYMAR001

EBE Faculty: Assessment of Ethics in Research Projects

Any person planning to undertake research in the Faculty of Engineering and the Built Environment at the University of Cape Town is required to complete this form before collecting or analysing data. When completed it should be submitted to the supervisor (where applicable) and from there to the Head of Department. If any of the questions below have been answered YES, and the applicant is NOT a fourth year student, the Head should forward this form for approval by the Faculty EIR committee: submit to Ms Zulpha Geyer (Zulpha.Geyer@uct.ac.za; Chem Eng Building, Ph 021 650 4791). Students must include a copy of the completed form with the thesis when it is submitted for examination.

Name of Principal Researcher/Student: MARIE MELISSA SANDY MARIAYE Department: MECHANICAL ENGINEERING

If a Student: Degree: MSC (Materials Engineering) Supervisor: Professor Robert Knutsen

If a Research Contract indicate source of funding/sponsorship:

Research Project Title: Effects of hydrogen as a temporary alloying element on the manufacturing and stages and properties of Ti-6Al-4V by powder metallurgy

Overview of ethics issues in your research project:

Question 1: Is there a possibility that your research could cause harm to a third party (i.e. a person not involved in your project)?	YES	(NO)
Question 2: Is your research making use of human subjects as sources of data? If your answer is YES, please complete Addendum 2.	YES	(NO)
Question 3: Does your research involve the participation of or provision of services to communities? If your answer is YES, please complete Addendum 3.	YES	(NO)
Question 4: If your research is sponsored, is there any potential for conflicts of interest? If your answer is YES, please complete Addendum 4.	YES	(NO)

If you have answered YES to any of the above questions, please append a copy of your research proposal, as well as any interview schedules or questionnaires (Addendum 1) and please complete further addenda as appropriate.

I hereby undertake to carry out my research in such a way that

- there is no apparent legal objection to the nature or the method of research; and
- the research will not compromise staff or students or the other responsibilities of the University;
- the stated objective will be achieved, and the findings will have a high degree of validity;
- limitations and alternative interpretations will be considered;
- the findings could be subject to peer review and publicly available; and
- I will comply with the conventions of copyright and avoid any practice that would constitute plagiarism.

Signed by:

	Full name and signature	Date
Principal Researcher/Student:	MARIE MELISSA SANDY MARIAYE	02/02/15

This application is approved by:

Supervisor (if applicable):		02/02/2015
HOD (or delegated nominee): Final authority for all assessments with NO to all questions and for all undergraduate research		02/02/2015
Chair : Faculty EIR Committee For applicants other than undergraduate students who have answered YES to any of the above questions.		

ADDENDUM 1:
Please append a copy of the research proposal here, as well as any interview schedules or questionnaires:

ADDENDUM 2: To be completed if you answered YES to Question 2:

It is assumed that you have read the UCT Code for Research involving Human Subjects (available at http://web.uct.ac.za/depts/educate/download/uctcodeforresearchinvolvinghumansubjects.pdf) in order to be able to answer the questions in this addendum.

2.1 Does the research discriminate against participation by individuals, or differentiate between participants, on the grounds of gender, race or ethnic group, age range, religion, income, handicap, illness or any similar classification?	YES	NO
2.2 Does the research require the participation of socially or physically vulnerable people (children, aged, disabled, etc) or legally restricted groups?	YES	NO
2.3 Will you not be able to secure the informed consent of all participants in the research? (In the case of children, will you not be able to obtain the consent of their guardians or parents?)	YES	NO
2.4 Will any confidential data be collected or will identifiable records of individuals be kept?	YES	NO
2.5 In reporting on this research is there any possibility that you will not be able to keep the identities of the individuals involved anonymous?	YES	NO
2.6 Are there any foreseeable risks of physical, psychological or social harm to participants that might occur in the course of the research?	YES	NO
2.7 Does the research include making payments or giving gifts to any participants?	YES	NO

If you have answered YES to any of these questions, please describe how you plan to address these issues (append to form):

ADDENDUM 3: To be completed if you answered YES to Question 3:

3.1 Is the community expected to make decisions for, during or based on the research?	YES	NO
3.2 At the end of the research will any economic or social process be terminated or left unsupported, or equipment or facilities used in the research be recovered from the participants or community?	YES	NO
3.3 Will any service be provided at a level below the generally accepted standards?	YES	NO

If you have answered YES to any of these questions, please describe how you plan to address these issues (append to form)

ADDENDUM 4: To be completed if you answered YES to Question 4

4.1 Is there any existing or potential conflict of interest between a research sponsor, academic supervisor, other researchers or participants?	YES	NO
4.2 Will information that reveals the identity of participants be supplied to a research sponsor, other than with the permission of the individuals?	YES	NO
4.3 Does the proposed research potentially conflict with the research of any other individual or group within the University?	YES	NO

If you have answered YES to any of these questions, please describe how you plan to address these issues(append to form)

Table of contents

List of Figures

List of Tables

List of Equations

Chapter 1: Introduction

1.1 Purpose of study

Titanium and titanium alloys (mainly Ti-6Al-4V) are known for their excellent physical, chemical and mechanical properties [1]. The reluctance in manufacturing Ti-6Al-4V by the PM route remains the inferior mechanical properties as compared to wrought Ti-6Al-4V [1]. Hydrogen is expected to enable sintering at lower temperatures resulting in improved density and mechanical properties while remaining a cost effective process [2]. Hydrogen can be introduced either by sintering in a hydrogen atmosphere and/or by using TiH_2 instead of CP Ti. However, TiH_2 is very brittle during compaction. The purpose of this research was to firstly, determine the optimal ratio of TiH_2 to CP Ti in a powder blend that can result in reasonable green properties and be used as a starting material to manufacture Ti-6Al-4V via the PM route. Secondly, the effects of hydrogen by sintering TiH_2 based compacts and/or sintering in a partial hydrogen atmosphere on the sintering properties (density and microstructure) were evaluated in different atmospheres with the aim to determine whether the sintering temperature could be lowered and thus provide a more cost efficient manufacturing route for Ti-6Al-4V alloys.

1.2 Significance of study

Titanium alloys have various applications namely in the aerospace, military and automotive industry [1][2]. However, the major hindrance in using titanium alloys lies in their high manufacturing cost which, makes them less commercially viable for many applications. In order to use titanium alloys for a wider range of applications, the PM route is expected to be the most cost efficient method provided mechanical properties comparable to the wrought alloys are achieved[3]. Hence, there is a rising need to conduct innovative research with the aim to reduce the costs of the PM route for the manufacturing of Ti-6Al-4V alloy by using hydrogen as a temporary alloying element. Hydrogen lowers the β-transus temperature and prevents the formation of surface oxides which, in turn promotes sintering and densification at lower temperatures while refining the microstructure [2][3]. Hydrogen introduction, in the form of TiH_2, has successfully resulted in higher densities when sintered under vacuum

at 1200°C for 2-4 hours [2][3][4]. Sintering at an even lower temperature can be expected, if a hydrogen atmosphere is used for sintering TiH_2, provided that hydrogen gas in the sintering atmosphere delays dehydrogenation. Hence, the presence and retention of hydrogen in TiH_2 samples should be studied in depth to evaluate and optimise the role that hydrogen (in a TiH_2 and/or H_2 form) plays on the sintering and resulting properties of Ti-6Al-4V.

1.3 Scope of research

This study looks at assessing the following:

1) the effects of the ratio of TiH_2 to CP Ti on the compaction behaviour, density and strength of the green compacts.
2) the decomposition behaviour of the selected powder blends over a temperature range similar to the sintering temperature profile. This decomposition study will determine whether there are any additional benefits of using TiH_2 in the powder blend as well as the benefits of sintering in a partial hydrogen atmosphere.
3) the improvement from green to sintered densities of the different samples in the various atmospheres. These improvements shall be explained in depth based on particle shape, size, composition as well as sintering atmosphere and temperature.
4) Evaluate the effects of hydrogen, in the form of TiH_2 and H_2 (from the partial hydrogen atmosphere), on the sintered densities and microstructures of the selected samples.

1.4 Limitations of research

Due to time constraints, safety concerns and limitations of the equipment for this particular study, the following could not be assessed:

- the effect(s) of compaction pressures greater than 500MPa on the green density and strength of the various powder blends.

- the effect(s) of increasing the hydrogen content in the sintering atmosphere on the densities and microstructures of the selected samples.
- the effects of a wider matrix of sintering temperatures and times on the microstructures and densities of the various CP Ti / TiH_2 powder blends compacts.
- the decomposition behaviour of the powder blends under vacuum. The vacuum pump causes vibration of the mass balance in the Netzsch which, gave very erratic results.
- Conduct partial sintering of TiH_2-6Al-4V green compacts to determine the exact sintering profile that would provide indication of the vanadium and aluminium diffusivity prior to homogenisation.
- Element mapping of all the Ti-6Al-4V and TiH_2-6Al-4V samples subjected to sintering conditions to determine the element distribution.

1.5 Plan to development

This dissertation follows with a literature review (Chapter 2) describing the different stages of the PM route and the role of hydrogen as a temporary alloying element. A critical review of the research related to the role that hydrogen plays in the sintering of TiH_2, CP Ti and their blends with either elemental or pre-alloyed 60Al-40V MA powders, is then described. The findings of these research are then discussed in terms of the significance and importance of this dissertation. Chapter 3 illustrates the methodology of this dissertation explaining the different tests and procedures that were conducted to evaluate the role of hydrogen on the compaction and sintering stages involved in manufacturing Ti-6Al-4V by the PM route. Chapters 4-7 show, compare and discuss the various results obtained and compare then to the data in the current literature. Any unexpected results are discussed in depth and possible explanations are provided. The outcomes of this dissertation are then summarised and possible future work are recommended in Chapter 8 and 9 respectively.

1.6 Expected outcomes

Based on the existing literature and the results of previous research the following are expected:

- TiH_2 is more brittle and will therefore break and rearrange resulting in higher green densities. However, the difference in particle size and shape will also play a role in the densities of the various green compacts.
- TiH_2 is more brittle and hence the particles are expected to break during compaction. Thus no bond formation is expected which should be denoted by a lower green strength as compared to CP Ti which can deform under cold welding forming bonds.Thus, powder blends with higher levels of TiH_2 are expected to have lower green strength.
- The higher the compaction pressure, the higher will be the green strength and density of the compact.
- During decomposition of the powder blends, hydrogen absorption will not take place in compounds with no CP Ti levels and hence no decomposition will take place in an argon atmosphere. For powder blends, containing both CP Ti and TiH_2, both an absorption and decomposition steps are expected.
- Hydrogen is expected to enable the sintering of the green compacts at lower temperatures. This is due to the stabilisation of the β-phase as opposed to the α-phase at relatively low temperatures. In addition, the reducing properties of hydrogen (by forming H_2O (g) when reacting with surface oxides present) promotes sintering and densification. Thus, higher sintered densities are expected in samples sintered in a partial hydrogen atmosphere or samples containing higher levels of TiH_2. However, for temperatures below 1200°C, whether the same rate of H_2O (g) release is still not documented.
- Sintering in a partial hydrogen atmosphere should result in higher sintered densities compared to similar sintering trials conducted in an argon atmosphere.
- It is expected that aluminium will diffuse first for CP Ti-6Al-4V and that vanadium will diffuse first for TiH_2-6Al-4V during the initial stages of sintering respectively since CP Ti is an alpha phase stabilizer whereas TiH_2 is a beta phase

stabiliser. Thus, the diffusion of the MA is expected to differ for these two samples which could affect the sintered densities.

Chapter 2: Literature review

This chapter provides an in-depth background understanding to this research as well as a critical review on the role and effects of hydrogen as a temporary alloying element during the compaction and sintering stages of the PM route to manufacture Ti-6Al-4V.

2.1 Titanium

Titanium, in the form of its ore, is the ninth most commonly occurring element on earth [1]. Titanium is well known for its excellent strength to weight ratio as well as good corrosion properties as compared to other alloys such as steel. For example, in its unalloyed condition, titanium has comparable strength with steel but is 45% less dense [1].

2.2 Ti-6Al-4V alloy

The most commonly used titanium alloy is Ti-6Al-4V, which is more commonly referred to as the 'workhorse alloy' of the titanium industry [2]. This alloy equates to 50% of the amount of titanium used in various applications. Ti-6Al-4V is an alpha plus beta (α+β) alloy that can be heat treated to achieve moderate increase in strength. The change in mechanical properties is achieved by modifying the microstructure of Ti-6Al-4V.

2.2.1 Microstructure of Ti-6Al-4V

The microstructure of Ti-6Al-4V alloy depends on:

1) The heat-treatment that the alloy is subjected to.
2) The amount of α and β phase present in the alloy.
3) The type of alloying element; for example hydrogen as a temporary alloying element in the manufacture of Ti-6Al-4V by the PM route is expected to result in finer microstructures [2][3].

2.2.1.1 Modification of Microstructure

The modification of microstructure is commonly achieved through a combination of cold or hot working followed by heat treatments such as annealing or solution heat treatment [3]. Most Ti-6Al-4V castings alloys, produced commercially today, are supplied in the annealed condition. However, research has been conducted in altering the microstructure of cast titanium alloys so as to improve the fatigue and strength properties. These treatments include solution-treatment and aging, or other post-cast thermal processing such as selective laser melting [4].

In the case of titanium casting alloys, the main goal is to eliminate the grain-boundary α phase, the large α plate colonies, and the individual α plates [3]. These plates are 100% α and hence do not result in Ti-6Al-4V alloy having a homogeneous $\alpha+\beta$ microstructure. This is accomplished either by solution treatments or by temporary alloying will hydrogen. Hydrogen, present in TiH_2, is expected to lower the sintering temperature of Ti-6Al-4V made by the PM route. This is further discussed in Section 2.4 and 2.5.

2.3 Powder metallurgy (PM) of Ti-6Al-4V

PM is a process of blending fine elemental or pre-alloyed metal powders, pressing them into a desired shape and then heating the material under a controlled atmosphere [5]. The PM route can be illustrated using the flow diagram shown in Figure 2.1.

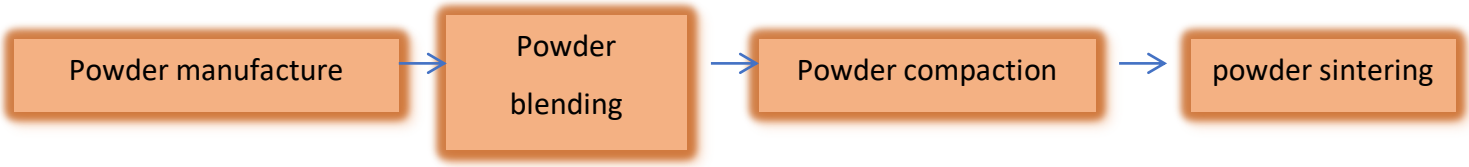

Figure 2.1: Main steps in PM route

Figure 2.2 is a schematic that illustrates the manufacturing of Ti-6Al-4V products by the PM route.

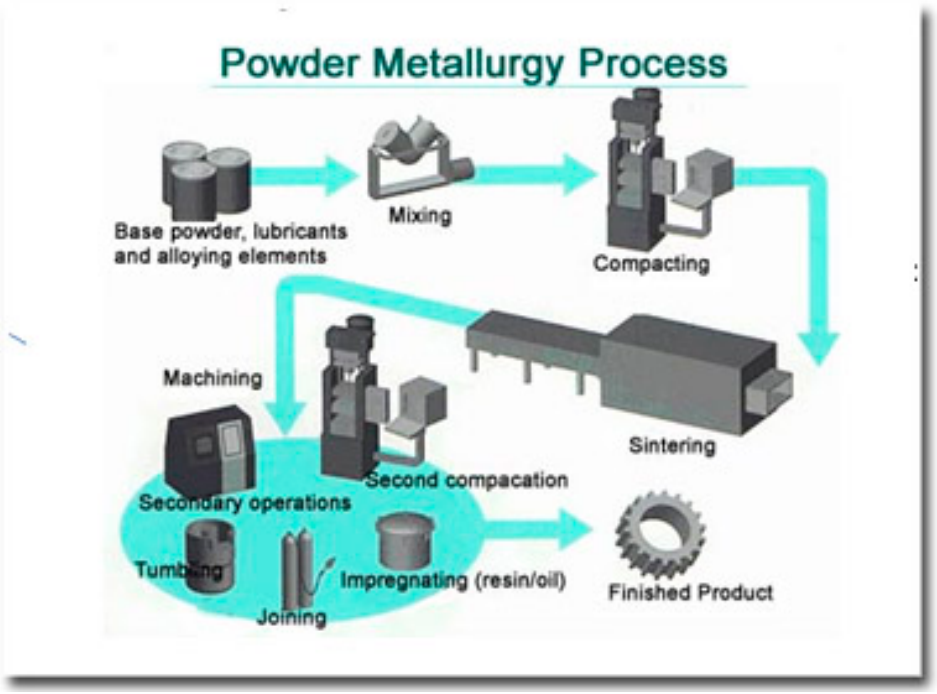

Figure 2.2: Different processes involved in PM [6]

The type of metal powder as well as the powders' particle size and shape used in PM affect the properties of the finished products. The powders' shape and size are determined by their manufacturing methods [7].

2.3.1 Starting powders

2.3.1.1 Powder manufacture

Titanium sponge fines are the most common elemental powder used in PM. These particles are obtained as by-products of the Hunter or Kroll reduction process used to primarily extract pure titanium from its ore [8]. The titanium sponge fines that are too small to be used in the melting process are available at a relatively low cost. This powder has an irregular shape (see Figure 2.3) which, enables them to be cold pressed into green compacts. There are two main ways in which metal powders can be produced: mechanical fabrication and atomisation technique. The mechanical fabrication technique includes impaction and compression which involves the use of exerting high forces to crush the metal parts into powders [8]. Compared to mechanical fabrication techniques, the atomisation technique allows easier processing which, in turn enables better control over particle size. The atomisation

technique (water or gas atomisation) involves heating the pure metal or alloy above its melting point and allowing the molten stream to be subjected to high gas or water pressures. On cooling the fine molten sprays result in the formation of solid powders [9].

2.3.1.2 Powder type

There are two main types of starting powders that can be used when manufacturing Ti-6Al-4V by the PM route. They are; blended elemental (BE) powder or pre-alloyed (PA) powder. A blended elemental powder refers to a powder blend formed by mixing each individual elemental powder to form the desired alloy whereas a pre-alloyed powder already contains all the element in the correct ratio for the alloy. Thus, no blending is required for pre-alloyed powders.

BE powder

The BE powder is cheaper and thus more commercially viable. BE powders will allow alloy modification but result in lower mechanical properties of the sintered compacts when compared to their equivalent PA sample [10]. A study conducted suggests that the homogenisation or uniform distribution of elements is not achievable using blended elemental powders. This in turn resulted in lower density and mechanical properties of the Ti-6Al-4V alloy. It was suggested that a master alloy (MA) (aluminium and vanadium powder in the ratio of 60:40) could be a better alternative in manufacturing Ti-6Al-4V [10].

PA powders

A PA Ti-6Al-4V powder will consist of all three elements already mixed in the correct ratio and will not require any blending before compaction. Hence, when using pre-alloyed powder, the issue of homogenisation is eliminated [10]. However, production of PA powders are limited due to high production costs.

Hence, a compromised powder blend of titanium with a 60Al40V MA powder will be a more commercially feasible alternative in manufacturing Ti-6Al-4V by the PM route [11].

2.3.1.3 Powder characterisation

The particle size of metal powders is difficult to characterise due to their irregular shape and geometries. Figure 2.3 shows the different shapes that powder particles can exhibit [12].

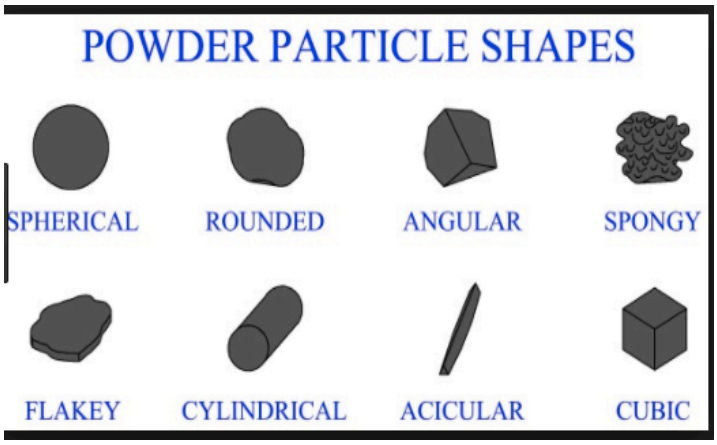

Figure 2.3: Schematic of different powder particle shapes [12]

A reliable method to measure particle size entails the use of molecular sieves (see Figure 2.4. Each sieve allows a particular particle size and shape to go through it. The particle size and shape are categorised in terms of the 'mesh' number. The larger the mesh number, the smaller is the size of the powder particles. For example, a powder with a mesh size of -200 (75 µm) has smaller particles as compared to the same powder with a mesh size of -100 (150 µm). The (-) sign suggests that the powder particles go through the sieve. Figure 2.4 shows a schematic drawing of a molecular sieve that is used to determine powder size [13].

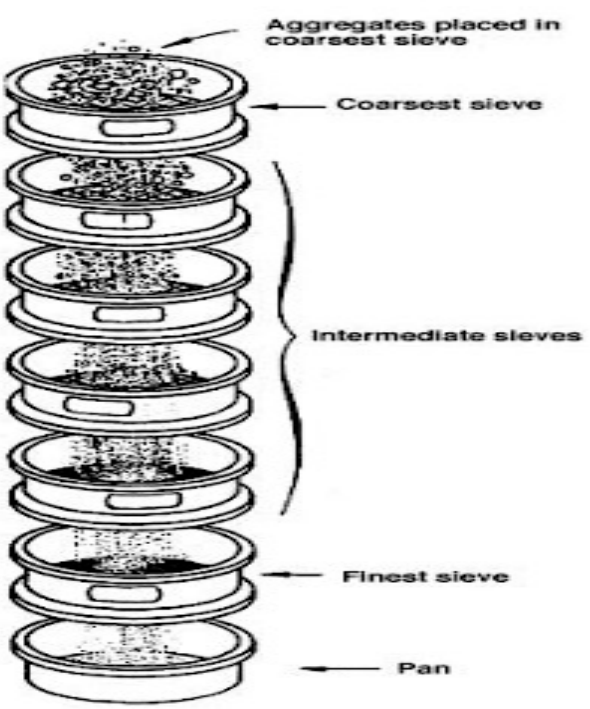

Figure 2.4: Molecular sieve used to determine mesh size of powder particles [13]

2.3.1.4 Effect of particle size and shape on the properties of resulting green compacts

The particles' size and shape affect the behaviour of the powders during compaction. A study conducted [14] looked at the effects of compaction pressure and particle shape on the porosity of the resulting green compacts. Two powders were used; namely Powder A and Powder B. The former was spherical and uniform in size whereas the latter was angular and irregular in shape. Powder A (average particle size of 140 µm) could only be compressed in shape for compaction pressures higher or equal to 400MPa. Powder B (average particle size of 170 µm) could easily be compressed at lower compaction pressures (<400MPa). Thus, it can be said that the compressibility of the powders is better with irregular shaped powders. This is due to the locking and cold welding abilities of the powders which, results in better packing ratio of the resulting green compacts. Thus, angular and highly facetted powders are expected to be easily compressed at low compaction pressures (<400MPa) [14].

The particle size also affects the compressibility and green density of the compacts. A study that looked at the process models for the press-and-sinter titanium [15]

compared the green density between coarse (average particle size 77.6 µm) and fine (average size of 32.3 µm) powders at various compaction pressures. The green density of the coarse powder was higher than the fine powders (75% as opposed to 71% relatively densities respectively) for a compaction pressure of 400MPa. Based on this study, it was concluded that the green density increases with increasing particle size up to a compaction pressure of 450MPa for CP Ti. A general compaction model is mathematically expressed as shown in Equation 2.1.

Equation 2.1: $\ln[(1/(1-\rho)) = KP + \ln[(1/(1-\rho_a)) + B$ [15]

where K: proportionality constant

ρ_a : apparent density of powder before any loading is applied

B: constant related to mechanical properties of the powder

P: Pressure

From this general compression model, it is clear that the mechanical properties of the powders also have a role to play in the compressibility of the powders [15]. On the one hand, a ductile powder will start to plastically deform under pressure until a pressure at which the powders can no longer deform is reached (relative green density will plateau). On the other hand, a brittle powder can only fracture during green compaction. Hence, the compaction pressure at which the brittle powders fracture is key in understanding the density results of compacts made from brittle powders [15]. The compaction pressure must be high enough to result in fracture of the brittle powder particles to allow good compression.

CP Ti and TiH_2 are examples that can be used in the context of this research project. TiH_2 will require a minimum pressure to fracture the particles that will in turn result in densification of the compact. It is stated in current literature [16] that a compaction pressure higher than 250MPa is sufficient to fracture TiH_2 powder particles. If fracture does not take place, the densification rate will be lower resulting in compacts with low green densities. In current literature [17], a study reports the effects of compaction pressures on CP Ti and TiH_2 based compacts with either elemental aluminium and

vanadium or aluminium-vanadium MA powder. The results show that compacts with bigger particle size results in higher green densities. Table 2. 1 and Figure 2.5 show the different powder blends and their relative green densities respectively.

Table 2. 1: Different powder blends used [17]

Mixture	Description	Methods of addition
1	Ti, −100 μm, 1% impurities, including 0.29%O	Elemental powders Al: 98%, −100 μm V: 99%, −100 μm
2	Ti, +100–200 μm, 0.7% impurities, including 0.29%O	Elemental powders Al: 98%, −100 μm V: 99%, −100 μm
3	TiH_2, −100 μm, 1% impurities, including 0.30%O	Elemental powders Al: 98%, −100 μm V: 99%, −100 μm
4	Ti, −100 μm, 1% impurities, including 0.29%O	Elemental powders Al: 95%, −20 μm V: 98%, −40 μm
5	TiH_2, −100 μm, 1% impurities, including 0.30%O	Elemental powders Al: 95%, −20 μm V: 98%, −40 μm
6	Ti, −100 μm, 1% impurities, including 0.29%O	Master alloy powders Ti-35Al: 98.5%, −100 μm V-25Al: 98.3%, −100 μm
7	TiH_2, −100 μm, 1% impurities, including 0.30%O	Master alloy powders Ti-35Al: 98.5%, −100 μm V-25Al: 98.3%, −100 μm

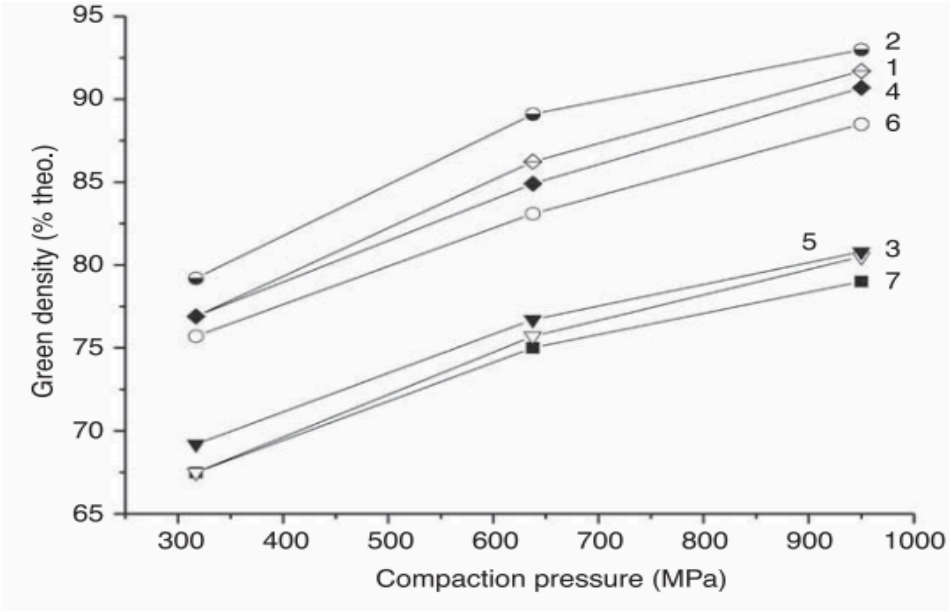

Figure 2.5: Effects of compaction pressure on relative green densities [17]

Even though, the addition of elemental aluminium and vanadium alloying powders as opposed to MA powder results in higher green densities, the effects associated (inhomogenisation and formation of undesired $TiAl_3$ phase) with blended elemental powders during sintering, limits the use of elemental alloying powders [10][17].

A different study [18] also supports that titanium compacts with bigger particle size (average particle size of 100μm) result in higher green densities as compared to similar compacts with finer powder particles (average particle size of 25μm). Even though the voids between two particles are smaller in a compact made from the finer powder particles, the frequency of the voids are extremely high and consequently result in an overall lower relative green density as compared to similar compacts formed from powders with bigger particle size. The results of the study led to the conclusion that for finer particle size, higher compaction pressures were required to result in comparable densities that were obtained at lower compaction pressure for coarse powders. Also, TiH_2 powder blends fracture at compaction pressures lower than 320MPa. This supports the argument, stated previously, that TiH_2 powders fracture at compaction pressure higher than 250MPa. The study also confirms that at 400MPa, TiH_2 based compacts reach their maximum green density [18]. Therefore compaction pressures from 300-500MPa will be enough to fracture TiH_2 samples to result in acceptable green densities.

Another research conducted shows the difference in relative green densities for CP Ti and CP TiH_2 which, is depicted in Figure 2.6 [19].

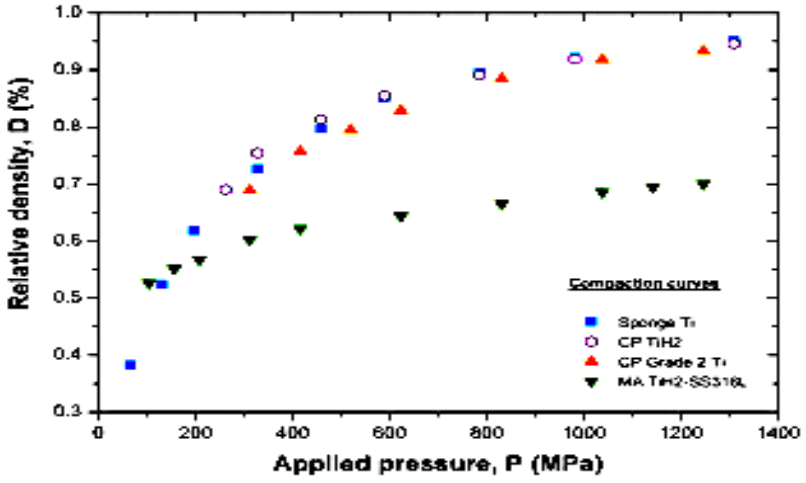

Figure 2.6: Effect of compaction pressure on relative green densities of CP Ti and TiH_2 [19]

Figure 2.6 shows that the relatively green densities of TiH_2 and CP Ti as a function of compaction pressures, follow similar trends. Here again, it can be pointed out that CP TiH_2 was not pressed at a compaction pressure lower than 300MPa. Figure 2.6 shows that 80% relative density for both powders is achieved at 500MPa. The powders used are of varying size but their shapes are also significantly different as shown in Table 2. 2.

Table 2. 2: Powder characteristics [19]

Material	Ti Sponge	TiH_2	CP Grade 2 Ti	MA TiH_2-SS316L
Supplier	Industrial Analytical (Pty) Ltd.	AG Metals Inc.	TLS Technik GmbH & Co.	—
Particle characteristics				
Mean sphericity	0.844	0.825	0.887	0.845#
Mean roundness	0.683	0.671	0.804	0.633#
Size, D_{10} (μm)	159.4	11.4	22.8	#
Size, D_{50} (μm)	250.0	18.7	32.1	#
Size D_{90} (μm)	668.0	28.6	41.06	#
Morphology	spongy	angular	spherical	mixed#
Theoretical density (g/cm^3)	4.51	3.76	4.51	5.56
Initial porosity (pct)	82.3	62.3	45.4	62.6

Based on Figure 2.6, the Ti sponge, TiH_2 and CP Grade 2 Ti have similar green densities at various compaction pressures. However, since the particle shape and size are both different, it is difficult to evaluate the effects of particle size on green densities for this study. For example, the relatively green densities of Grade 2 CP Ti and CP TiH_2 are

more or less the same (76%) but their average particle size are substantially different (32.1 µm and 18.7 µm respectively). Based on the general trends in current literature, smaller particles should result in lower relative green density. However, the particle shape of Grade 2 CP Ti is spherical, and as discussed previously regular shaped powders will have a lower relative green density [19].

It is important to note here, that CP TiH_2 was not pressed at pressures lower than 250MPa. This again confirms that a pressure higher than 250MPa are required to fracture TiH_2 powders. Therefore, the use of a compaction pressure range of 300-500MPa is expected to be sufficient enough to fracture TiH_2 particles to promote green densification. Even though a higher compaction pressure would still result in a significant improvement in green density for the TiH_2 based compacts, sample ejection at such high pressure can be very difficult and would result in cracking and fracturing of the sample.

Based on the results discussed in this section, it is expected that the relative green densities of coarse CP Ti (average particle size of 100 µm) should be higher than that of TiH_2 (average particle size of 67 µm) provided that both powders have similar shape.

2.3.2 Stages in PM

The main steps in making Ti-6Al-4V by the PM route are: blending, compaction and sintering as shown in Figure 2.2.

2.3.2.1 Powder blending

A cost-effective method to result in a Ti-6Al-4V powder blend that can possibly improve the alloy's final properties is by blending titanium powder with MA powder. The use of MA powder as opposed to aluminium and vanadium elemental powder minimises the additional homogenisation issues between aluminium and vanadium [20]. The MA powder is easily produced and also does not entail a significant increase in production costs.

The blending of titanium and MA powders can be easily conducted by using a blending equipment for 15 minutes. The time required to blend these powders was established to be 15 minutes based on a study conducted at the University of Stellenbosch. This study titled “The optimisation of a Homogenising Metal Powder Mixer” concluded that 15 minutes was the minimum required mixing time that would result in a uniform distribution of the powders within the blend [21].

2.3.2.2 Compaction

Powder compaction is a mass-conserving shaping process. During powder compaction, each powder blend is placed inside a die and high pressure is then applied for consolidation resulting in the formation of a green compact [22]. The most common type of die tooling will press the powders in the vertical orientation, otherwise known as uniaxial pressing. The die pressing method is the most commercially viable pressing method as compared to other pressing methods such as cold isostatic pressing. Figure 2.7 is a schematic diagram of the compaction process that is used and Figure 2.8 shows a representation of a die mould that can be used for the vertical pressing of the powders to result in the formation of green compacts.

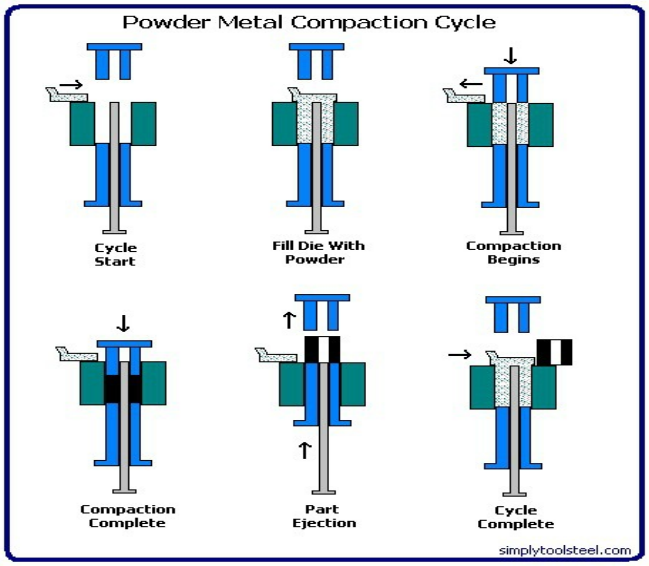

Figure 2.7: Pressing process forming green compact [22]

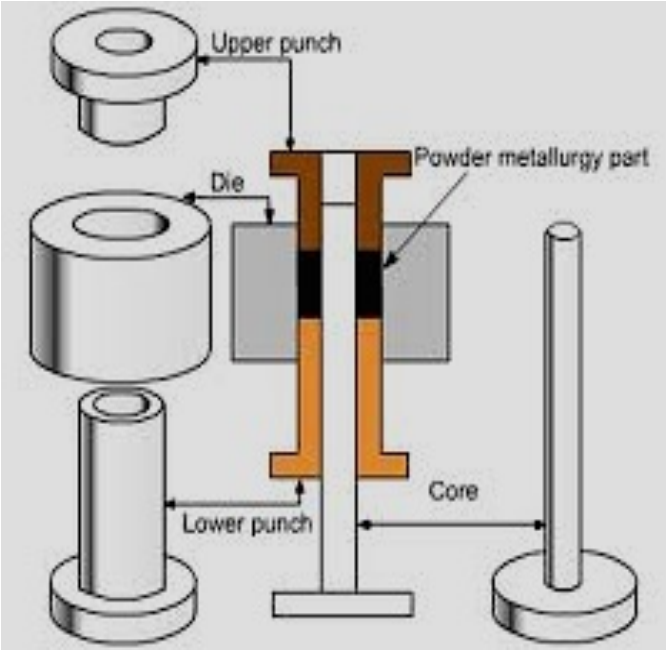

Figure 2.8: Die mould for uniaxial pressing [22]

2.3.3 Sintering

Sintering is defined as a heat treatment process whereby previously compacted metal powders are heated to elevated temperatures (but below the melting point of the metal or alloy) in order to allow the particles to diffuse and bond together [23]. Sintering occurs in several stages, which are initial, intermediate and final. Figure 2.9 illustrates the main stages of sintering.

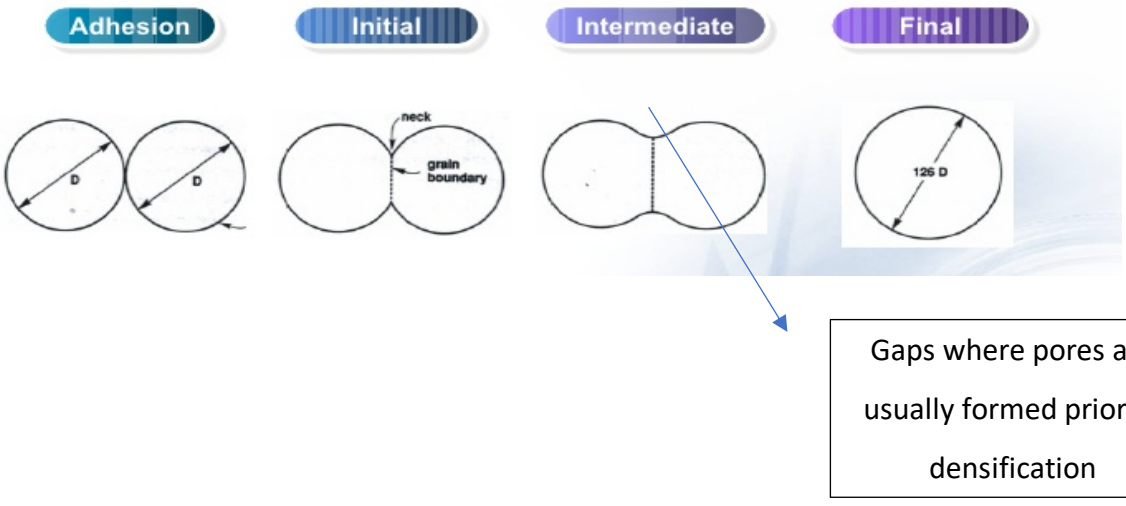

Figure 2.9: The main stages of sintering [23]

From Figure 2.9, the following stages can be briefly described as follows [23]:

1) Adhesion: This is the stage that occurs when the particles come into contact. This stage can also be achieved during compaction. During this stage, weak cohesive bonds hold the powder particles.
2) Initial: During the initial stage, there is rapid growth of the inter-particle neck resulting in the formation of a grain boundary.
3) Intermediate: During the intermediate stage, the pore structure becomes smooth and interconnected thus giving rise to larger but fewer grains.
4) Final: During the final stage, the pores are completely spherical and closed giving rise to grain growth (formation of a bigger grain).

2.3.3.1 Sintering of titanium powder

Titanium powder is sintered at temperatures in the range of 1150 to 1315°C under vacuum to prevent oxidation. The high sintering temperature is needed to allow excellent bonding between the particles to result in a more homogenous distribution of the particles. This temperature is well above the β transus of all common titanium alloys. As a result, the microstructure in α + β alloys is composed of colonies of similarly aligned coarse α plates [24]. This microstructure is substantially finer than ingot material treated at the same temperature due to the inherent porosity of the powder compact. This refined microstructure is an indication of improved strength properties, which favours the PM route. In many cases, significant porosity of the sintered sample is the result of sodium chloride residues (from the Kroll process) in the sponge from the reduction process. Hence, it is vital that the titanium powder used in the PM process is free from any chloride contamination [25].

Sintering of titanium powders starts around 700°C, the sintering temperatures for making Ti-6Al-4V will be above 700°C. At temperatures above 450°C, under normal atmospheric conditions, titanium powder oxidises which is undesirable due to the formation of surface oxides [26].

In the current literature, the following is known for the sintering behaviour of Ti-6Al-4V:

1) The sintering of loose powders is known to start at a temperature of 700°C.
2) Mechanical and physical contact begins at 650°C and 1100°C respectively
3) The boundaries of titanium start to dim at a temperature of 900°C. This alteration in the grain boundaries suggests that diffusion is initiated at 900°C [26].

2.3.3.2 Sintering atmosphere

Sintering of titanium and titanium alloys must be conducted under a controlled atmosphere due to titanium's high affinity with oxygen. The use of a partial hydrogen atmosphere is expected to be beneficial due to the reducing abilities of hydrogen in preventing the formation of surface oxides thus promoting sintering to take place at lower temperatures. The role of hydrogen in making Ti-6Al-4V by the PM route is discussed in depth in Section 2.4. Figure 2.10 and Figure 2.11 illustrate a sintering profile of titanium powders sintering under vacuum followed by a controlled cooling profile in partial hydrogen atmosphere.

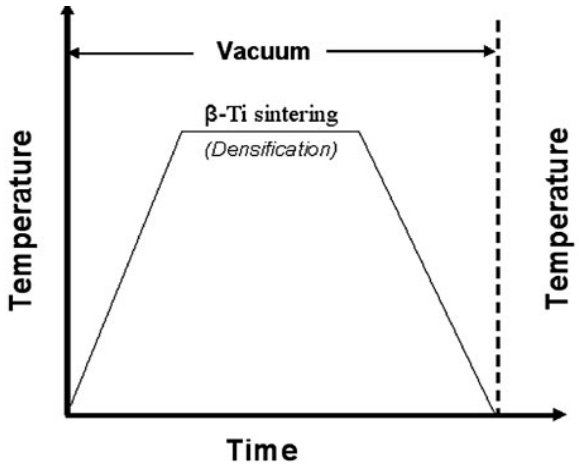

Figure 2.10: Temperature versus time profile during vacuum sintering of Ti-6Al-4V [27]

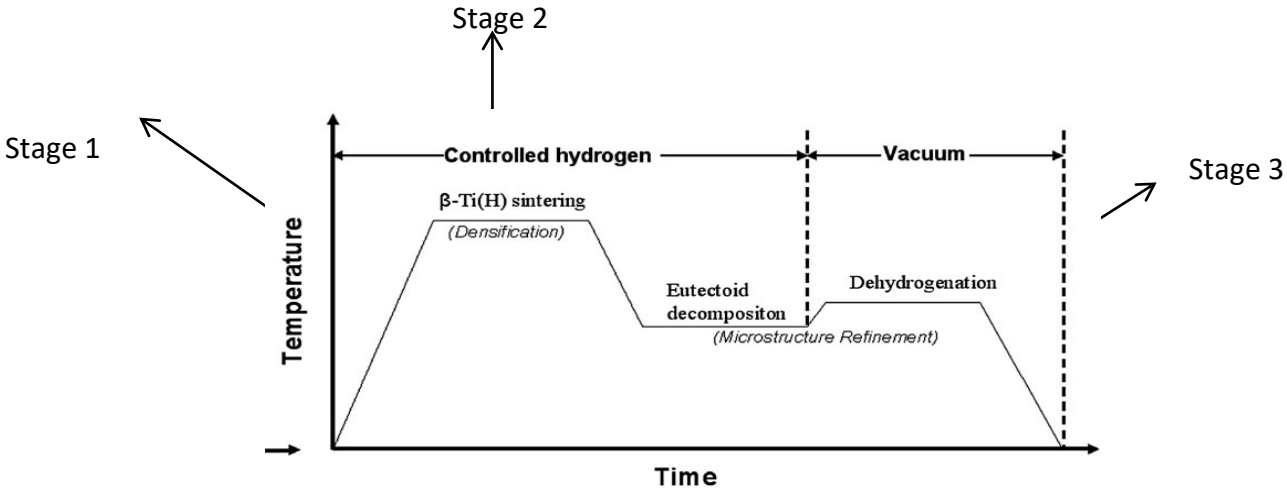

Figure 2.11: Temperature versus time profile during hydrogen sintering followed by vacuum of Ti-6Al-4V [27]

The results of this study concluded the following:

1) In a controlled hydrogen atmosphere, [β-(Ti)] contains a substantial amount of hydrogen. A solid solution of hydrogen in titanium will lower the activation energy of titanium. Consequently, there is a decrease in the strength of Ti-Ti bonds which can result in self diffusion of titanium. This process enables densification of titanium at a lower sintering temperature.
2) After β-Ti densification, the samples were cooled in a controlled hydrogen atmosphere to temperatures below the eutectoid temperature and held for a time period of 8-16 hours. This resulted in the breaking up of fine coarse grains into fine dispersed grains.
3) The vacuum annealing conducted further refined and modified the microstructure of the Ti-6Al-4V alloy while removing any residual hydrogen present in the sample.

The study conducted and referred in Section 2.3.1.4 [14] also looks at the sintering properties of titanium compacts. This study confirms that fine powders as compared to coarse powders resulted in higher sintered densities (98% as opposed to 91% relative density) for sintering conditions of 1300°C for 2 hours under vacuum. Figure 2.12 and Figure 2.13 show the improvement in the number and size of pores present in sintered samples made from a coarse to fine titanium powder, which supports the difference in sintered densities.

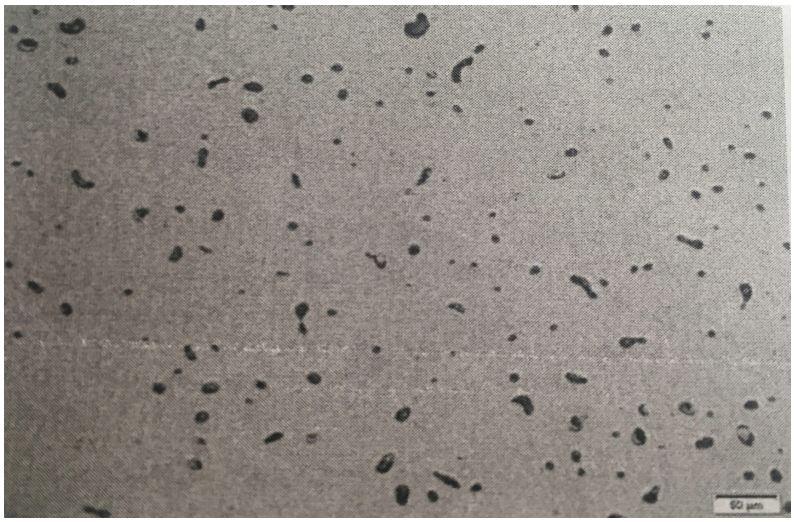

Figure 2.12: Sintered microstructure of compacts (from fine powders) pressed at 400MPa and sintered at 1300°C with relative sintered density of 98% [14]

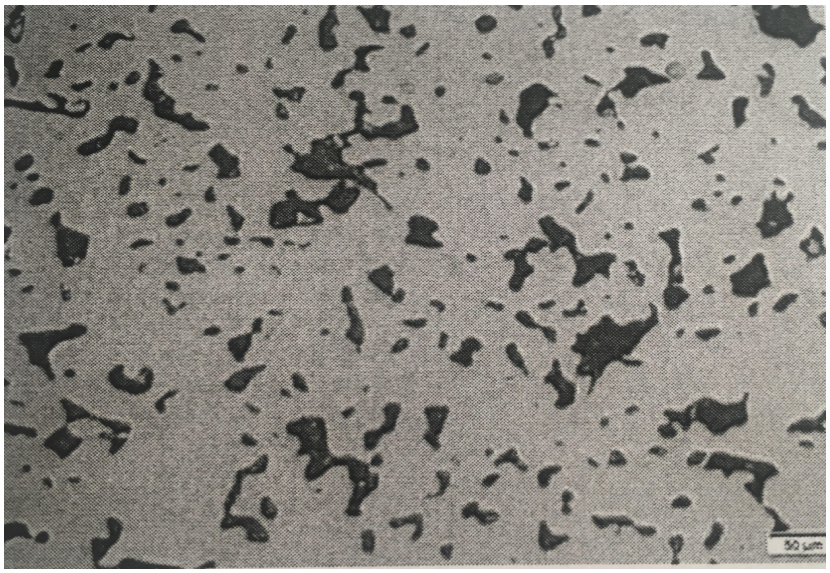

Figure 2.13: Sintered microstructure of compacts (from coarse powders) pressed at 400MPa and sintered at 1300°C with relative sintered density of 91% [14]

2.4 The role of hydrogen in manufacturing titanium and Ti-6Al-4V alloy by the PM route

Hydrogen is an alloying element that can be added and removed without melting of the metal powders. Several benefits of having hydrogen as a temporary alloying element during the sintering of titanium and titanium alloys by the PM route, were investigated and proven. Hydrogen is known to decrease the β-transus temperature as well as rendering post sintering treatments such as hot deformation possible. It is stated in current literature [28] that hydrogen alloying destabilises the low temperature α-hcp (hexagonal close pack) phase and stabilises the β-bcc (body centered cubic) phase in both titanium and Ti-6Al-4V. Hence, the α-phase partially dissolves in the β-phase, above the eutectoid temperature, resulting in the decrease of the β-transus temperature and an increase in the temperature interval of the two phase (α and β) range. When the hydrogen levels in the systems are increased, a decrease in the critical rate and the temperature of martensitic transformation can be observed. In addition, the shear strength and Young's moduli of the β-phase increases which, are highly favourable.

The addition of hydrogen in Ti-6Al-4V (α+β titanium alloy) results in the redistribution of alloying elements between the phases which, in turn results in unequal changes in specific volumes of the different phases. The larger volume changes are concomitant when α-titanium transforms to TiH_2. During this phase transformation, a 17.2% volume expansion occurs causing a high strain level in the matrix [29]. Hydrogen has a role to play in the diffusivity of the alloying elements together with the dislocation slip systems, since it activates the surface of the material hence, promoting better diffusion bonding and welding. The decrease in β-transus temperature results in a reduction in grain growth associated with long sintering hours and high temperatures. A key role that hydrogen plays is in the post heat treatments such as hot deformation. Hydrogen results in an increase in temperature interval of the α+β phase and a decrease in the flow stress of the α, pseudo-α and α+β phases. Altering the phase transformation temperatures and allowing hot deformation treatments, allows hydrogen additions to result in the generation of various novel microstructures that

have improved strength, toughness and hardness properties comparable to those of wrought Ti-6Al-4V. Thus, understanding to what extent hydrogen can lower the sintering temperature of titanium and Ti-6Al-4V, while resulting in good densities and mechanical properties is critical.

2.4.1 Hydrogen absorption in CP titanium

The absorption of hydrogen by titanium depends on the time, temperature as well as the composition of the alloy. Titanium and titanium alloys are known to have relatively high affinity with hydrogen and can absorb up to 60 atomic percent (at%) of hydrogen at 600°C and even higher contents at lower temperatures [28]. It is therefore expected that at the higher end of the sintering temperature profile, hydrogen loses its affinity with titanium which, will lead to the decomposition of TiH_2 to β-Ti. Therefore, investigating the temperatures at which hydrogen absorption and decomposition takes place during sintering, is key in assessing the benefits of hydrogen as a temporary alloying element in the manufacturing of Ti-6Al-4V by the PM route [28][29]. In other words, chosen sintering treatments will provide some indications as to whether there are any positive benefits of sintering TiH_2 in a partial hydrogen atmosphere to allow small levels of hydrogen to be retained at higher temperatures (higher than 700°C) [28][29].

Reaction of titanium and hydrogen begins at 332°C which, results in the formation of TiH_2. Based on a study conducted [30], it has been experimentally proven that at 350°C for two hours, a maximum of 42.96L of hydrogen can be absorbed by 100g of CP titanium. However, in the compact form, under similar experimental conditions, only 38.14L of hydrogen is absorbed which, shows that the geometry of the sample has a role to play in the maximum level of hydrogen that can be absorbed (hydrogen saturation) [30]. The resulting TiH_2, that is formed, starts to then dissociate at higher temperatures (between 344-388°C) and final liberation of hydrogen from TiH_2 occurs at 900°C. Thus, hydrogen absorption and phase transformation (from CP Ti to TiH_2) changes the thermodynamics of the sintering mechanism which, is expected to promote densification at lower temperatures. Hence, it is critical to understand over which temperature range hydrogenation and dehydrogenation takes place for CP Ti/

TiH_2 samples as well as for Ti-6Al-4V and TiH_2-6Al-4V to conclusively determine whether or not the introduction of hydrogen plays a positive role during sintering [28]. It is expected that under a partial hydrogen atmosphere (15%H_2/85%Ar), hydrogen will dissolve in the CP Ti matrix [30][31]. This reaction occurs from 332°C up to about 600°C [31]. Since hydrogen dissolves in the CP Ti matrix, a phase transformation from α-Ti to β-Ti occurs. This phase transformation is an exothermic reaction. No dehydrogenation takes place at higher temperatures. In the case of TiH_2 powder blends, in a partial hydrogen atmosphere, hydrogenation cannot take place since TiH_2 is already saturated with hydrogen (maximum of 67 at% or 3-4wt%) and hence only dehydrogenation [31] (an endothermic reaction) is expected for TiH_2 compacts. However, the temperature range over which the various steps associated with dehydrogenation will take place for TiH_2/CP Ti blends is unknown. This is a key finding that will be investigated in this dissertation.

2.4.2 Diffusion of hydrogen in CP Ti, Ti-6Al-4V and TiH_2

There are two main types of diffusion which are: interstitial and vacancy diffusion. Due to the small size of a hydrogen atom as compared to a titanium, aluminium or vanadium atom, hydrogen occupies interstitial sites in a Ti-6Al-4V alloy. For a hydrogen atom to jump into an interstitial site, it requires energy, which is known as the activation energy.

Looking at the crystal structure that titanium and Ti-6Al-4V alloy can have (BCC or HCP), it can be said that in the β phase, the crystal structure (BCC) is less packed as compared to the HCP crystal structure (α-phase). This is confirmed by the packing factor of 0.68 for BCC and 0.74 for HCP [32][33]. Hence, hydrogen diffusion in the β-phase is expected to occur at a faster rate as compared to its diffusion in the α-phase.

The diffusion time of hydrogen is roughly proportional to the square of the thickness of the material (at a given temperature) and inversely proportional to hydrogen diffusion coefficient as shown by Equation 2.2.

Equation 2.2 [34]…… **($t = x^2/D$)**

Where t: diffusion time

X: thickness of the material

D: hydrogen diffusion coefficient

Fick's First law of diffusion (Equation 2. 3) is based on the assumption that diffusion is a steady state process. This implies that that the diffusion flux or mass of atoms diffusing through a unit area per unit time is constant throughout the whole diffusion process.

Equation 2. 3 [34][35]……**$D= D_0 \exp(-E_a/RT)$**

Where D: Diffusion coefficient of hydrogen in Ti-6Al-4V alloy

D_0: Diffusion coefficient of Ti-6Al-4V; 6.6×10^{-3} m^2/s

E_a: E; pre-exponential factor and a; activation energy of hydrogen; 432 kJ/mol

R: Gas constant; 8.314J/mol

T: Temperature in Kelvin

From Equation 2. 3, it can be said that as the temperature increases, the diffusion of hydrogen will be more or less equal to the diffusion coefficient of Ti-6Al-4V.

Hydrogen, being a smaller atom, will have a lower activation energy as compared to a bigger molecule such as oxygen and thus sintering in a partial hydrogen atmosphere will limit the formation of surface oxides since hydrogen absorption will be favoured [34][35]. The prevention of surface oxides formation allows the sample to have more open pores which, can thus shrink even further or even be eliminated at the higher temperatures. Additionally, this could allow near full sintering to take place at lower temperatures. Thus, hydrogen assists in further shrinkage during sintering which could imply that sintering could take place at temperatures lower than 1200°C [34][35].

Most sintering treatments documented in the current literature are conducted at 1200°C. Thus, sintering at temperatures, such as 1050°C, could indicate whether or not hydrogen can reduce the sintering temperature of Ti-6Al-4V while maintaining

similar or better densities and microstructures. Since the aim is to lower the sintering temperature to reduce the production cost, sintering trials at 1050°C could be the benchmark that could indicate whether the sintering temperatures could be lowered. Hence, the sintering temperature used in this dissertation is 1050°C.

Dehydrogenation of TiH_2 depends on the diffusivity of hydrogen in the crystal lattice of TiH_2 as well as in the α and β phase [34]. Hydrogen diffusivity in TiH_2 at room temperature is very low (10^{-14} m^2/s). As temperature increases, diffusivity increases which in turn onsets dehydrogenation. Dehydrogenation increases further in the temperature interval of δ (phase where TiH_2 decomposes to $TiH_{1.74}$ forming a fluorite structure) →β phase transformation as hydrogen diffusion in bcc β titanium is higher than that in TiH_2 by 2-3 orders of magnitude [34]. At this point, the level of hydrogen in the β-titanium experiences a reduction to the level that allows β→α transformation. However, the formation of the hcp α-phase in the final stage of dehydrogenation again slows down the rate of dehydrogenation because of the lower hydrogen diffusivity in the α phase [34][35].

The temperatures at which CP Ti and TiH_2 experience hydrogenation and dehydrogenation respectively in the sintering atmosphere should be investigated by means of thermogravimetric (TG) and differential scanning calorimetry (DSC) analyses. The temperatures at which hydrogenation and dehydrogenation onset and ends for the selected samples are critical in understanding the role that hydrogen plays in the sintering as well as evaluating whether there are any positive benefits in sintering TiH_2 in a partial hydrogen atmosphere.

2.4.3 Optimal level of hydrogen in Ti-6Al-4V alloy

To fully understand the effects of hydrogen on the sintering behaviour of Ti-6Al-4V, the phase transformations that occur in Ti-6Al-4V with increasing hydrogen content and temperature must be investigated. A research conducted [36] reproduced the phase diagram of Ti-6Al-4V as shown in Figure 2.13.

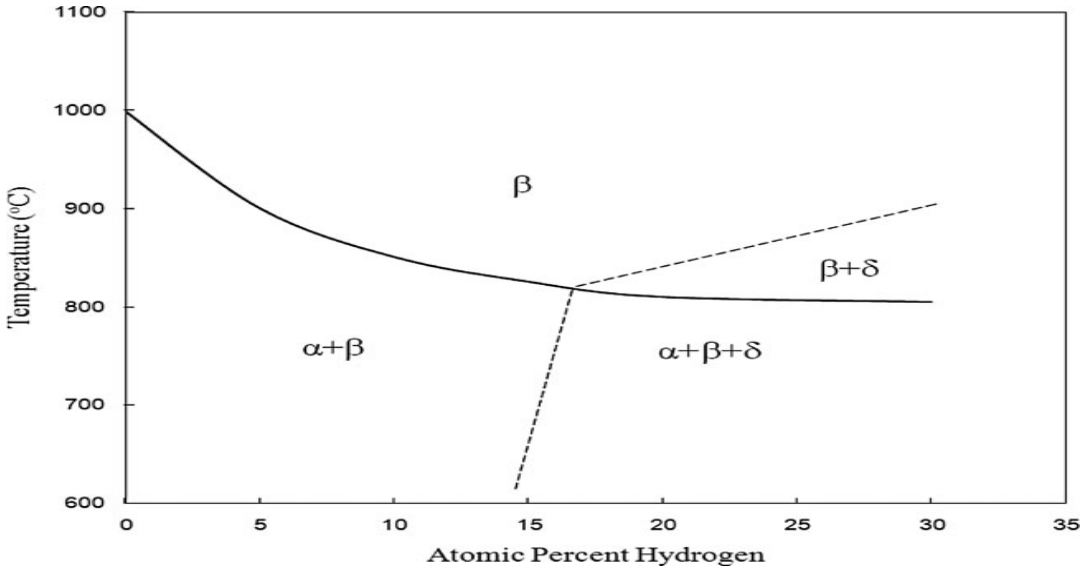

Figure 2.14: Phase diagram for Ti-6Al-4V-xH [36]

From Figure 2.14, the higher the hydrogen content, the lower is the β-transus temperature up to 20 at%. However, it can also be observed that a hydrogen concentration greater than 15 at% will result in the formation of an additional phase (hydride phase) which, is not desirable because this phase results in the embrittlement of the alloy. Embrittlement will eventually result in fracture of the sample at room temperature after sintering or during post mechanical heat treatments. Hence, it can be said that the atomic percentage of hydrogen must not exceed 15% during the sintering of Ti-6Al-4V alloy.

An increase from 5% to 15% hydrogen content in the sintering atmosphere will result in higher levels of hydrogen absorption for a temperature of 650°C. Figure 2.15 shows the differences in atomic percentage of hydrogen in Ti-6Al-4V for various temperatures and times. Figure 2.15 shows that three hours at 650°C with a 15% hydrogen content in the atmosphere results in the highest level of hydrogen absorption in Ti-6Al-4V [37]. Thus, sintering in a hydrogen atmosphere instead of a vacuum is expected to allow hydrogen to still be present at higher temperatures in the CP Ti matrix, which could enable sintering of the compacts at lower temperatures due to hydrogen's ability to promote faster sintering. However, since whether the

same benefits will occur for TiH_2 is unknown and therefore a key area that was investigated during this project.

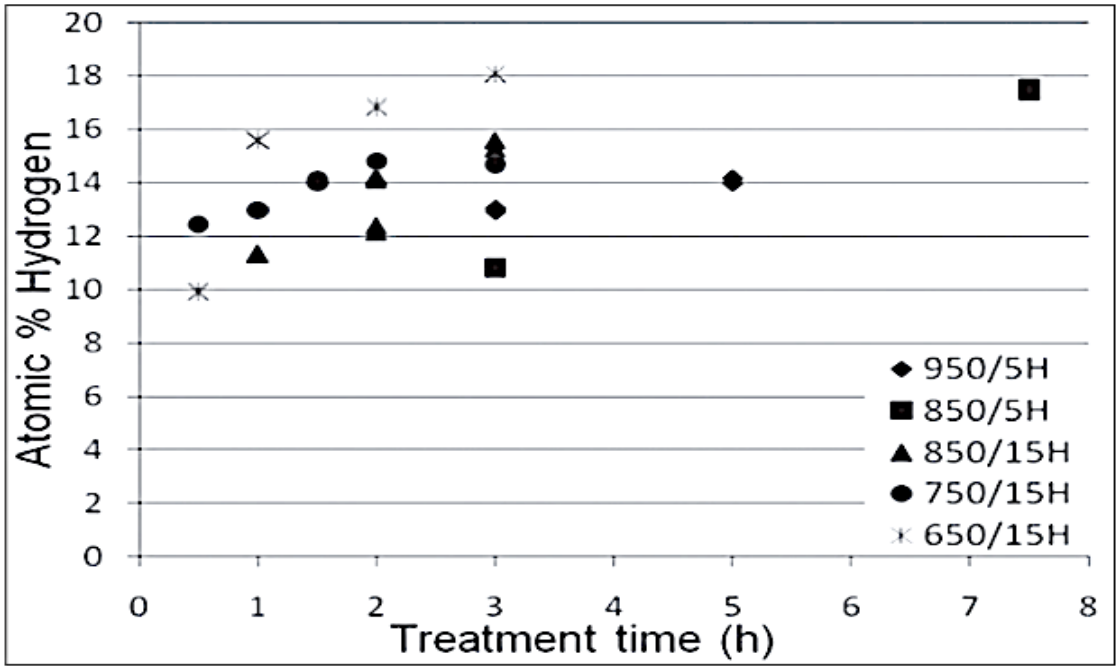

Figure 2.15: Atomic percentage of hydrogen absorbed in Ti-6Al-4V at various temperatures with varying hydrogen levels in atmosphere and treatment times [37]

2.4.4 Using titanium hydride (TiH_2) as opposed to CP Ti

The role of hydrogen is well documented and proven in the current literature. A kinetic study on non-isothermal dehydrogenation of TiH_2 powders [31] used TiH_2 (approximate particle size of 50μm) heated at rates of 10, 15, 20 and 40°C/min up to a temperature of 1000°C as shown in Figure 2.16.

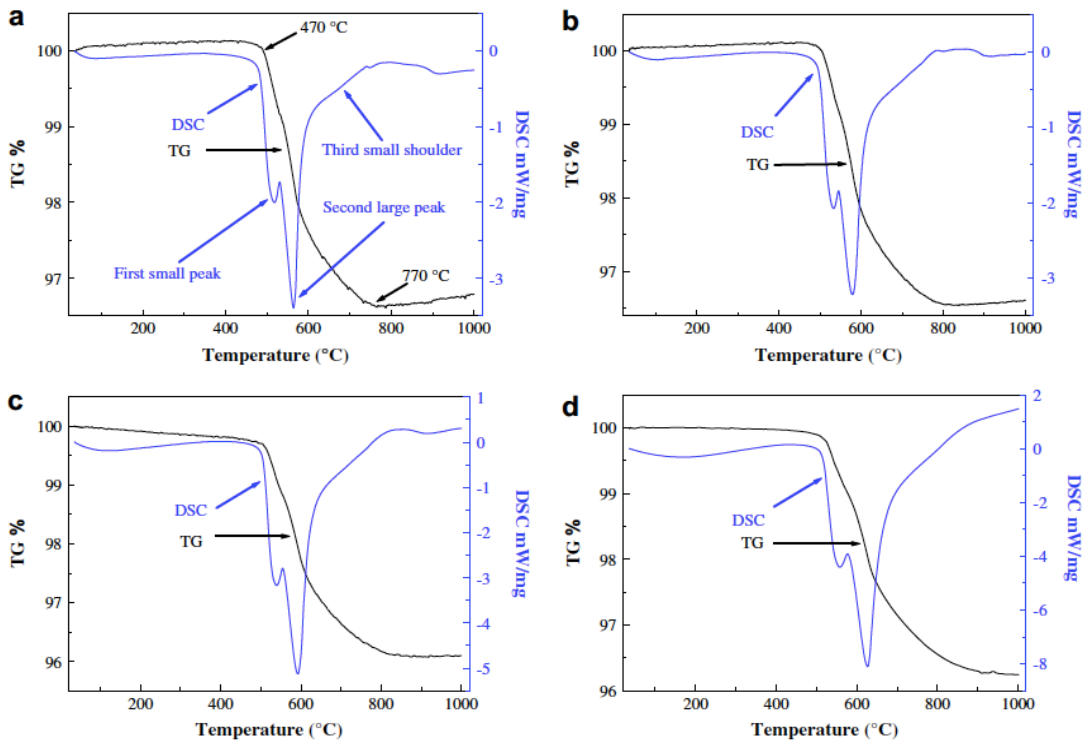

Figure 2.16: TG/DSC curves of TiH_2 powders with heating rates of (a) 10℃/min; (b) 15℃/min; (c) 20℃/min; (d) 40℃/min [31]

The TG curve for a heating rate of 10°C/min shows a mass loss between 470°C and 770°C which corresponds to the dehydrogenation of TiH_2. The curve also shows an increase in mass for temperatures higher than 770°C. This oxidation was due to the use of roughing pump which did not allow high vacuum to be achieved. This research also uses Ti-6Al-4V powders to confirm the oxidation process that was taking place in TiH_2 as well. Figure 2.17 shows that the TG curve for Ti6Al4V which denotes a significant increase in mass.

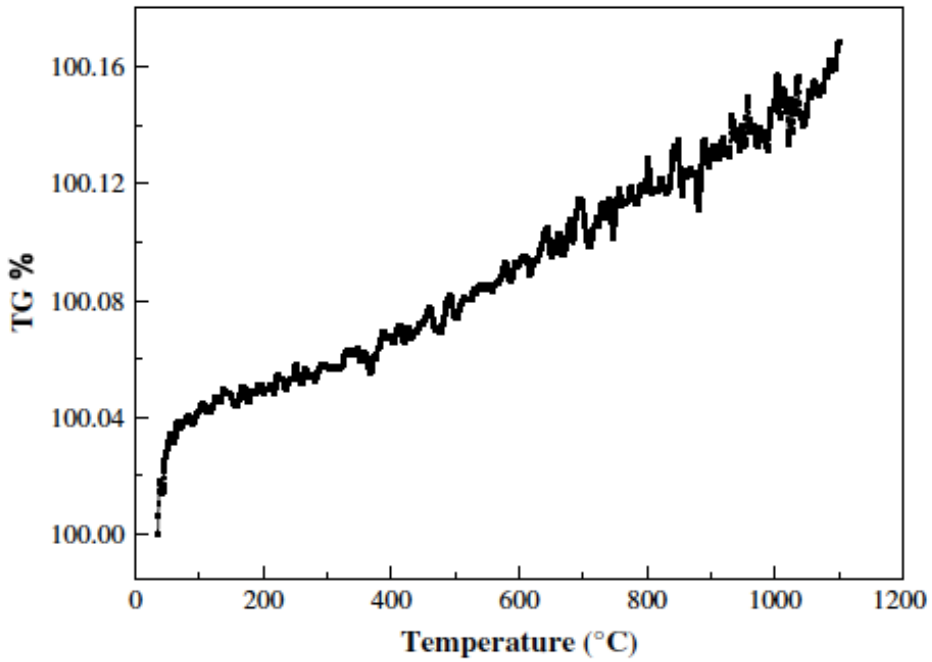

Figure 2.17: TG curve of Ti6Al4V alloy at a heating rate of 20℃/min [31]

The weight gain observed at room temperature was accounted as a result of the unstable TG baseline. The TG curve for TiH_2, showing oxidation after dehydrogenation, confirms the reducing properties of TiH_2 as a starting material to prevent oxidation of the powders before 700°C. Even though the mass gain, representing oxidation, was obvious in the TGA curve, a corresponding exothermic peak (oxidation is exothermic) was not observed on the DSC curve. This is because the slight exothermic peak could have been masked by the larger endothermic peak (as a result of dehydrogenation) occurring at very similar temperatures.

The role of hydrogen during sintering of Ti-6Al-4V is partially established in the literature. There are two ways in which hydrogen can be introduced which are; by using TiH_2 as opposed to CP Ti as a starting powder or by sintering in a hydrogen atmosphere. The basic difference between CP Ti and TiH_2 is the hydrogen content. Research that looks at the role of hydrogen in the sintering of titanium [38] suggests that the use of TiH_2 (as a starting powder) can significantly improve the density and thus final mechanical properties of the resulting titanium alloy. The results led to the conclusion that 67 at% of hydrogen which equates to the atomic percentage of

hydrogen in TiH_2, increases the density and mechanical properties of the resulting alloy as compared to the same alloy sintered in the absence of hydrogen. The main findings and conclusions of this research [39] were as follows:

- Hydrogen helps in decreasing the β-transus temperature of Ti-6Al-4V. For sintering to take place dissolution of aluminium and vanadium is required. This dissolution can only take place above the β-transus temperature. Hence, if the β-transus temperature can be lowered, sintering can take place at lower temperatures.
- Hydrogen stabilises the more ductile BCC β-phase as opposed to the HCP α-phase in an α+β alloy such as Ti-6Al-4V.This is again critical since dissolution of the alloying element that is required for sintering can only take place when the alloy is in the beta phase.
- Hydrogen prevents the formation of surface oxides. Oxides scales at the powder surface are effective barrier for diffusion. In the presence of atomic hydrogen the sintering kinetics are altered. Atomic hydrogen reduces any oxides that are located on the surface of the powder particles. In other words, hydrogen cleans the inter-particle interfaces, which in turn enhances the diffusion between all components of the powder mixture. Hence, the diffusion process can occur at a lower temperature [39].

Hence, it is expected that the sintered density of compacts containing TiH_2 will be higher than that of similar blends containing CP Ti instead. However, the behaviour of TiH_2 in a partial hydrogen atmosphere is not yet documented in the current literature. Due to the positive effects of hydrogen in the form of TiH_2, there can be a strong argument made for using TiH_2 in an partial hydrogen atmosphere to further improve density and potentially lowering the sintering temperature. This is investigated during the course of this dissertation.

2.5 Effects of hydrogen on the properties of CP Ti, TiH_2 and Ti-6Al-4V during the different stages of PM

The density, microstructure and final properties depend on the chemical composition and mechanical properties of the starting powder, the particular consolidation method employed and on post-compaction treatment; namely sintering. The role of hydrogen in the various studies that were most relevant to this dissertation are summarised in the following sub-sections.

2.5.1 During compaction

There are several factors that have proven to affect the density and strength of the green compacts. They are namely: powder particle size, shape and mechanical properties, compaction pressure and powder composition.

During pressing, CP Ti powder is plastically deformed. A higher pressure will result in more deformation and a decrease in the number and size of the voids which, implies an increase in green density. The size of the voids in turn depends on the size of the titanium powder. When TiH_2 is pressed (under high loading), the hydride particles are not deformed because of their low ductility. Instead, the particles disintegrate into fragments with sharp edges. Figure 2.18 shows the effects of compaction pressure on the densities of coarse and dispersed CP Ti and TiH_2.

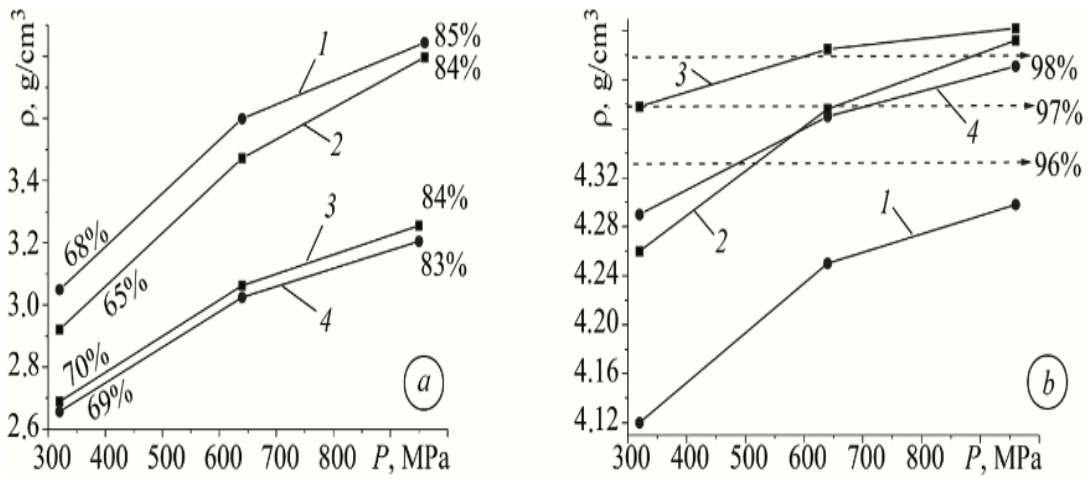

Figure 2.18: Influence of compaction pressure of pressed and sintered specimens [39]; (1) coarse Ti; (b) dispersed Ti; (3) dispersed TiH_2; (4) coarse TiH_2 [18]

Coarse CP Ti and TiH_2 powders (average particle size of 100μm) and that of dispersed CP Ti and TiH_2 powders (average particle size of 25μm) resulted in the density of the coarse CP Ti pressed specimen to be higher as compared to the specimen formed from fine CP Ti (73% versus 70% relatively densities respectively) at 500MPa [18]. This research supports the results of various research discussed previously; since the increase in particles size increases the relative green density. For low compaction pressures (325MPa), the relative green densities of dispersed TiH_2 (70%) is higher than that of dispersed CP Ti (65%). However, for the coarse powders, the relative green densities for both CP Ti and TiH_2 were more or less the same. This suggests that the mechanical properties of the powder does play a more significant role when the particle size are smaller [18]. Hence, investigating the densities of different powder size for TiH_2 and CP Ti could provide a clear indication of whether the particle's composition and mechanical properties outweighs the particle shape and size when it comes to their effects on the density of green compacts with CP Ti and TiH_2.

2.5.2 During sintering

The strength and hardness of the material increases significantly as a result of sintering due to the strong bonds that are formed between the different particles. The higher the sintering temperature, the higher is the strength and hardness of the material as a result of improved density [40].

The chemical composition and mechanical properties of the powder is critically important due to the shrinkage that occurs during sintering. For example, TiH_2 (density ranging from 3.7-3.95 g/cm^3) [41][42] occupies a larger molar volume as compared to CP Ti (density of 4.51 g/cm^3) and thus the shrinkage of a TiH_2 compact will be more significant which, is expected to result in higher sintered density. Additionally, further shrinkage occurs during dehydrogenation of TiH_2 to form β-Ti. Hydrogen gas is liberated into the sintering medium causing further shrinkage to occur as the voids, formed after hydrogen liberation, reduces in size. However, the sintering temperature will have a critical role to play in ensuring whether these voids can be eliminated. Sintering temperature below 1200°C could possible not provide sufficient energy

required to eliminate or close the voids. The volume change for a TiH_2 sample heated up to 1250°C under dilatometric conditions is about 27%, which, is substantially significant [34] and additionally 6.7%; further shrinkage occurs as a result of dehydrogenation. Hence, it can be said that even though TiH_2 compacts have lower densities in the green state (up to 68%), they can result in near full density products after sintering. Thus, the minimum green density that can lead to full densification is estimated to be 68%. TiH_2 samples should therefore not be disregarded if they have substantially lower green densities as compared to CP Ti samples. If TiH_2 samples achieve good densities in the green state, it is expected that sintering at a lower temperature (higher than the β-transus temperature) could result in near full densification of the sample. Thus, an argument for sintering at temperatures lower than 1250°C does stand good grounds based on the role of hydrogen in lowering the β-transus temperature during sintering. This supports the fact that the green density and compaction study of TiH_2 compacts as well as their limitations should be thoroughly investigated in determining the levels of TiH_2 in a compact that could result in acceptable relative green density and near full density after sintering. The benchmark for the minimum acceptable green density was 68% [34].

The sintering of pressed green compacts of CP Ti and TiH_2 at 1250°C for four hours under vacuum conditions shows that TiH_2 based samples have higher sintered densities in both the coarse (95.1-97.9% relative density) and dispersed (97.1-98.5% relative density) form when compared to the densities of coarse (91.4-95.3% relative density) and dispersed CP Ti (94.6-98.2% relative density) powders. This study argues that the compaction pressure affects the sintered density of the CP Ti based compacts more when compared to the TiH_2 based compacts [40]. Figure 2.19 (a) and (b) show the difference in microstructure confirming that sintered TiH_2 have higher density due to the presence of less pores as compared to CP Ti.

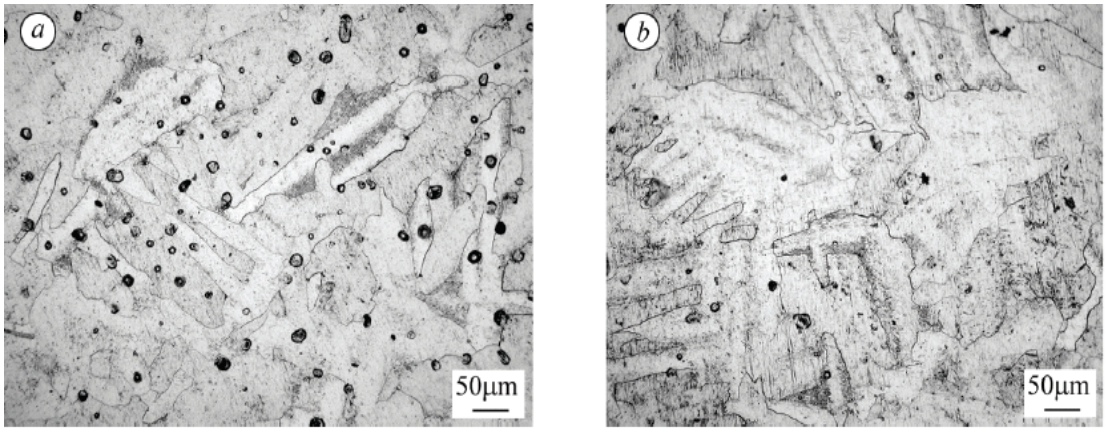

Figure 2.19: Sintering of CP Ti (a) and TiH_2 (b) sintered at 1250℃ for 4 hours under vacuum [40]

The relative green densities of the coarse powders were higher than those of the TiH_2 compacts. Hence, the improvement in density, from the green to the sintered state, is higher for TiH_2 as compared to CP Ti. This confirms the benefits of using TiH_2 as opposed to CP Ti due to the resulting higher sintered densities despite their lower densities in the green state. Since TiH_2 results in better sintered densities, it is expected that TiH_2 allows densification to take place faster and even at lower temperatures. Thus, conducting sintering trials at temperatures lower than 1250°C, for example at 1050°C (substantially lower) can possibly result in acceptable relative sintered densities due to the considerable increase in sintered density that the TiH_2 resulted in previous studies. Sintering at 1050°C can thus be used as a benchmark to evaluate whether sintering of Ti6Al4V using CP Ti/TiH_2 blends as a starting material in a partial hydrogen atmosphere can result in good sintering densities and microstructures.

Green compacts pressed between 320-960MPa and sintered between 1000-1350°C under vacuum show higher sintered densities in TiH_2 as opposed to CP Ti [41]. The study also found that the higher the sintering temperature, the higher the sintered density. This is because fragmentation of TiH_2 and additional cracking of fragments during compaction, result in an increase in surface contact which promotes diffusion. However, hindering of densification is possible due to the introduction of alloying elements such as 60Al40V MA. Diffusion dissolution of alloy particles in titanium matrix is accompanied with pore formation at the particle/matrix interfaces. Thus,

difference in diffusion mobility (opposite directions) between the different particles results in formation of pores and vacancies of Al and V particles. This is later discussed as the Kirkendall effect. Figure 2.20 (a) and (b) show that the microstructures of Ti-6Al-4V, at 1350°C, have less pores as compared to similar sample sintered at 1150°C.

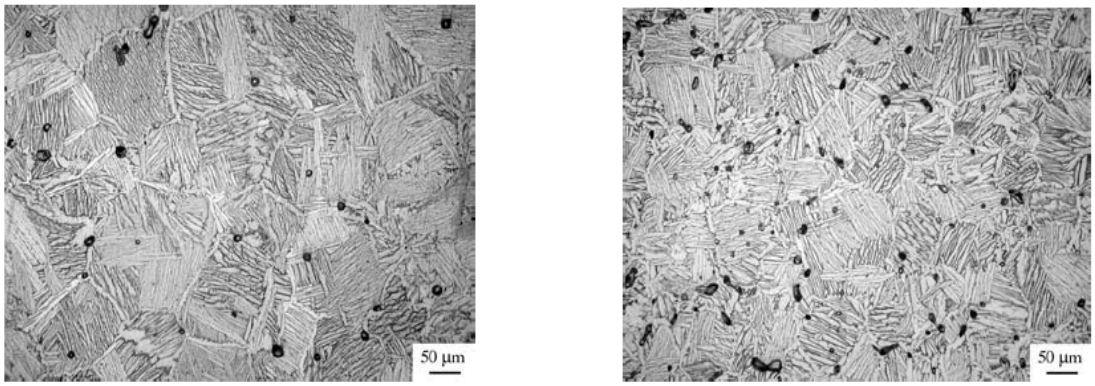

Figure 2.20: Microstructure of Ti-6Al-4V (a) 1350°C sintered relatively density of 98.8% with average grain size of 110µm (b) 1150°C sintered relatively density of 97% with average grain size of 62µm [41]

Another study [42] uses CP Ti and TiH_2 (particle size ranging from 20-100µm for both powders) with 60Al40V MA pressed at 294MPa and then sintered at 700, 800, 900, 1000, 1100, 1200 and 1300°C under vacuum for four hours. This study shows a significant improvement in sintered densities for both hydrogenated Ti-6Al-4V (from 81 to 97%) and CP Ti-6Al-4V (from 79 to 96%) when the temperature increases from 700 to 1300°C. At sintering temperatures of 1000 and 1100°C, the sintered density of CP Ti-6Al-4V is unexpectedly higher than that of the H-Ti-6Al-4V as shown in Figure 2.21 [42].

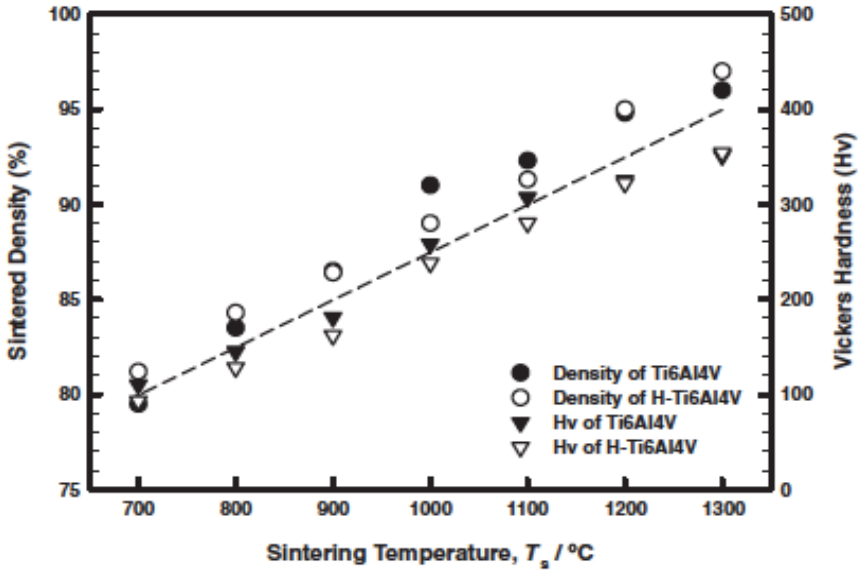

Figure 2.21: Variation of sintered density and Vickers hardness of the Ti6Al4V and H-Ti6Al4V alloys as a function of sintering temperatures [42]

No further details commenting on these unexpected results is provided in the paper. Hence, the sintering of hydrogenated Ti-6Al-4V and CP Ti-6Al-4V at a temperature of 1050°C could possibly result in unexpected density results. Sintering of TiH_2-6Al-4V and CP Ti-6Al-4V at temperatures lower than 1200°C either in an inert gas or partial hydrogen atmosphere is not very well documented or even present in the current literature. All researches discussed used a vacuum environment as their sintering atmosphere. As hydrogen is expected to allow near full sintering to occur at lower temperatures, this unexpected behaviour in the temperature range of 1000-1100°C could very well limit the lowest temperature at which sintering could take place for TiH_2-6Al-4V.

Another study that examines the hydrogen sintering of Ti-6Al-4V involves the blending of TiH_2 and Ti powders with 60Al40V MA pressed at 350MPa and sintered at 1200°C under vacuum and in a partial hydrogen atmosphere [27]. While the density of the compacts in both sintering atmospheres are more or less the same (approximately 99% relative density), the improvement in density results in a finer microstructure in TiH_2 and hence mechanical properties. In other words, the use of a partial hydrogen

atmosphere might only be beneficial in terms of grain refinement only for Ti-6Al-4V. Figure 2.22 (a) and (b) show the different microstructures obtained by using vacuum and partial hydrogen atmosphere for the sintering of Ti-6Al-4V with TiH_2 as a starting powder.

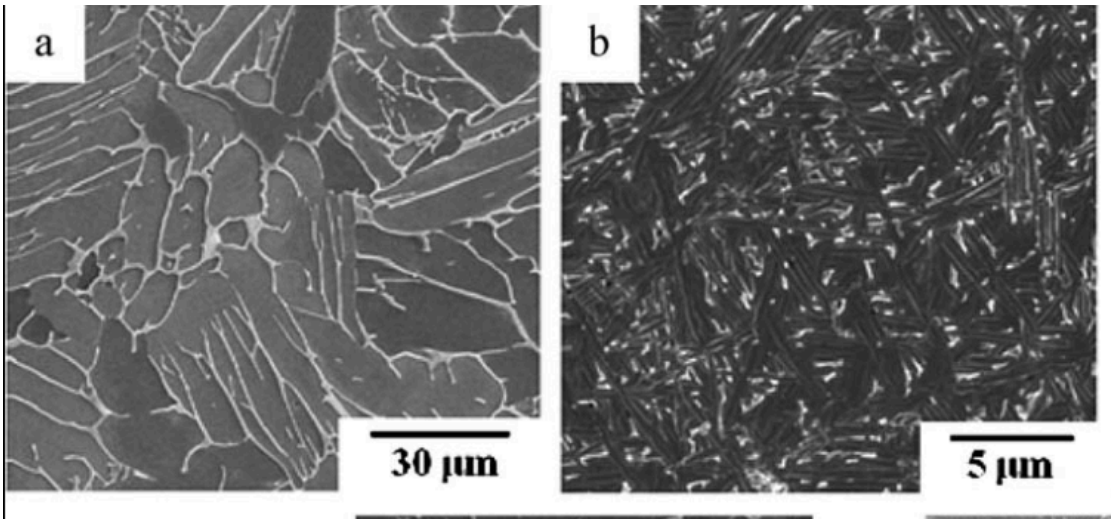

Figure 2.22: Microstructure of sintered TiH_2-6Al-4V under vacuum (a) and in partial hydrogen atmosphere (b) [27]

The final microstructure consists of coarse grains for vacuum sintering whereas in hydrogen sintering the final microstructure consists of fine dispersed grains, which are comparable to the microstructure of wrought Ti-6Al-4V alloys. A finer microstructure implies better mechanical properties.

Several studies that look at the effects of particle size, mechanical properties and composition of the powder particles on the final properties of resulting sintered products [17] [43] uses a compaction pressure range of 320-960 MPa and powder particles (CP Ti and TiH_2 with 65Al35V master alloys and elemental Al and V powders) with varying particle sizes. The compacts were then sintered under vacuum at 1350°C. The sintered densities of TiH_2 based compacts are higher (99%) with the MA. For mixtures 1 and 2 (see Table 2. 1), the addition of alloying elemental powders results in lower sintered densities (lower than 92%). However, the use of TiH_2 with elemental aluminium and vanadium powder resulted in higher densities (93% but increased from 66% which, is a lower green density to start with). Thus, TiH_2 significantly improves

the sintered density. This is because TiH_2 decomposes during sintering which, causes a phase transformation and eventual defects in the crystal structure. As a result, the reaction of aluminium and titanium occurs at a temperature below the melting point of aluminium which in turn promotes faster densification. However, the temperature (in terms of final temperature and heating rate) at which this takes place is not described. It is possible that this phase transformation only takes place due to sintering at 1350°C under vacuum. Further research is thus required to determine whether decomposition and crystal defects in TiH_2 is dependent on the sintering profile of the specimen.

The finer particle size also results in higher sintered densities. The various green and sintered densities of the mixtures from Table 2. 1 for both compaction pressures supports the statement made at the beginning of this paragraph and is graphically illustrated in Figure 2.23.

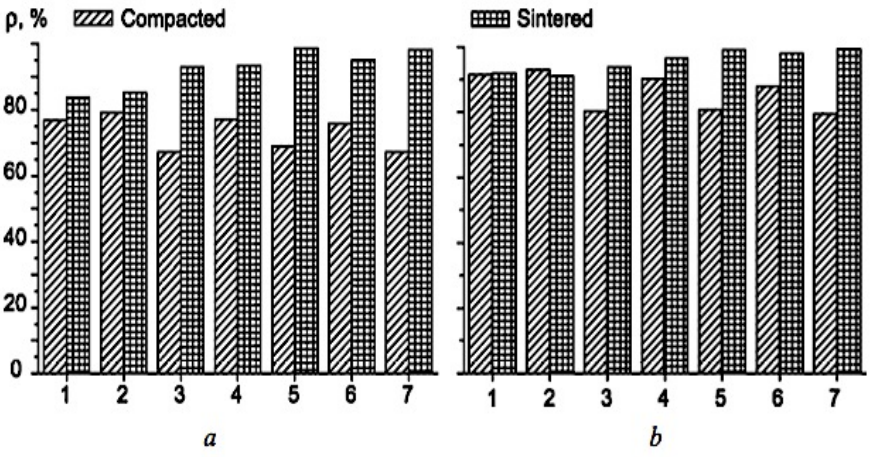

Figure 2.23: Density change of compacts of various mixtures upon sintering, compaction pressures of (a) 320 MPa and (b) 960 MPa [43]

2.6 Thermal decomposition of TiH_2 at high temperatures

Understanding the thermal decomposition of TiH_2 is key in establishing the various phase transformations that take place during sintering. The phase transformations affect the density as well as the sintering diffusion mechanism.

A study that investigates the thermal decomposition of TiH_2 states that hydrogen release starts at 390°C [44] and reaches a maximum at 525°C with noticeable endothermic peaks at 445°C and 610°C. The phase transformation that was derived from this study is expressed as follows:

$$\delta \longrightarrow \delta + \alpha \longrightarrow \beta + \delta + \alpha \longrightarrow \alpha + \beta \longrightarrow \alpha$$

Based on the Ti-H phase diagram the sequence of the phase transformations showed above is not the same as predicted by the Ti-H phase diagram in Figure 2.24. The reason for this difference is due to the presence of oxygen (in the form of surface oxides) that stabilises the α-phase. It is thus expected that the sequence of phase transformation outlined above will occur when using commercial TiH_2 powders particularly if the latter is not stored under inert conditions.

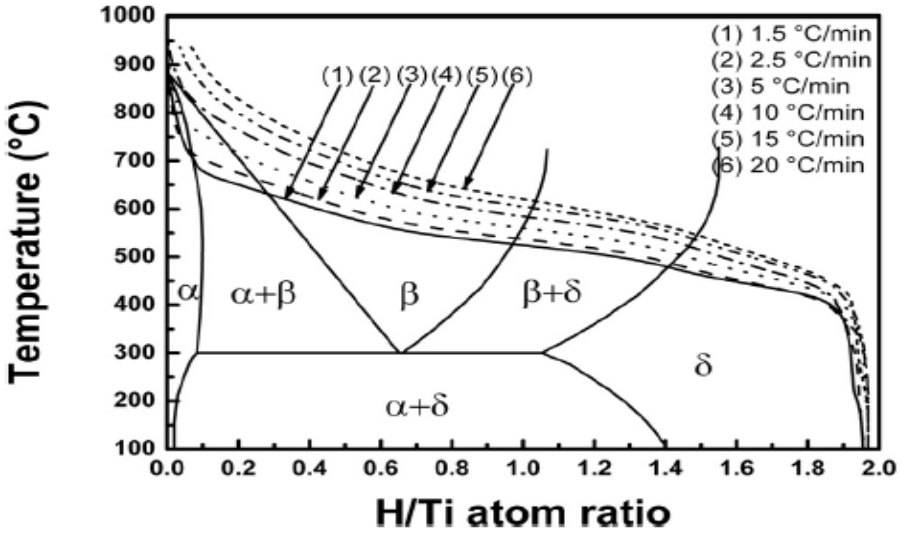

Figure 2.24: Ti-H phase diagram combined with changing trends of temperature/hydrogen content at different heating rate [45]

In the presence of surface oxides, the temperature at which hydrogen is released from the TiH_2 powders is expected to increase to 405°C. It is also documented in the current literature [44] that during decomposition of TiH_2 hydrogen gas results in the subsequent H_2O gas formation since the hydrogen reacts with the surface oxides. The release of H_2O gas is expected to take place from 466°C to 620°C with a peak at 535°C. The total mass loss for the decomposition of TiH_2 is expected to be 3.8wt%. The H_2O gas molecules being larger in size when compared to hydrogen gas molecules will result in bigger pores being formed between the TiH_2 particles during sintering [44]. Thus, more energy will be required to close or shrink the pores during densification and this can in turn hinder reasonable densification from taking place at lower temperatures. However, this is likely to be dependent on the diffusion rates of the H_2 and H_2O gases [44].

Another research that looks at the phase transformations that takes place in TiH_2 [45] confirms that the heating rate plays a critical role as seen in Figure 2.24. This study [45] confirms that the thermal decomposition of TiH_2 results in two main endothermic peaks at 540°C and 610°C for a heating rate of 10°C/min. The study concludes that the higher the heating rate, the higher is the temperature at which decomposition of TiH_2 takes place up to a heating rate of 15°C/min. The two endothermic peaks are attributed to the $\delta \longrightarrow \beta + \delta$ and the $\beta + \delta \longrightarrow \beta$ phase transformation respectively. The phase transformations are different from reference 44 which is only accountable by the difference in heating rate since the low heating rate (<10°C/min) allows for the co-existence of the $\alpha + \beta$.

A study on the decomposition of TiH_2 looks at the effects of the atmosphere under which thermal decomposition is conducted [46]. This study shows that the phase transformations that take place under a stagnant or flowing atmosphere are different. The two sequences below show the phase transformations that take place for both atmospheres.

Sequence 1 (flowing argon): $$\begin{cases} \text{heating}: \ \delta \xrightarrow{432\,^\circ\text{C}} \delta + \alpha \xrightarrow{514\,^\circ\text{C}} \delta + \alpha + \beta \xrightarrow{536\,^\circ\text{C}} \alpha + \beta \xrightarrow{702\,^\circ\text{C}} \alpha \\ \text{cooling}: \ \text{no phase transformation } (\alpha \text{ remains}) \end{cases}$$

Sequence 2 (Stagnant argon): $\begin{cases} \text{heating}: \delta \xrightarrow{448\,^{\circ}C} \delta+\alpha \xrightarrow{578\,^{\circ}C} \delta+\alpha+\beta \xrightarrow{620\,^{\circ}C} \alpha+\beta \xrightarrow{744\,^{\circ}C} \beta \\ \text{cooling}: \beta \xrightarrow{568\,^{\circ}C} \beta+\alpha \xrightarrow{264\,^{\circ}C} \beta+\alpha+\delta \xrightarrow{157\,^{\circ}C} \alpha+\delta \end{cases}$

Under stagnant conditions, the same phase transformations are observed under flowing argon but occurring at higher temperatures. However, under flowing argon the α phase is stabilised at the end of the heating cycle and no further phase transformation occurs upon cooling. The core-shell model investigated [46] confirms the presence of an α shell which affects the diffusion rate of hydrogen gas from the as received TiH_2 powders. For a CP Ti powder (similar to a pre-oxidised TiH_2 powders), a rutile (TiO_2) core shell was demonstrated to control the diffusion rate of the hydrogen released. Thus, the use of TiH_2 powders is likely to stabilise the α phase and not the beta phase as one would expect. Hence, sintering using TiH_2 is not expected to favour the diffusion of β stabilisers (such as vanadium in MA).

The decomposition study being conducted at high temperatures provides some indications of the sintering behaviour of TiH_2 powders. The sintering conditions are therefore expected to play a critical role in the phase transformation of different TiH_2 powder blends which will in turn affects their sintered densities and microstructures.

2.7 Sintering mechanism of various Ti-6Al-4V powder blends

The sintering mechanism of Ti-6Al-4V using various starting powders is a key investigation that can provide insights on the shrinkage rate and levels during sintering. It is well known that sintering of Ti-6Al-4V green compacts at temperature above 1200°C can result in near full density samples. However, the various steps such as shrinkage rate and levels that will lead to the near full density of Ti-6Al-4V is critical in investigating whether or not sintering below 1200°C is possible.

A study that looks at the sintering mechanism of Ti-6Al-4V powder from diffusion path analysis [47] makes use of hydride-dehydride (HDH) CP Ti, 60Al40V MA and HDH pre-alloyed Ti-6Al-4V with average particle sizes of 75-150μm, 45-150μm and 75-150μm

respectively. The HDH CP Ti with MA (first mixed in the correct ratio to give Ti-6Al-4V) as well as the pre-alloyed Ti-6Al-4V powder were pressed at 690MPa and heated to 1370°C for two hours. The values of the relative green densities were 82% for the blended Ti-6Al-4V, 79% for the PA and 83% for the HDH CP Ti. The shrinkage ratio during sintering of all three compacts were studied, and it was shown that the blended Ti-6Al-4V experiences a 50% greater shrinkage as compared to the other two samples. The onset of that shrinkage begins at about 910°C which corresponds to the α/β phase transformation temperature. At 1100°C, the shrinkage rate shows a further increase which is not equivalent to the maximum shrinkage. Figure 2.25 and Figure 2.26 show the difference in shrinkage ratio between the theoretical and experimental data for the PA and blended Ti-6Al-4V respectively [47].

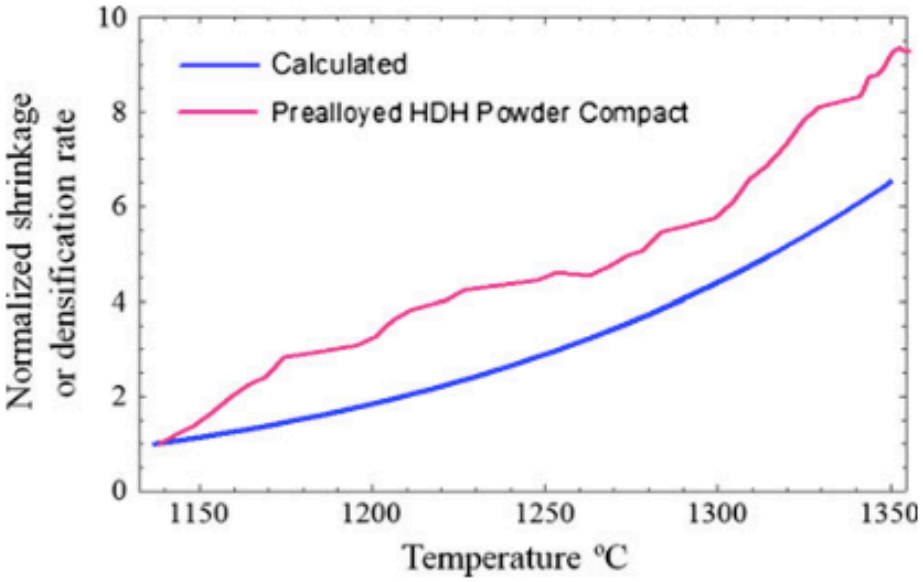

Figure 2.25: Normalised linear shrinkage for HDH pre-alloyed Ti-6Al-4V powder compacts and normalised densification from theoretical calculations [47]

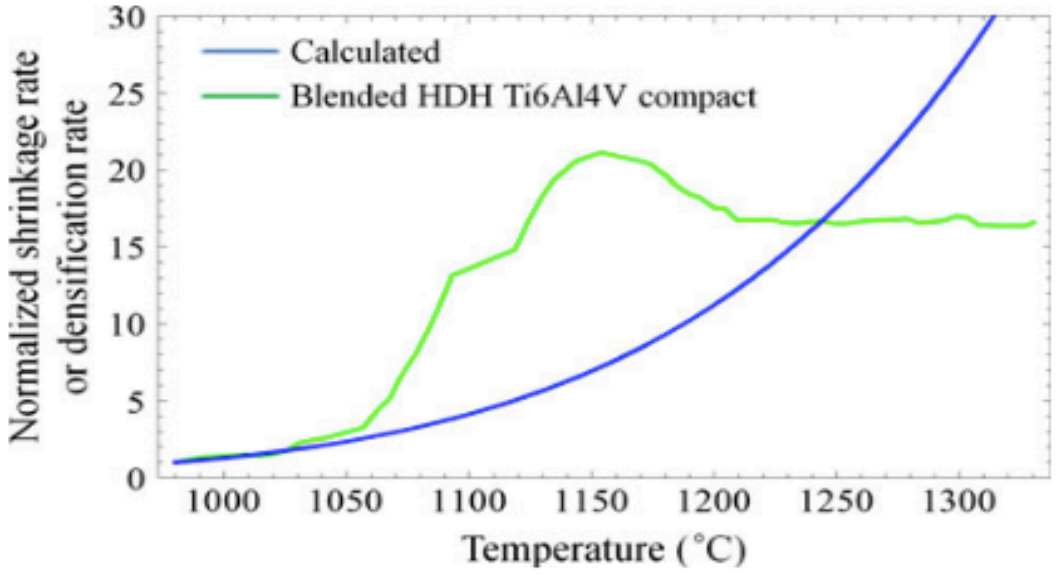

Figure 2.26:Normalised linear shrinkage for blended HDH Ti-6Al-4V powder compacts and normalised densification from theoretical calculations [47]

The shrinkage rate of the blended Ti-6Al-4V powder shows a substantial increase by a factor of 10 between 1000°C and 1150°C. Hence, further studies of the sintering of blended Ti-6Al-4V was conducted at 980°C and 1040°C.

The study of the different phases formed in the blended Ti-6Al-4V samples demonstrate that a quasi-peritectoid reaction takes place between 1000°C and 1100°C [47] based on the phase diagram as shown in Figure 2.27.

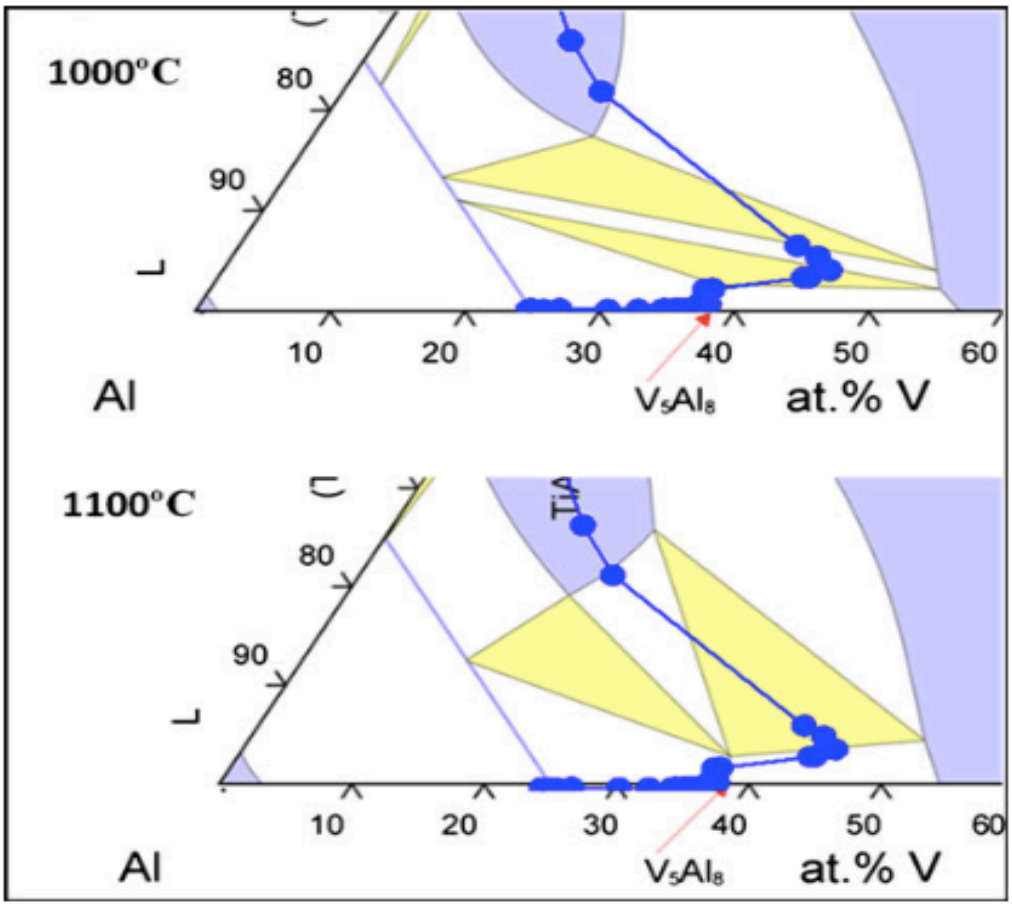

Figure 2.27: Portion of the experimentally determined diffusion path at 1040 °C plotted on the 1000 and 1100 °C isothermal ternary-phase [44]

The volume change before and after the reactions at both temperatures will result in stresses which can further improve sintering. The diffusion path at 1040°C gathered during the experiment [47] was plotted on the graph shown in Figure 2.27. The volume change during the reaction was noted to be positive since TiAl has a larger atomic volume when compared to the other phases present. This results in compressive stress being localised at small areas within the sample due to the low percentage of aluminium originally present.

An important conclusion of the study conveys that the sintering of blended Ti HDH 90wt% CP Ti and 10wt% 60Al40V master alloy is not determined by the CP Ti powder but rather by the interaction of the MA powder with the CP Ti powder through the diffusion of the intermetallic phases. The study confirms that the rapid densification

only starts at 1040°C which is the result of the stress generated by the quasi-peritectoid reaction as a result of volume changes of the phases, lattice diffusion enhanced by the potential gradient for aluminium in Ti and the localised adiabatic heating resulting from the formation of Ti-Al intermetallic compounds [47]. Thus, this could limit the lowering of the sintering to not be below 1040°C. Thus, sintering at 1050°C could provide a good indication of whether sintering of Ti-6Al-4V using CP Ti and/or TiH_2 can result in good densities.

2.8 Implications on further research based on critical review

The critical review from Section 2.4 and 2.5 suggests that using coarser powder will result in better green densities. While the compaction pressure does play a role in the increase in green density, very high compaction pressures cannot be used particularly for TiH_2 powders. The brittle nature of TiH_2 will affect sample ejection from the die as TiH_2 particles do not plastically deform. Therefore, cracks could very likely form along the edges of the sample. While the use of TiH_2 results in high sintered density, its brittleness in the green state results in the green compacts having very low green strength. Therefore, using a 90 wt% TiH_2 with master alloy to form TiH_2-6Al-4V could entail difficulties in terms of sample handling. Thus, the maximum level of TiH_2 that would result in good green densities and strength as well as high sintered densities is something that needs to be investigated.

Most of the sintering treatments that uses either CP Ti or TiH_2 are conducted under vacuum at 1200°C. While it is suggested that sintering in the presence of hydrogen (either in the sintering atmosphere or in the form of TiH_2) will lower the sintering temperature, insufficient data with sintering temperatures lower than 1100°C are documented in the current literature. There are a few density results at 1000°C and 1100°C (under vacuum) which, shows that Ti-6Al-4V containing hydrogen have lower sintered densities compared to similar samples without hydrogen. This unexpected difference is not discussed in depth in the current literature. In addition, while the sintering mechanism suggest that most of the densification starts at 1040°C [44], it is very crucial that the effects of various temperature points between 1000°C and

1150°C are investigated further to establish better sintering models. Sintering at 1050°C and 1200°C could shed light on the extent to which hydrogen can reduce the sintering temperature of Ti-6Al-4V while achieving near full densities. Further, most studies use vacuum as the sintering atmosphere. The use of other inert atmosphere such as argon or partial hydrogen should be explored further, to determine the effects of various sintering atmospheres on the sintered densities and microstructures of CP Ti, TiH_2 and their various blends with and without MA.

Chapter 3: Methodology

This chapter outlines the different tests and experimental procedures conducted to investigate the effects of different processing parameters and material composition on the density and mechanical properties during compaction and sintering. The first step was to analyse the starting powders. This consisted of a series of tests including scanning electron microscopy (SEM) which, was used to determine the particle shape and laser diffraction particle size analysis (LDPSA) was a technique used to determine the particle size of each powders. CP Ti and TiH_2 were blended for 15 minutes to form various CP Ti/ TiH_2 powder blends. In addition, CP Ti and TiH_2 were also blended with MA to form two additional powder blends. The next phase of the experimental approach of this dissertation was to press the different powder blends at various compaction pressures. The green density and strength were measured based on the relevant American Society for Testing Materials (ASTM) standards. In order to determine whether and to what extent, hydrogen lowers the sintering temperature, the behaviour of the selected powder blends from the compaction and green density study were investigated by means of thermogravimetric analysis (TGA) and differential scanning calorimetry (DSC). The sintered densities and microstructures at the various sintering conditions and atmospheres were then measured and recorded accordingly.

3.1 Analyses of starting powders

Since the particle shape and size affect the green compaction, density and sintering properties of the different compacts, it was vital to determine these powder properties for the different powders used. Table 3.1 summarises the expected particle size (based on the information provided by the powder suppliers) of the different powders used for this research.

Table 3.1: Powder size and chemical composition

Powder description	Chemical composition	Mesh size	µm
Commercially Pure (CP) titanium	Ti	-100	149
Titanium hydride	TiH_2	-200	70-74
Master alloy	60Al-40V	-230	55-63

The different tests conducted on the starting powders were:

3.1.1 Laser diffraction particle size analysis (LDPSA)

Laser diffraction uses the Mie theory which is a theory of absorption and scattering of electromagnetic pattern by an uniform sphere generated using the samples' optical properties. If the samples to be analysed have unknown optical properties, the Fraunhofer approximation is used. The latter is better for larger particles but not suitable for transparent particles or particles that are smaller than 50 μm [48].

LDPSA is the analytical method used to determine the particle size distribution of the starting powders by laser scattering. Particles scatter light in all direction and the scattering patterns is directly proportional to the particle size based on the Fraunhofer diffraction theory [48]. The angle of the laser beam and particle size are inversely proportional and hence the laser beam angle increases as particle size decreases [49].

Laser diffraction analysis is achieved by using a red He-Ne laser which is a popular laser used. The particle size that the laser can analyse is dependent on the distance from the lens to its point of focus (focal length). The focal length is directly proportional to the area detected by the laser [48][49]. A programmed computer is used to detect the particle sizes in the sample from the data generated by the light energy produced and its subsequent pattern. The computer in turn processes the data collected on the particle frequencies and wavelengths to plot the particle size distribution of the sample.

The laser scattering equipment used was the Saturn DigiSizer model which, can measure particle size between 0.1-1000 microns (μm). The Saturn DigiSizer uses light scattering models based upon the complete Mie Theory [48][49] and the Fraunhofer Diffraction approximation for calculating particles size distributions for measured light scattering patterns [48][49]. About 1g of each powder was placed in a sample vial for analysis and the powder size distribution of the sample was generated graphically.

3.1.2 SEM analyses

SEM allows one to observe the particle shape and relative size under very high resolution in order to determine the shape of the powders. The SEM used was the Nova NanoSEM which allows for both high resolution imaging as well as energy dispersive X-ray spectroscopy to be conducted on small samples. A small spatula tip of each powder was placed and spread uniformly on a small piece of carbon tape on the specimen holder to improve the conductivity of the powders during analysis. A good conductivity is required to obtain high resolution images of the powders. A working distance of 5mm and accelerating voltage of 20 keV was used to obtained several SEM images of the different powders used in this dissertation.

3.2 Blending of powders

The first mechanical process conducted on the CP Ti, TiH_2 and MA powders is the blending process. Table 3.2 is an example of the amount of powders mixed during blending. The amount of TiH_2 added to form TiH_2-6Al-4V was calculated according to results in a 90% titanium, 6% aluminium and 4% vanadium sample.

Table 3.2:Mass of powders added per blending cycle

Powder combination	Mass of CP Titanium (g)	Mass of titanium hydride (g)	Mass of master alloy (g)	Total mass of sample (g)
TiH_2 and master alloy (TiH_2-6Al-4V)	94.23	0	10	104.23
Titanium and master alloy	90	0	10	100
CP Ti/ TiH_2 (X:Y mix)	X	Y	0	X+Y

The blender that was used for this research was from Stellenbosch University. From a study conducted [21] it was found that a blending time period of 15 minutes at 15 revolutions per minute was enough to ensure the homogeneous distribution of the various powder mixtures based on the chemical composition [21]. The mass of the various powders to make up the different powder blends was accurately weight and

place in a closed fit container. The total mass of the mixture was 100g. This mass was chosen since a few grams of each powder blend was required to make a sample. The samples were allowed to blend for 15 minutes at 15 revolutions per minute.

3.3 TGA and DSC analyses

Thermogravimetric analysis allows one to observe the decomposition of the various selected powders blends from 20-1200°C under a desired atmosphere. While the TGA allows one to observed any mass change during the analysis, the DSC allows one to determine the type of reactions that can take place. The reactions that takes place during oxidation or dehydrogenation or phase transformation can be denoted by the presence of exothermic or endothermic peaks. The TGA and DSC analyses were critical in determining the corresponding temperatures at which the various reactions or phase transformations were taking place. Additionally, since the TGA and DSC analyses are conducted at a temperature higher than that of the sintering trials, the TGA and DSC results could potentially explain the results of the sintering study by relating the relative sintered densities to the various reactions or phase transformations that take place.

TGA and DSC analyses of the powder blends entail heating a small mass (20-30 mg) of each powder blend from 20-1200°C to observe the decomposition of each powder blend under partial hydrogen and argon atmospheres. The aim was to evaluate whether or not the heating atmosphere affects the temperature as well as the energy associated with hydrogenation and dehydrogenation. The TGA and DSC results are expected to provide the following:

- The temperature at which hydrogen is released from the sample.
- The temperature range over which hydrogenation and/or dehydrogenation would occur for each powder blend.
- Whether the atmosphere plays a role in hydrogen retention at higher temperatures for TiH_2.

The Netzsch SAT 409 CD, was used to determine the thermal decomposition of various powder blends under an argon and 15% hydrogen/ 85% argon (partial hydrogen) atmosphere. Investigating the powder blends' behaviour under vacuum was not possible due to the noise effects associated with the vacuum pump, which interfered with the signal of the mass balance and hence the TGA and DSC results.

The parameters of the tests conducted were as follows:

1) Heating rate of 10°C/minute.
   The heating rate was chosen as such, since all the correction and calibration runs of the equipment were conducted at this heating rate.

2) From room temperature to 1200°C under argon and partial hydrogen atmosphere. A temperature of 1200°C was chosen since the sintering temperatures were 1050°C and 1200°C. Thus, the decomposition behaviour of the powders over the sintering temperature range could be observed.

3.4 Green compaction

3.4.1 Uniaxial pressing

Based on current literature, the compaction pressure range that affects the density and compaction properties of CP Ti and TiH_2 is 300-900 MPa. The 110kN press is only able to press the desired 10mm diameter and 10mm height specimens (mass of 2.70g of the powder blend) up to a maximum pressure of 500MPa. The 100kN press was chosen since the samples dimensions are desirable. Additionally no significant improvement after 600MPa was documented to substantially improve the green density. Hence, the parameters for the uniaxial pressing of the selected powder blends ranged from 300 to 500MPa at intervals of 50MPa. A zinc stereate lubricant is used during green compaction to improve the ejection and also prevent the formation of micro cracks in the pressed samples [15]. The zinc stereate was particularly important when ejecting samples with higher levels of brittle TiH_2 powders. The use of zinc stereate was deemed to be necessary after each TiH_2 sample was ejected. Zinc

stereate burns off easily during the initial stages of sintering and does not react with any of the powders [15] which is highly desirable.

This pressure range was chosen to assess the effects of compaction pressure on the density and strength of the different green compacts. The different powder blends that were used are summarised in Table 3.3.

Table 3.3: Powders blends used during compaction study

Pressure (MPa)	**Different ratio CP Ti: TiH_2 : 60Al-40V powder blends**							
300	**100:0:0**	**90:0:10**	**0:90:10**	**0:100:0**	**80:20:0**	**60:40:0**	**40:60:0**	**20:80:0**
350	**100:0:0**	**90:0:10**	**0:90:10**	**0:100:0**	**80:20:0**	**60:40:0**	**40:60:0**	**20:80:0**
400	**100:0:0**	**90:0:10**	**0:90:10**	**0:100:0**	**80:20:0**	**60:40:0**	**40:60:0**	**20:80:0**
450	**100:0:0**	**90:0:10**	**0:90:10**	**0:100:0**	**80:20:0**	**60:40:0**	**40:60:0**	**20:80:0**
500	**100:0:0**	**90:0:10**	**0:90:10**	**0:100:0**	**80:20:0**	**60:40:0**	**40:60:0**	**20:80:0**

3.4.2 Green density

The green densities were measured according to ASTM B962-13 [50]. The apparatus used to measure the green density is shown in Figure 3.1. The detailed methodology is described in Appendix 11.1.1 in Chapter 11.

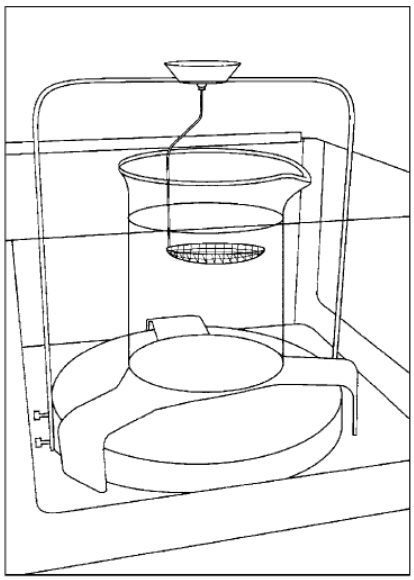

Figure 3.1: Apparatus used to measure green density of compacts

The effects of pressure and powder composition on the green density of the different compacts are discussed in Chapter 5.

3.4.3 Pressing of specimens for green strength measurements

The green strength of the compacts were measured to determine the influence of powder compaction pressure and composition on these properties. The green strength measurement was conducted according to ASTM B312-09 [51]. Due to the specimen size specified by the standard, the specimens had to be pressed using a 250kN press.

Three specimens from each powder blend (9.00g of powders for each specimen) were pressed with dimension of about 30mm length, 12mm width and 7mm height). Only two pressures were selected for the pressing of the samples which were 300 and 500 MPa. A total of 48 samples were pressed (eight different powder blends with three specimens at each pressures).

3.4.4 Green strength measurements

To measure the strength of the green compacts from the 250kN press, the dimensions of each specimen in terms of length, breadth and thickness were measured and recorded to three decimal places in millimeters as prescribed by ASTM B312-09.

However, due to the very low magnitude of the green strength of the compacts, the measurements on the 200kN tensile tester were not accurate. Hence, an apparatus was designed and assembled based on ASTM B312-09. Figure 3.2 shows the apparatus described in ASTM B312-09 and Figure 3.2 shows the apparatus made based on the standard. The stepwise procedure for the green strength measurements are outlined in Chapter 11 Appendix 11.2.

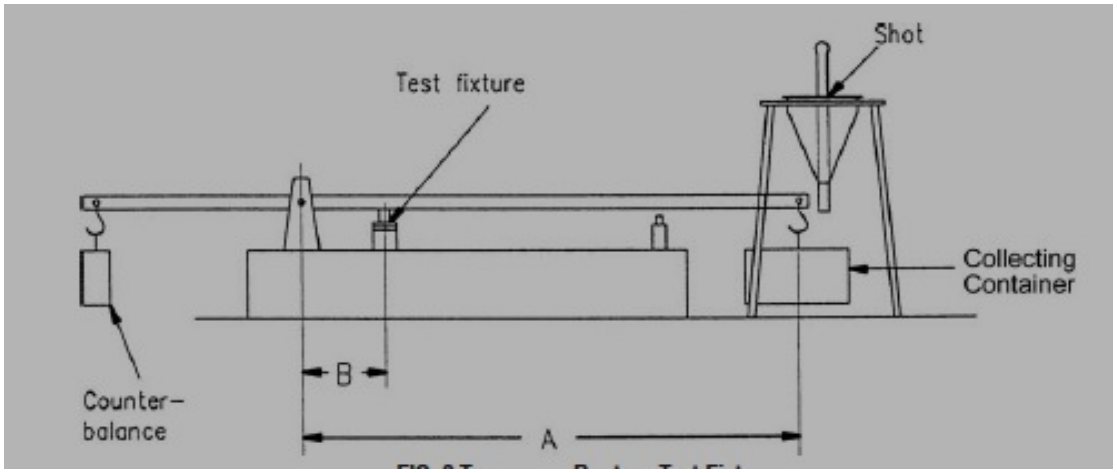

Figure 3.2: Schematic of apparatus for green strength measurements based on ASTM B312-09

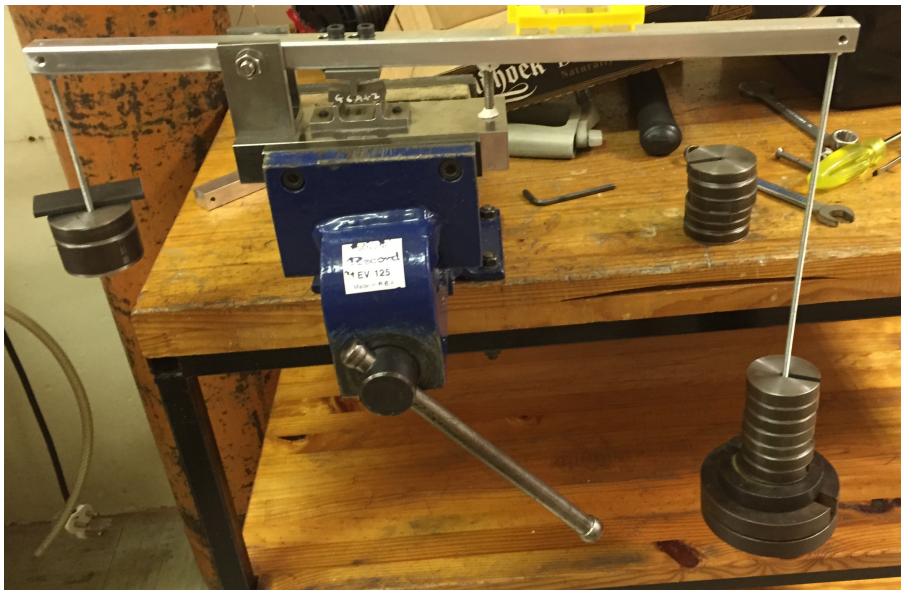

Figure 3.3: Apparatus manufactured for green strength measurements

3.5 Sintering

The sintering conditions were chosen based on the aim of this dissertation which is to lower the sintering temperature of Ti-6Al-4V. In current literature, the sintering of CP Ti and Ti-6Al-4V at 1200°C for four hours is expected to result in good densities and microstructures. Since hydrogen has the potential to decrease the sintering temperature, a temperature of 1050°C was selected.

3.5.1 Sintering temperature and time

It was critical that a furnace that can allow vacuum and positive gas atmosphere is used during the sintering study of this dissertation. Since hydrogen can also be introduced by sintering in a partial hydrogen atmosphere it was vital that the safety of the furnace was ensured. Thus, cracker valves and a correct exhaust system as seen in Figure 3.4 were set. The cracker valves were set to ensure that a positive atmosphere was obtained during sintering in an argon and partial hydrogen sintering. Additionally, any pressure build up in the furnace will be prevented thus ensuring the safety of the experimental conditions.

Nine green compacts were then sintered at a temperature of 1050°C with a heating rate of 5°C/min, a dwelling time of eight hours and left to cool in the furnace. To sinter at 1050°C for more than eight hours in both positive and negative atmosphere, a new furnace that can sinter up to a temperature of 1500°C was acquired. The new furnace is shown in Figure 3.4. A calibration curve recording the temperature in the furnace tube and the corresponding temperature on the furnace monitor was derived. From this curve, a temperature of 1065°C on the temperature monitor results in middle of the furnace to be at 1050°C. Additionally, a temperature of 1200°C on the calibration curve is equivalent to 1200°C on the furnace tube.

The stepwise procedure for the sintering treatment occurred in the following chronological order:

1) Pre-setting the heating rate, dwell time and final temperature on the sintering profile monitor on the furnace.
2) Insert the nine samples for the selected powder blends in the middle of the horizontal tube and close the horizontal tube.
3) The auxiliary pump was switched on and as soon as the pressure decrease to a 10^{-2} magnitude, the turbo pump is switched and maintained until a 10^{-6} pressure is reached.
4) The valve connecting the vacuum pump to the horizontal tube of the furnace is then closed and the tap of the gas cylinder and inlet valve of the respective

gas to be used are opened and the gas is allowed to flow until a constant flow of 5 litres per minute is recorded on the flow meter.

5) The gas is allowed to flow for three minutes and the inlet valve and gas cylinder tap are closed. The valve connecting the vacuum pump to the furnace tube is opened again and Step 3 is repeated.
6) Step 4 is repeated and once the gas flow is constant, the sintering treatment begins by switching on the sintering profile monitor and furnace. When the sintering treatments is complete the furnace is allowed to cool and the samples are only removed when the temperature of the furnace is lower than 100°C.
7) When sintering under vacuum, the sintering monitor is only switched on when the vacuum from Step 3 is stable for at least 30 minutes.

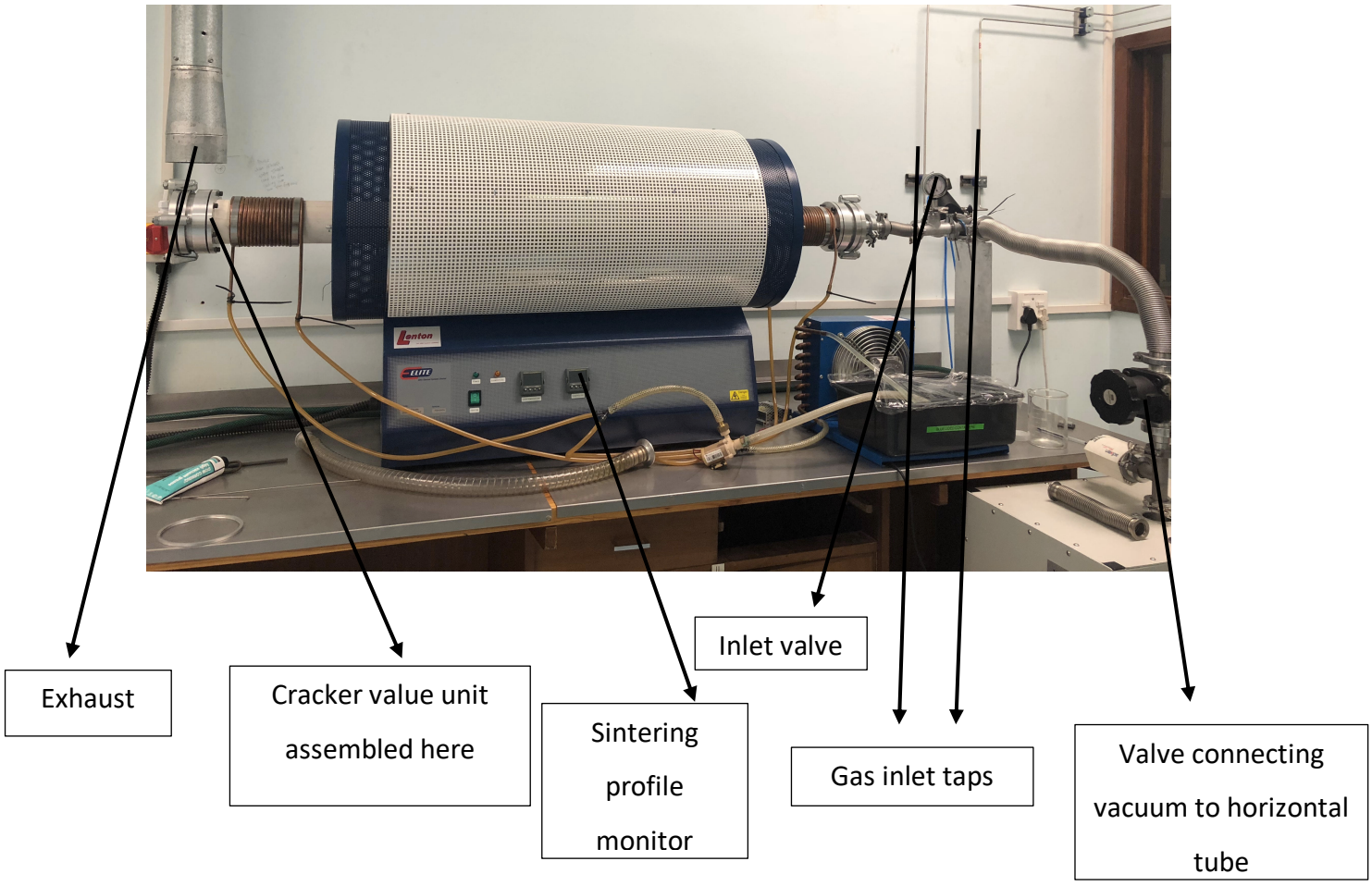

Figure 3.4: Sintering furnace TSH/15/45/300

3.5.2 Sintering atmospheres

Nine pressed samples for each of the selected powder blends were sintered in an argon atmosphere and the same procedure was repeated for a 15% hydrogen/ 85% argon atmosphere. Additionally, it was critical to determine the sintered densities and look at the microstructures of the CP Ti-6Al-4V and TiH_2-6Al-4V (four samples) under vacuum at 1050°C for eight hours. Three samples from each sintering treatments were used to measure the density of the samples and the remaining samples were used for microstructural evaluation. Additionally, to validate the method used, two more sets of CP Ti-6Al-4V and TiH_2-6Al-4V (four samples each) were sintered at 1200°C for four hours under vacuum as well as under a 15% H_2/85% Ar atmosphere. The density and microstructural results, for the samples sintered at 1200°C for four hours under vacuum, can be compared to the results generated by past research to validate the sintering method used.

3.5.3 Tests on sintered samples

After sintering the microstructures and densities of the various samples were observed and measured respectively.

3.4.3.1 Optical microscopy

One sample from each powder blend was hot mounted and prepared, as per Table 3. 4 and Table 3.5, for microstructural evaluation.

Table 3. 4: Polishing procedure of sintered samples

Silicon carbide paper size	Solution	Time (mins)
1000 μm	water	1
4000μm	water	5
Diamond blue pad	Diamond 2-3μm paste	5
Colloidal black pad	Colloidal solution	5

Table 3.5: Etching procedure of sintered samples

Solvent	Volume (cm^3)
Concentrated nitric acid (HNO_3) 67%	1
Hydrofluoric acid (HF)	2
water	97

The samples were swabbed for about 15-20 seconds after being polished and then washed immediately with water to prevent further etching. The samples were then dried and observed under the light microscope at various magnification.

3.5.3.2 Mass and Density measurements

The sintered density of the samples were measured and calculated by using the procedure outlined by ASTM B962-13 which is documented in Chapter 11 Appendix 11.1.

Chapter 4: Powder analysis

The particle shape and size affects the compaction as well as sintering behaviour of the resulting green and sintered compacts respectively [17][18][27]. To determine the extent to which particle shape and size affects the green density and hence sintered density, analysis of the starting powders is critical.

4.1 SEM

A series of SEM analyses were conducted on the three different powders to study the particle size of the powders. Figure 4.1 show representative SEM images of the CP Ti, TiH_2 and MA powders respectively.

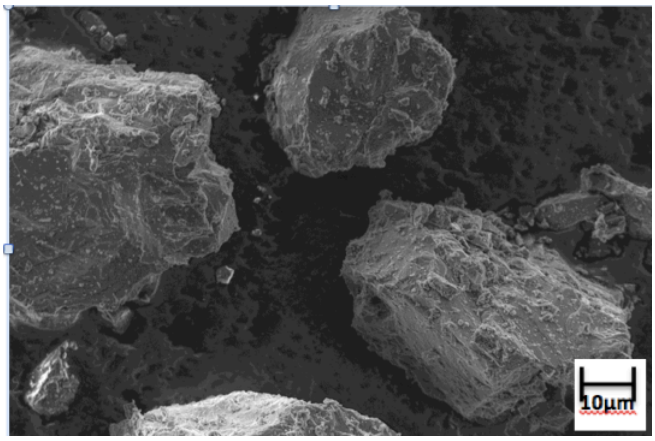

(a)

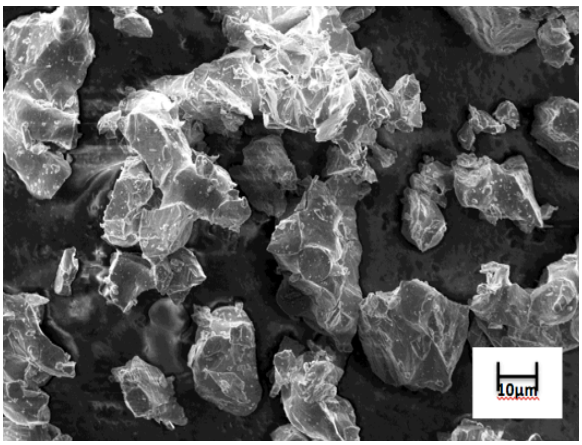

(b)

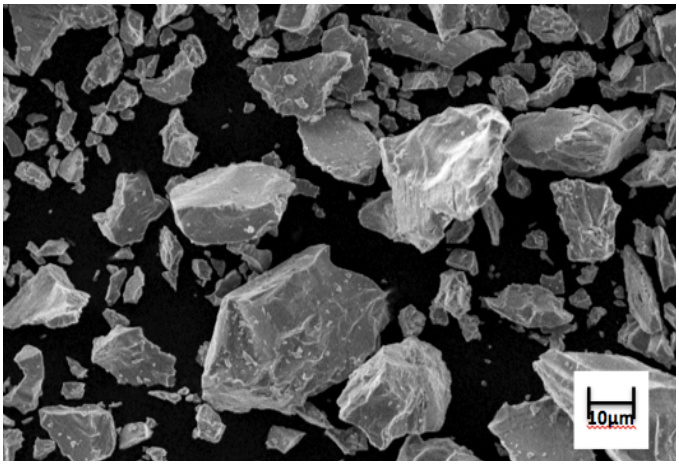

(c)

Figure 4.1: (a) SEM image of CP Ti powder, (b) SEM image of TiH_2 powder and (c) SEM image of master alloy powder (X5000)

4.2 Laser diffraction analysis

Determining the powder size and shape are key in explaining the compaction behaviour and green densities as well as the sintered properties of the various pressed compacts.

As displayed in Figure 4.1, CP Ti, TiH_2 and the MA are all of different sizes. Figure 4.2 shows the particle size distribution of the CP Ti, TiH_2 and MA powders respectively.

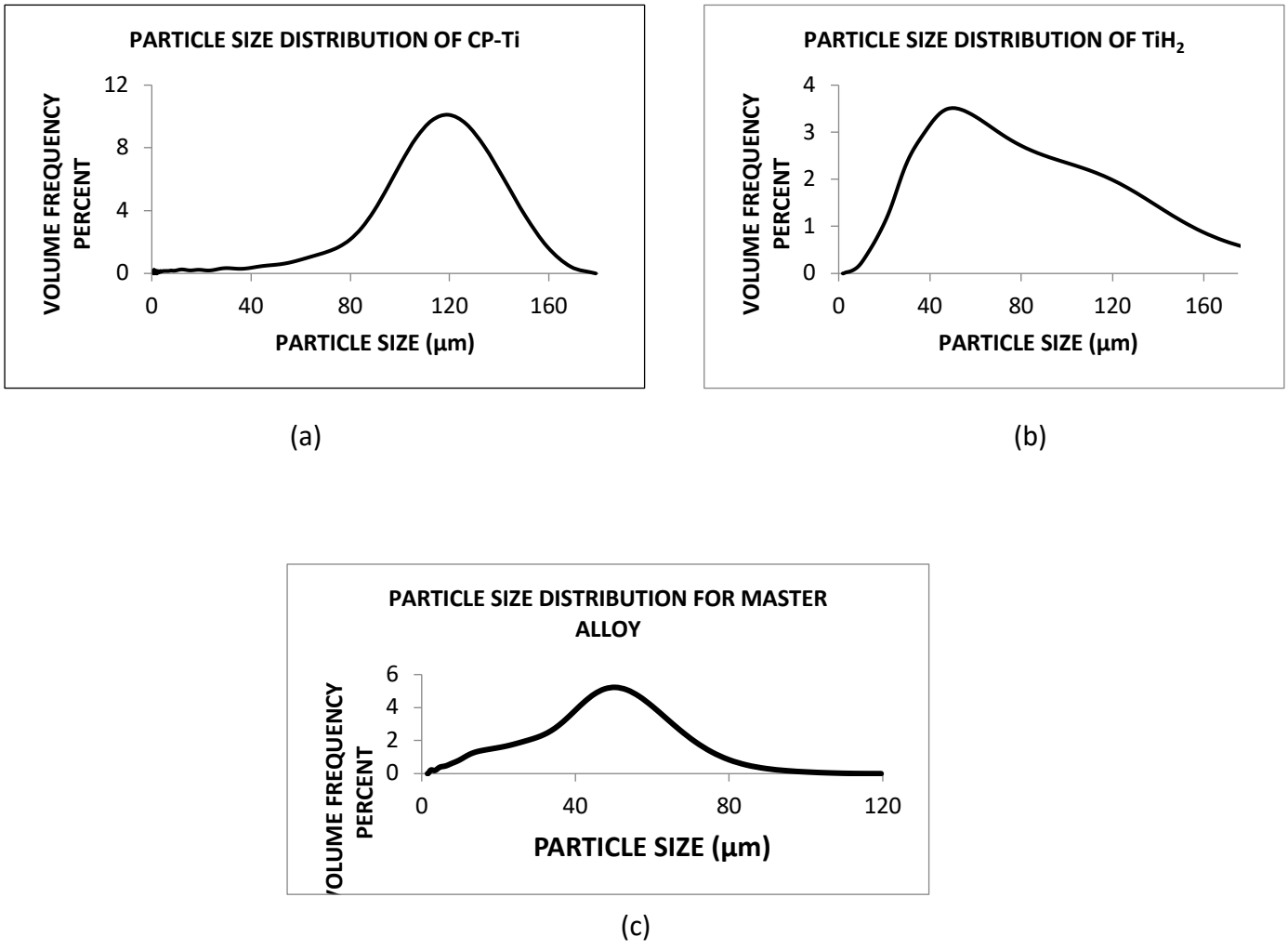

(a) (b)

(c)

Figure 4.2 (a)Particle size distribution of CP Ti (b)Particle size distribution of TiH_2 (c) Particle size distribution of master alloy

Figure 4.2 supports the results obtained and illustrated in Figure 4.1 for the average particle size of the three different powders used for this project.

Table 4.1 summarises the average particle size as well as the shape of the three powders.

Table 4.1:Powder size and shape

Powder type	Average particle size range (μm)	Particle shape
CP Ti	100±0.2	Angular and facetted
TiH_2	63±1.1	Angular and facetted
Master alloy (60Al-40V)	37±0.1	Angular and facetted

From Table 4.1, it can be said that the difference in particle size is significant. The values and errors were generated by the Saturn DigiSizer. In general, the compaction pressure required to achieve reasonable relative density (>80%) varies according to the shape of the CP-Ti powder. For example, a powder manufactured by the Amstrong method is a titanium powder with a dendritic "coral-like" morphology which requires a significantly higher compaction pressure (>1100 MPa) as compared to sponge fines or hydride de-hydride powder (HDH) (600-800MPa) to result in a relative density higher than 80% [48]. Thus, based on the shape of the CP Ti in Figure 4.1(a) powder a pressure of 600MPa should be more than enough to result in good compaction.

The shape and size of the powders have vital roles to play in terms of the density and strength of the green compact. Flowability of the powder affects the density of their resulting green compacts. According to a study discussed previously [14], irregular powders, as compared to spherical or regular shaped powders, are able to lock and undergo further cold welding, which assists in improving the density of the final product. Thus good green densities are expected from the compacts made from the three powders used for this dissertation due to their irregular shape.

Figures 4.2(a)-(c) graphically represent the particle size distribution of all three starting powders. The results of the laser diffraction analyses confirm that the average particle size of the supplied powders are within the acceptable range as per the powder size specification provided by the suppliers. The study discussed in Chapter 2

[16] suggests that the bigger the size of the powder particles, the higher is the green density. The reason being that while larger particles will result in bigger voids compared to compacts made from finer powder particles, the frequency of the smaller voids is so high that the overall final green densities of compacts with finer particles are lower than that of the compacts made from larger powder particles. Since CP Ti has a larger particle size, compared to TiH_2 as well as the MA powder, the green compacts with higher level of CP Ti are expected to have higher green densities solely based on their particle size.

However, the mechanical properties of the powders also affects the green density and strength of the compacts pressed from the various powder blends. This is further discussed in Chapter 5.

Chapter 5: Results of compaction study

The first phase of this project was to investigate the compactibility as well as the green density and strength of different CP Ti/TiH_2 powder blends. Since TiH_2 is known to be brittle, pressing 100% TiH_2 at relatively high compaction pressures (>500MPa) can result in crack formation within the compact. However, since TiH_2 represents potential benefits during sintering, determining the maximum level of TiH_2 powder that can be added to a CP Ti powder that would result in a compact being formed easily while achieving acceptable green densities was deemed vital.

5.1 General overview of the compaction process

CP Ti is ductile and hence compaction and ejection of the pressed samples is relatively easy and does not require any lubrication of the die. However, TiH_2 is very brittle and thus ejection of the pressed samples becomes problematic due to fracture and cracking of the compact. To counteract this issue, a lubricant (zinc stereate) was used during the compaction of the powder blends that contained TiH_2. Zinc stereate is non-reactive and is also not absorbed by the CP Ti, TiH_2 and MA powders. Zinc stereate also burns off relatively easy during sintering and hence will not alter or affect the properties of the compacts.

5.2 Green density

Table 5.1 summarises the results of the density measurements conducted on the green compacts at various compaction pressures.

Table 5.1 :Green density of powder blends

	Density of powder blends (g/cm^3)							
Compaction pressure (MPa)	**100% CP Ti**	**80% CP Ti/ 20% TiH_2**	**60% CP Ti/40% TiH_2**	**40% CP Ti/60% TiH_2**	**20% CP Ti/80% TiH_2**	**100% TiH_2**	**CP Ti-6Al-4V**	**TiH_2-6Al-4V**
300	83.4±0.1	71.7±0.1	67.6±0.1	67.5±0.1	67.3±0.1	66.0±0.1	80.9±0.1	74.1±0.1
350	84.3±0.1	73.1±0.1	69.1±0.1	69.9±0.1	69.5±0.1	67.7±0.1	83.3±0.1	74.8±0.1
400	85.5±0.1	73.8±0.1	71.8±0.1	73.8±0.1	70.3±0.1	69.4±0.1	85.4±0.1	77.3±0.1

450	86.5±0.1	76.3±0.1	74.8±0.1	73.5±0.1	72.7±0.1	71.0±0.1	85.2±0.1	78.5±0.1
500	87.4±0.1	77.9±0.1	76.2±0.1	75.4±0.1	72.8±0.1	75.5±0.1	86.4±0.1	79.3±0.1

Figure 5.1 shows the trends in densities of various powder blends as a function of the compaction pressure. Figure 5.2 shows the relationship between relative green density and levels of TiH_2 powder in the green compacts.

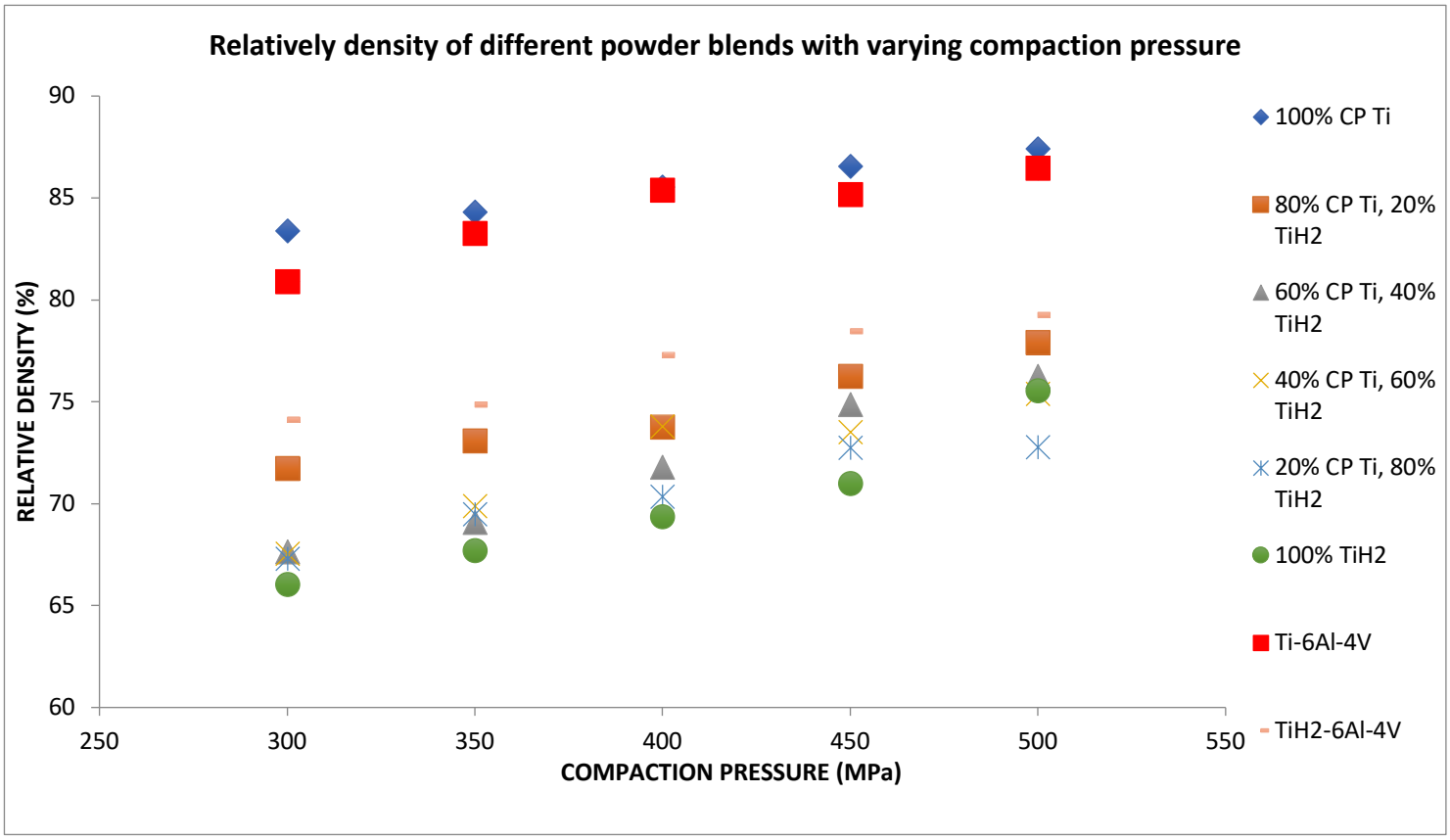

Figure 5.1 : Green density trends of different powder blends

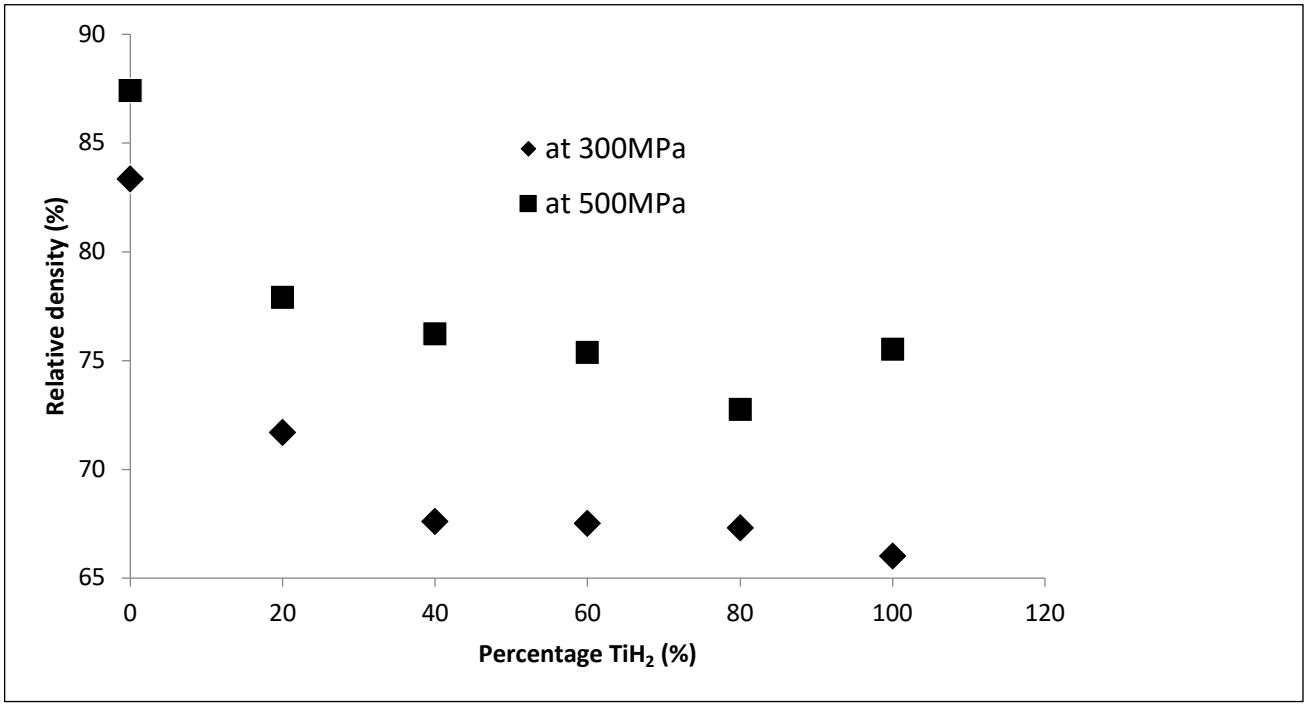

Figure 5.2: Green density versus % TiH_2

From Table 5.1 and Figure 5.1 and Figure 5.2, the following can be deduced:

- The higher the compaction pressure, the higher is the density of the green compact.
- The higher the percentage of TiH_2 in the blend, the lower is the green density.
- A percentage of 40% or more of TiH_2 no longer significantly affects the rate of decrease in relative green density of the CP Ti/TiH_2 powder blends.

Based solely on the chemical composition and mechanical properties of the powder blends, it was expected that the higher the level of TiH_2, the higher would be the green density of the compact. This is because the hydride particles (being brittle), as opposed to CP Ti particles (being ductile), can rearrange and break during compaction. Smaller irregular size particles form smaller voids during compression. However, for the compaction study conducted, it was found that the green density decreases with increasing TiH_2 content. This decrease in density is dominated by the difference in particle size between CP Ti and TiH_2 (discussed in Chapter 4). The particle size of the

TiH_2 used is smaller prior to compaction and thus when particles break (during compaction) there is a substantial difference in particle size compared to CP Ti. This results in the size of the voids in TiH_2 compacts being smaller in size compared to compacts with CP Ti, However, the frequency of the small voids is so high that it results in a lower overall density as compared to CP Ti compacts. The results are supported by various research papers discussed in Chapter 2 [17][18], where larger particle size of CP Ti had better relative green densities as compared to smaller CP Ti as well as smaller TiH_2 powders. While, it could be argued that bigger particles should be used, the effects of smaller particles on the sintering behaviour of compacts do confirm their ability to improve sintered density.

Therefore, the difference in particle size is significant and in this case outweighs the chemical composition and mechanical properties of the powders. To evaluate the difference in green density solely based on the chemical composition and nature, the powders used should have the same particle size and shape. Nevertheless, the green density results do suggest that a powder blend containing both CP Ti and TiH_2 can result in good green and sintering densities. The CP Ti will enable easy compaction while resulting in good green densities whereas the smaller TiH_2 will potentially result in improved sintered density (smaller particle size provides bigger surface area that promotes densification during sintering).The reducing ability of TiH_2 (due to the presence of hydrogen) is also expected to reduce the formation of surface oxides which in turn promotes sintering and densification. These factors are further discussed in Chapter 7.

5.3 Green strength

Figure 5.3 and Figure 5.4 show the results of the average green strength as a function of compaction pressure and TiH_2 content respectively at both selected compaction pressures. The number of tests conducted for the green strength were done as per ASTM B 312-09.

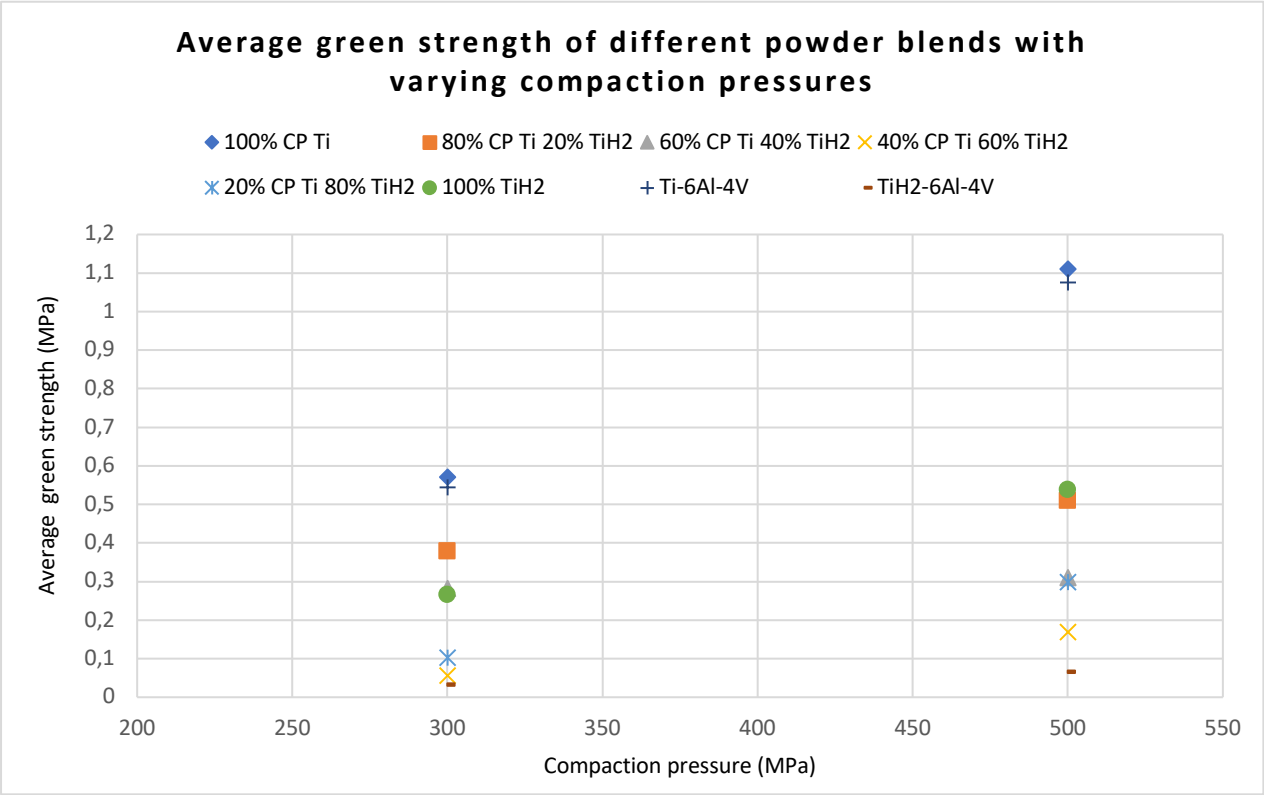

Figure 5. 3: Green strength (MPa) of different powder blends versus compaction pressure (MPa)

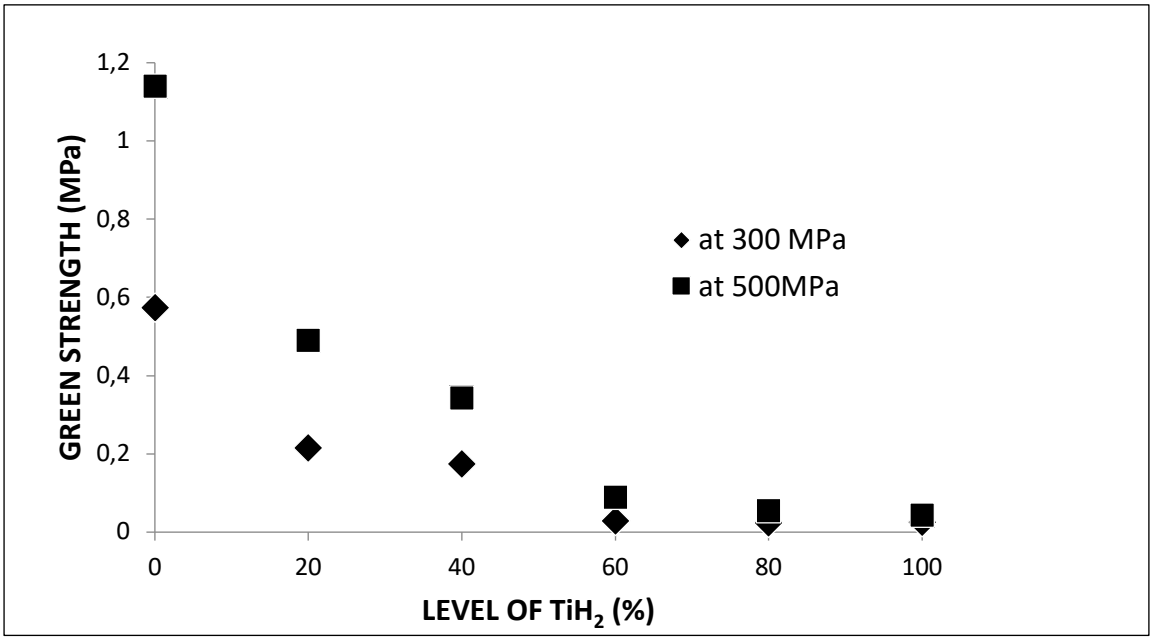

Figure 5.4: Green strength (MPa) of compacts versus TiH_2 content

From Figure 5.3 and Figure 5.4, the following can be deduced:

- The higher the percentage of CP Ti in the blend, the higher is the green strength.

- The green strength decreases significantly as the level of the TiH_2 in the blend increases from 0 to 40%. As the percentage of TiH_2 in the blend becomes greater than 40%, the decrease rate in green strength is less significant.

The green strength of the compacts are highly influenced by the chemical composition and brittle nature of the powder. As discussed in Section 5.2, CP Ti is ductile whereas TiH_2 is brittle. On the one hand, CP Ti powder particles are deformed during compaction. This breaks the oxide layer and leads to exposed metal surface being more susceptible to cold welding which in turn results in stronger bonds forming between the powder particles [14]. On the other hand, TiH_2 powder particles do not plastically deform but are rather crushed and rearranged, which does not result in the formation of bonds between the powder particles. In this respect it is not surprising that powder blends with higher levels of CP Ti are expected to have higher green strength as confirmed by the results shown in Figure 5.4.

5.4 Relationship between green strength and density

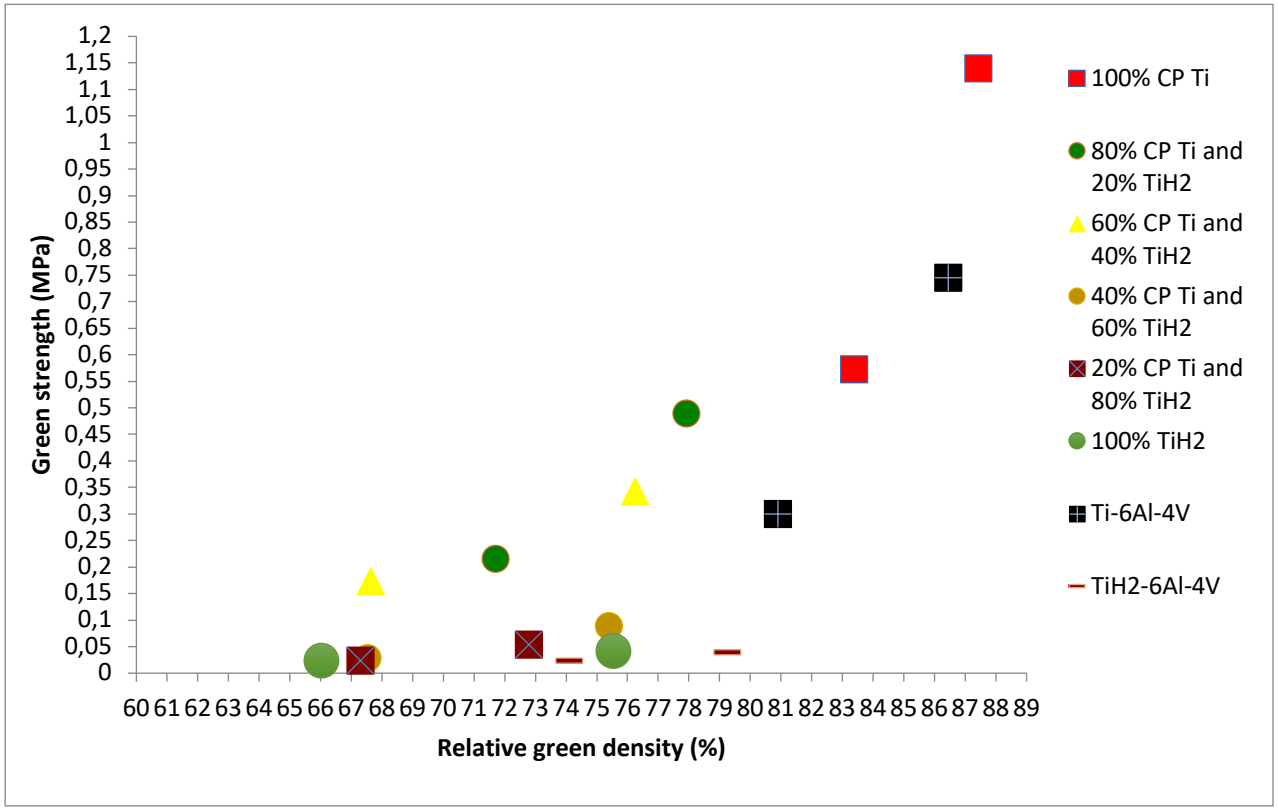

Figure 5. 5 :Green strength of powder blends (MPa) versus relative green densities (%)

Figure 5.5 shows the relationship between density and green strength for the different powder blends used in this project. From Figure 5. 5, it can be observed that the higher the green density of a compact, the higher is its green strength. However, the chemical composition, mechanical properties and size of the powders also have a role to play in terms of the strength of the resulting green compacts. When the percentage of TiH_2 in the powder blend is higher than 40%, the green strength remains more or less the same irrespective of the green density.

It was primarily concluded that the higher the relative green density, the higher is the green strength of the compact since there are less voids present. Voids or pores can act as stress concentrators when the samples are subjected to a force which in turn increases the risk of fracture. For CP Ti and Ti-6Al-4V an increase in compaction pressure (300 to 500MPa), which results in an increase in green density, leads to

improved green strength. As the levels of TiH_2 increases in the powder blend, the increase in compaction pressure barely improves the green strength of the sample even though the density of the samples are still affected by the compaction pressure. Thus, the primary factor that governs the green strength of the TiH_2 blends is the chemical composition and mechanical properties of the powders used to form the green compacts and not necessarily the compaction pressure. Hence, higher levels of TiH_2 would result in lower green density, which in turn limits the level of TiH_2 that can be added to the powder blend for compaction and sintering to make Ti-6Al-4V by the PM route. The green density and strength studies confirm that a powder blend containing more than 40wt% TiH_2 will not likely result in the desirable green strength and densities.

The green strength, lowering substantially with increasing level of TiH_2, indicates that direct powder rolling of TiH_2 will possibly not provide sufficient green strength to manufacture green TiH_2 sheets. However, it is possible that an additive could be used to provide green strength to manufacture green TiH_2 sheets.

Chapter 6: TGA and DSC analyses

From the results of the compaction study, five powder blends were selected for sintering. DSC and TGA analyses were conducted on these powder blends as well as on 100% TiH_2 powder. The powder blends that underwent DSC and TGA analyses were: 100% CP Ti, 80% CP Ti/20% TiH_2 powder blend, 60% CP Ti/40% TiH_2 powder blend, CP Ti-6Al4V, TiH_2-6Al-4V powder blends and 100% TiH_2. Figure 6.1 and Figure 6.2 show the TGA and DSC curves of all powders in an argon atmosphere respectively.

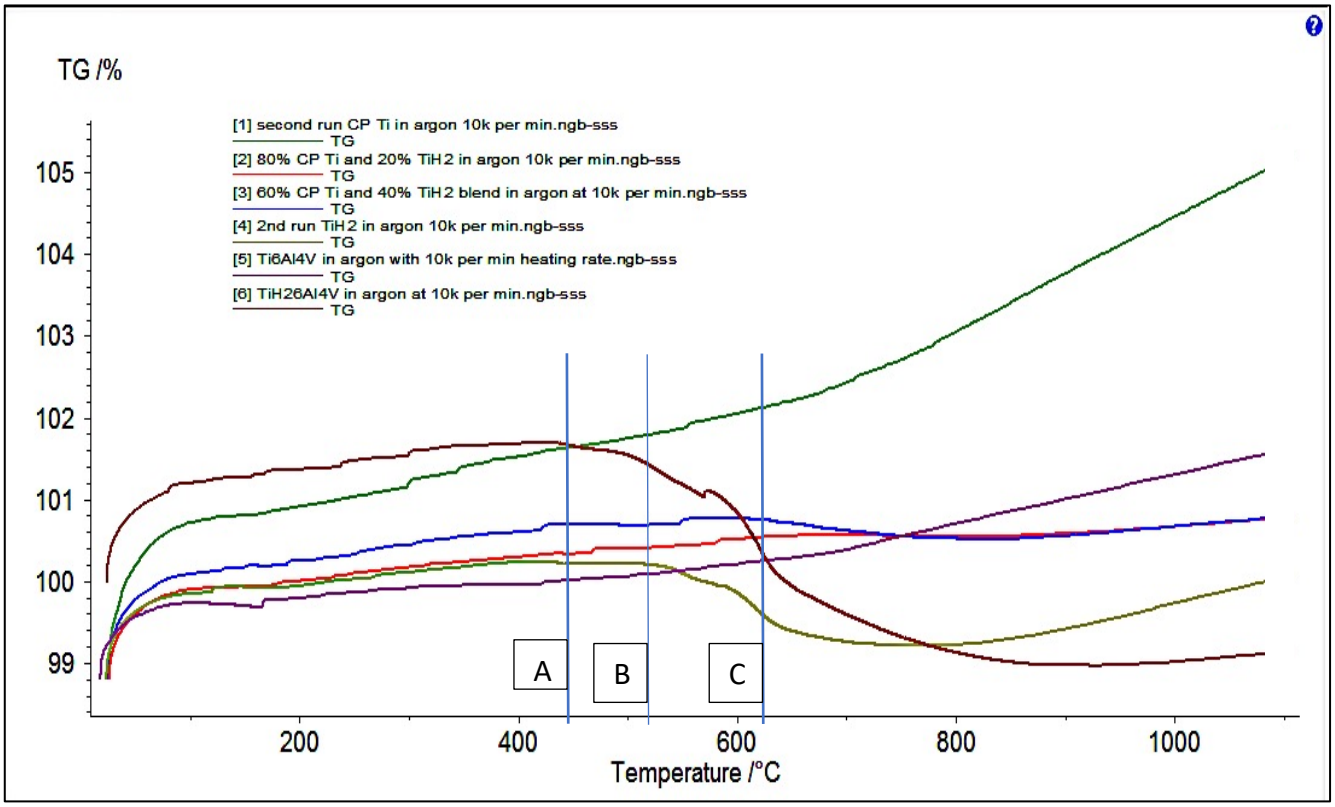

Figure 6.1: TGA curves of powder blends in argon (TGA)

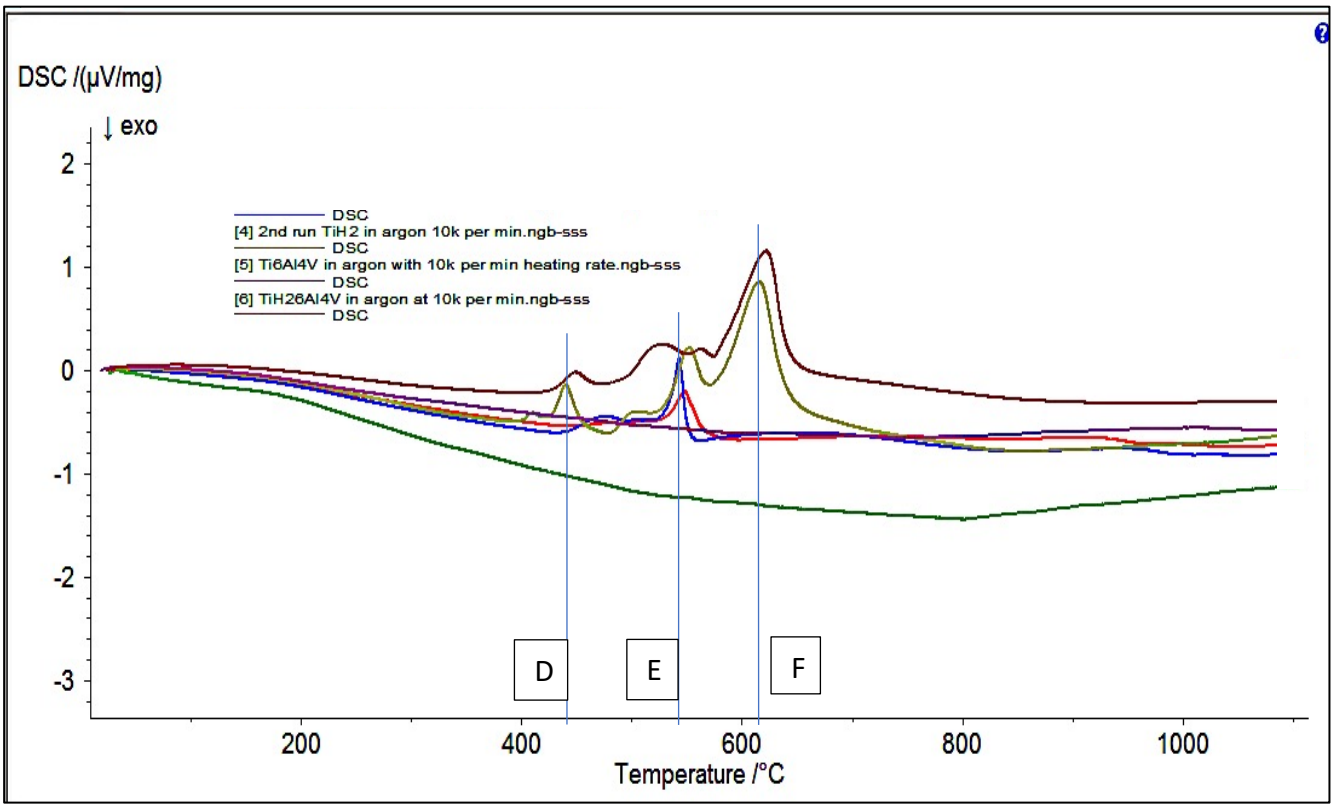

Figure 6.2 :DSC curves of all powder blends in argon

Figure 6.1 shows that for powder blends with no levels of TiH_2, the mass increase after 610°C (Temperature C), is significantly higher when compared to other powder blends with levels of TiH_2. However, in an argon atmosphere, no mass increase is expected since argon is an inert gas and oxidation should not take place. Hence, it can be argued, that either the argon gas used was not 100% pure argon or that the powders were slightly oxidised since they were not stored under inert conditions before or after the blending process. The slight oxidation of the powders during storing will result in the formation of an additional surface oxide layer upon heating which will cause an increase in mass. Previous research also argued that the mass increase observed in the TGA curves for powder blends containing CP Ti and Ti-6Al-4V is due to the titanium being highly reactive and will hence absorb oxygen at high temperature particularly if the atmosphere is not 100% inert. The initial mass increase (similar observation by past studies: refer to Figure 2.17 in Section 2.4.4) could be ignored since it is likely due to the unstable TG baseline [38].

The mass decrease of the 100% TiH_2 and TiH_2-6Al-4V powders also confirm dehydrogenation of TiH_2 from 430°C (Temperature A) [38][45]. Hence, this provides an indication that no mass loss for powder blends containing TiH_2 should be denoted. These are confirmed by their corresponding DSC curves which, show three endothermic peaks over a temperature range of 430-620°C (temperatures D-F; Figure 6.2) [38][45]. In a previous study dehydrogenation of TiH_2 starts at 390°C while reaching a maximum at 525°C [44]. However, if the powder is slightly oxidised, the oxide layer creates an effective barrier for hydrogen diffusion which results in an increase in the heat absorption temperature [44]. The DSC curves for both TiH_2 and TiH_2-6Al-4V (see Figure 6.2) confirm that both of these powder blends were slightly oxidised which is why dehydrogenation begins at a much higher temperature than expected.

The DSC curve for 100% TiH_2 (see Figure 6.2) confirms the presence of three endothermic peaks which is also sometimes referred as a two peak and one-shoulder structure at a heating rate of 10°C/min [45]. These three endothermic peaks are due to the different phase transformations that take place during dehydrogenation from 430°C to 620°C (similar results obtained as denoted by temperatures D-F). At a heating rate of 10°C/min or lower the phase transformation that takes place during the decomposition of TiH_2 is $\delta \longrightarrow \beta + \delta \longrightarrow \beta \longrightarrow \alpha+\beta$ (based on the Ti-H phase diagram as seen in Figure 6.3 [45].

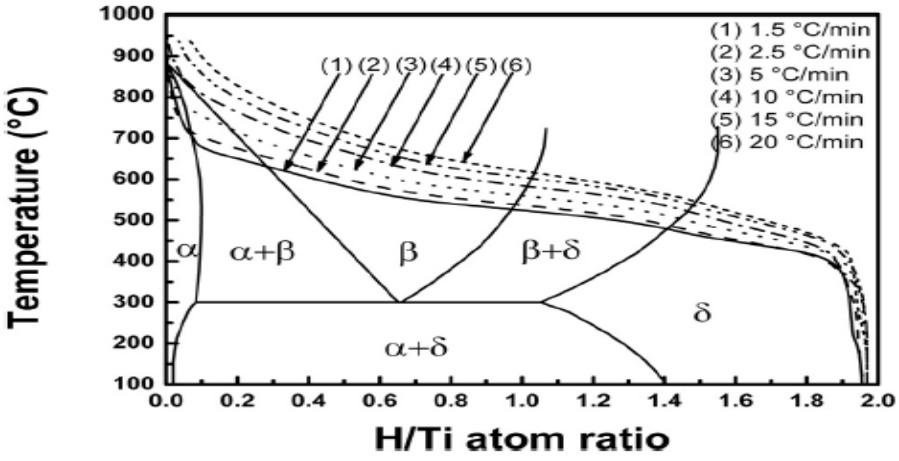

Figure 6.3: Ti-H phase diagram combined with changing trends of temperature/hydrogen content at different heating rate

These three different phase transformations correspond to three different endothermic peaks which are also observed in the TiH_2 and TiH_2-6Al-4V samples that were investigated in this dissertation. The first endothermic peak observed at 430°C (Temperature C) is due to hydrogen atoms being transferred from tetrahedral to octahedral lattice sites which in turn onsets hydrogen desorption. The second endothermic peak is due to the hydrogen desorption from the δ phase to $\beta + \delta$ phase which is completed when the remaining hydrogen is removed from the octahedral sites. The complete removal of hydrogen in the octahedral sites results in no more δ phase being present. Thus, the only phase present is the β phase. The latter is a high temperature phase where hydrogen atoms only occupy tetrahedral sites. However, in the α phase, hydrogen can occupy both tetrahedral and octahedral sites. The third endothermic peak is due to the β to $\alpha+ \beta$ phase transformation [45]. While other researchers have obtained different phase transformation steps, the difference is solely due to the presence of the α phase as a result of oxygen being present during the experiment (this is described later in this Chapter). Even though the DSC/TGA experiments conducted during the course of this dissertation were at very high vacuum prior to the flow of positive gas atmosphere, it is likely that the argon gas was not 100% inert and this could very likely result in slight oxidation of the powders. Additionally, the powders were most likely oxidised since they were not stored under inert conditions.

The presence of an oxide layer or oxygen enrichment would lead to hydrogen desorption not only resulting in the release of H_2 gas but also H_2O (g) release as well. A previous study [44] investigated and showed that TiH_2 powders start to release hydrogen from 405°C as denoted by a corresponding mass loss in the TGA curve. H_2O (g) only starts releasing at 446°C and the peak of H_2O (g) release appears at 554°C with a complete release at 620°C (concurrent with the results obtained in Figure 6.1 and 6.2 showed by temperatures A-F). However, during decomposition of TiH_2 due to the release of H_2 (g) and H_2O (g) occurring over the 466°C to 620°C temperature range, it can be difficult to distinguish between these two reactions on the DSC curve without measuring the mass flow rate of the evolved gases. The DSC results (see Figure 6.2)

cannot allow one to distinguish between the endothermic peaks of H_2 and H_2O (g) being release. It is very likely that the peaks associated with the release of these two gases overlap. However, the higher mass loss (higher than 2%) does confirm that H_2O (g) is also released. In previous studies the total mass loss as a result of H_2 and H_2O gas can correspond to 3.8wt% mass decrease during decomposition of TiH_2. The mechanism and reactions that lead to the formation of the H_2O gas in TiH_2 power compacts are discussed in Chapter 7.

For the powder blends containing low levels of TiH_2, the same phase transformations observed in TiH_2 and TiH_2-6Al-4V powder blends are not observed due to the overlapping effects of the phase transformation from α Ti (HCP) to β Ti (BCC). This is why only one distinct endothermic peak is observed for powder blends containing less than 50wt% TiH_2. The temperatures at which the endothermic peaks are observed are lower for powder blends containing lower levels of TiH_2. Hence, there is some evidence that suggests that having high levels of TiH_2 can assist in hydrogen being retained at slightly higher temperatures are discussed below.

From the TGA and DSC curves of all the powder blends heated in argon, it can be said that the presence of TiH_2 is expected to prevent oxidation at higher temperatures during sintering (the higher the level of TiH_2 the less is the mass increase at temperatures higher than 620°C). However, whether the delay in dehydrogenation is significant enough to establish any substantial benefits of using TiH_2 based solely on its hydrogen content is yet to be investigated by sintering treatment. The same TGA and DSC experiments were conducted in a partial hydrogen atmosphere to establish whether the hydrogen atmosphere can allow hydrogen retention at even higher temperatures.

Figure 6.4 and Figure 6.5 show the TGA and DSC curves of the selected powder blends in a partial hydrogen atmospheres (15% H_2 /85% Ar). Figures 6.6-6.13 show the relevant DSC and TGA curves that are discussed more in depth in this chapter.

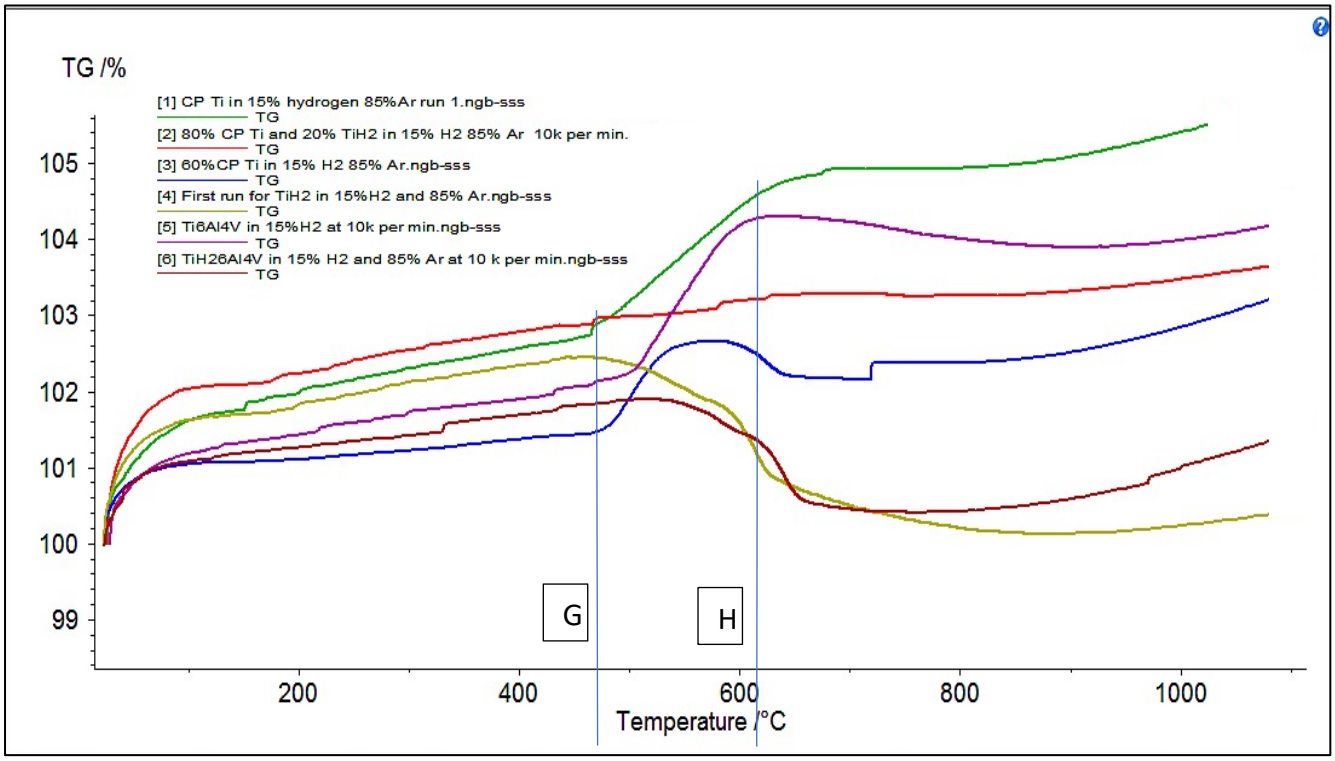

Figure 6.4: TGA curves of all powder blends in 15%H_2/85% Ar atmosphere

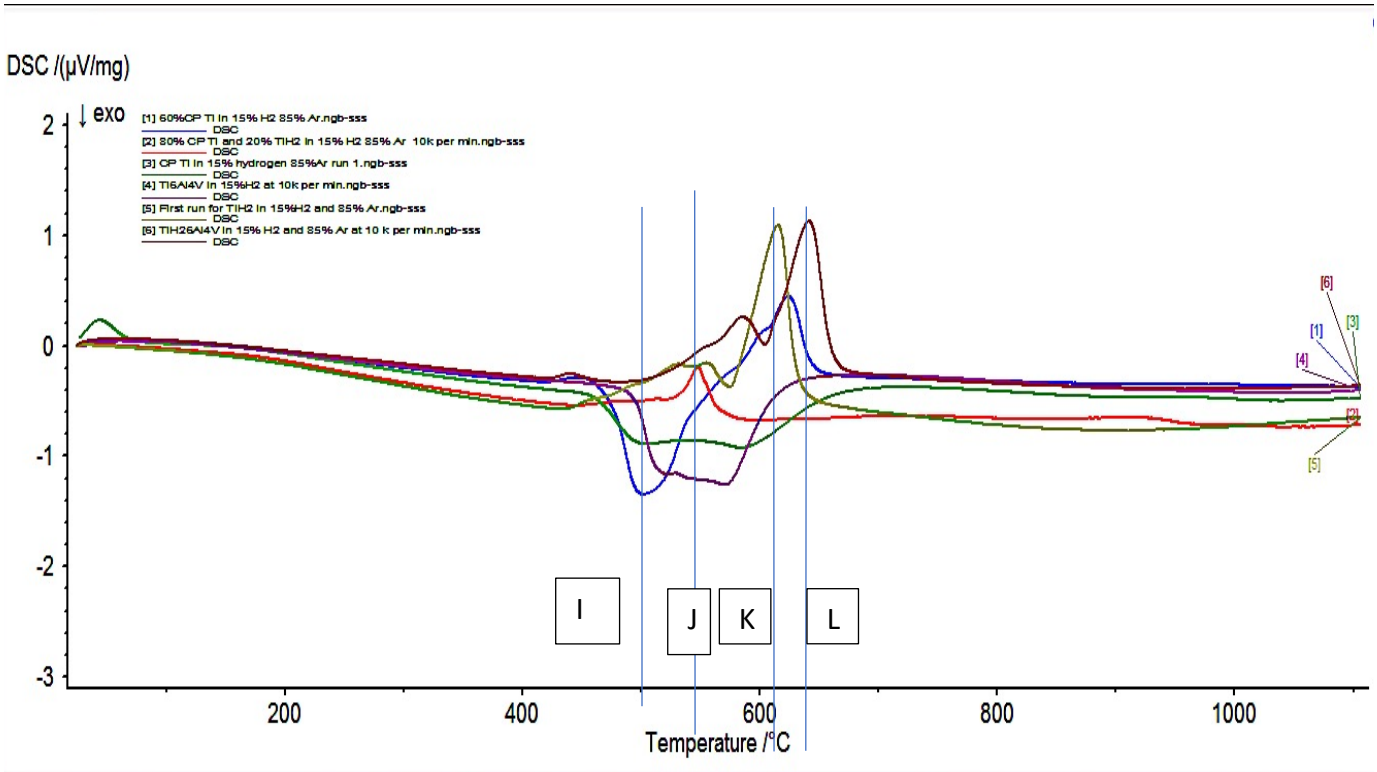

Figure 6.5: DSC curves of all powder blends in 15%H_2/85% Ar atmosphere

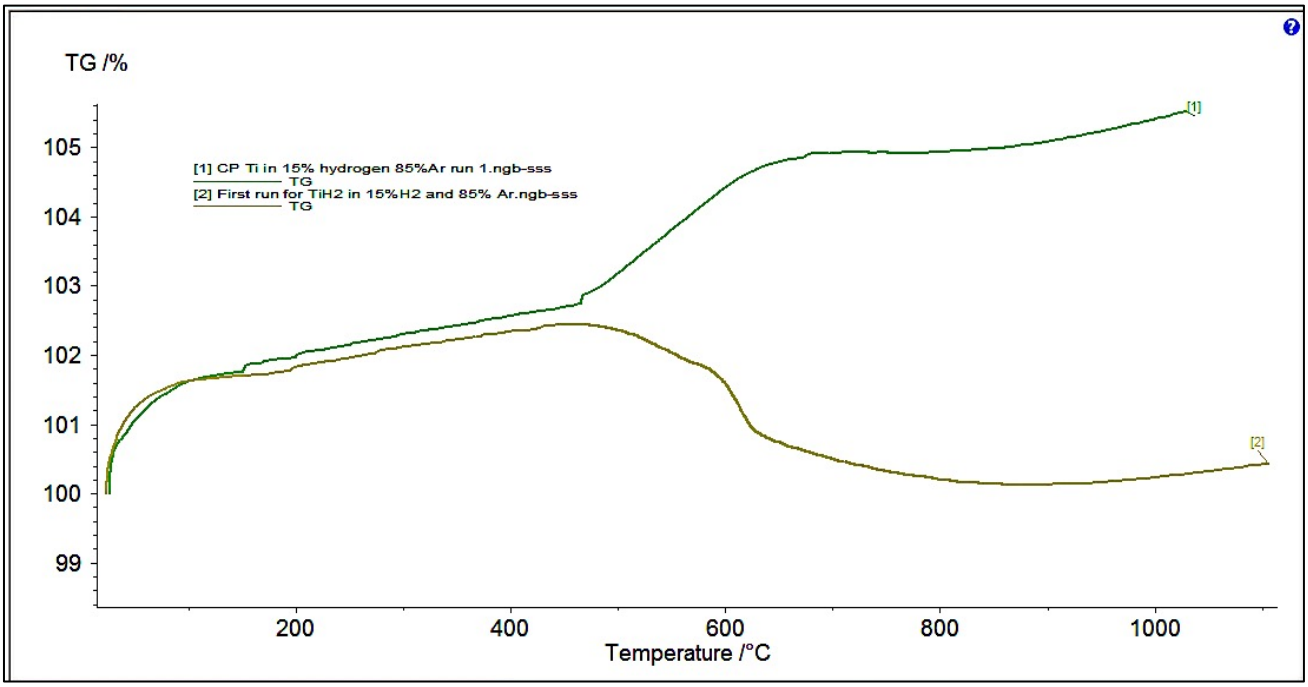

Figure 6.6: Comparative TGA curves of 100 CP Ti and TiH_2 in 15%H_2/85%Ar

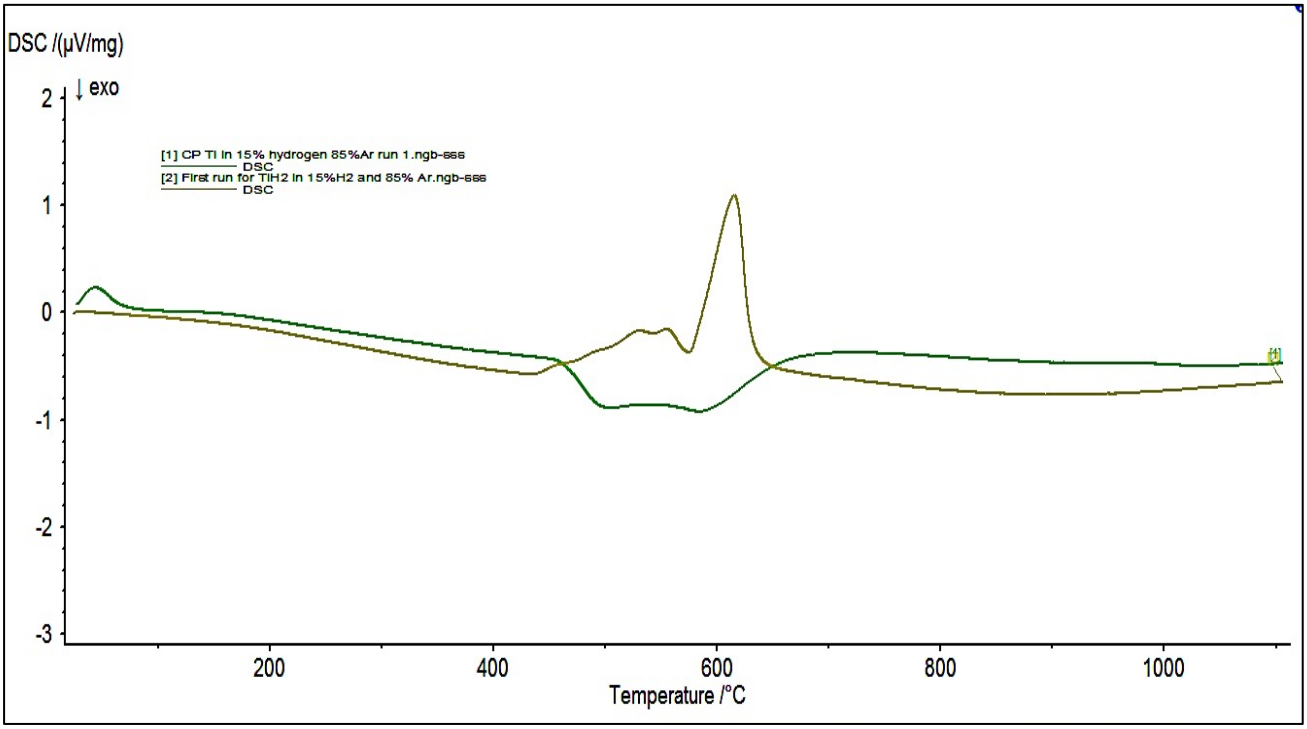

Figure 6.7: Comparative DSC curves for CP Ti and TiH_2 in 15%H_2/85%Ar

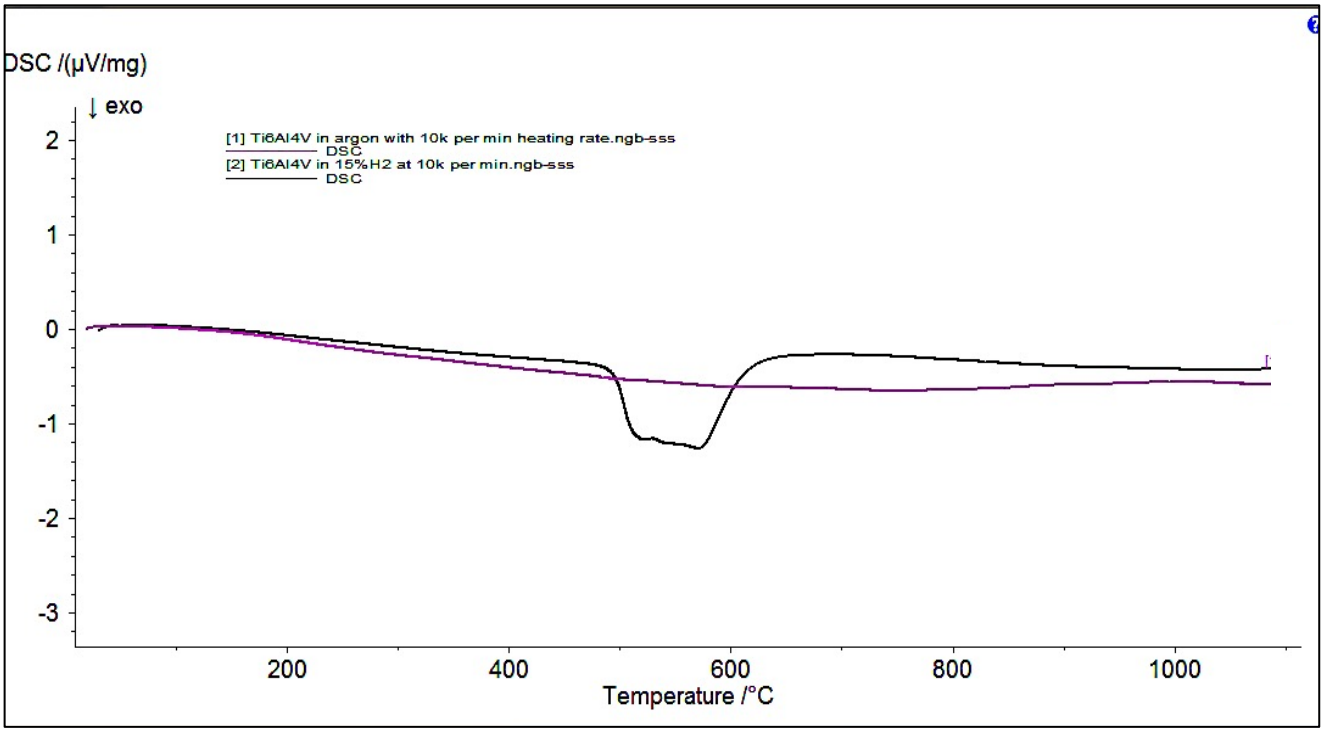

Figure 6.8 :Comparative TGA curves of Ti-6Al-4V in argon and in 15%H_2/85%Ar

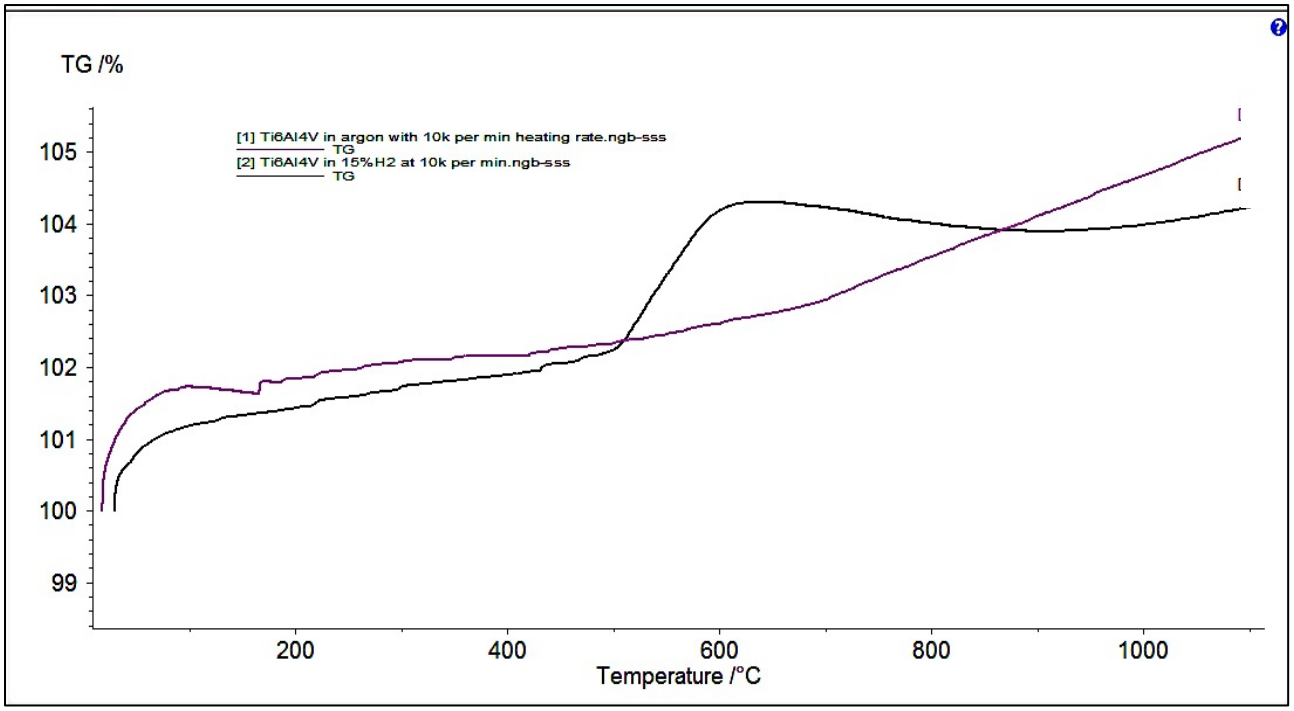

Figure 6.9: Comparative DSC curves of Ti-6Al-4V in argon and in 15%H_2/85%Ar

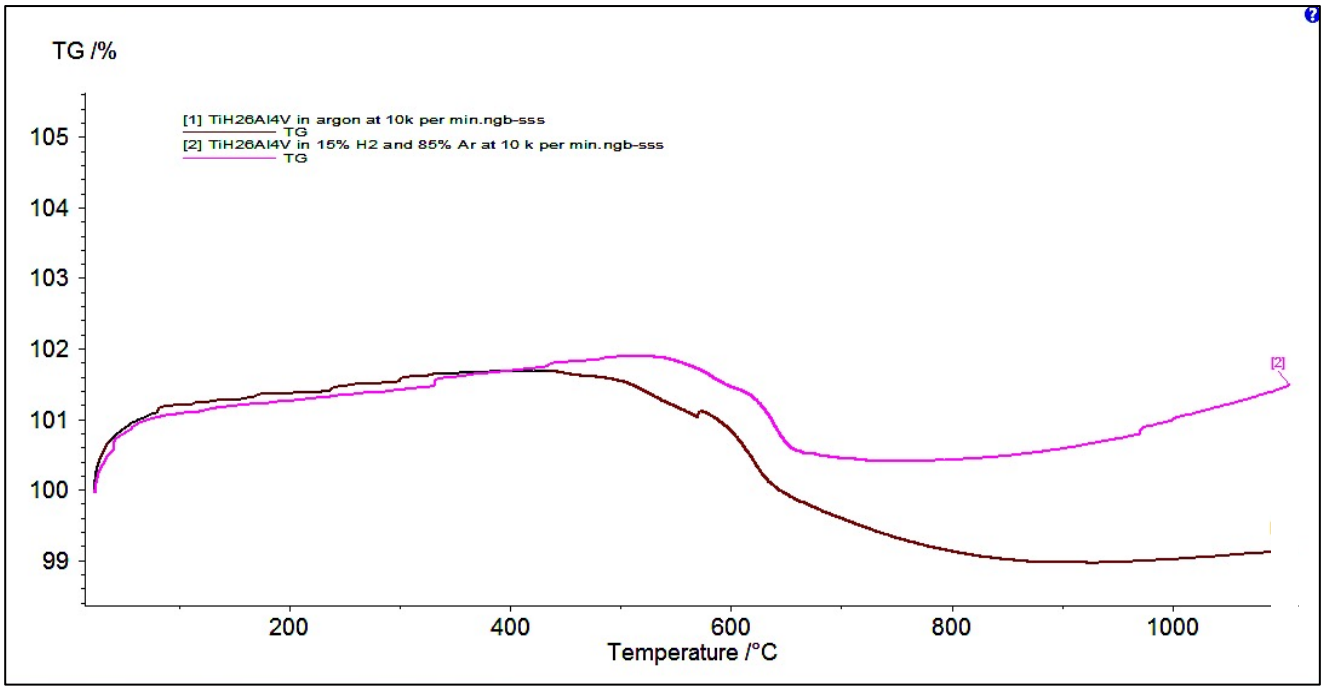

Figure 6.10: Comparative TGA curves of TiH_2-6Al-4V in argon and in 15%H_2/85%Ar

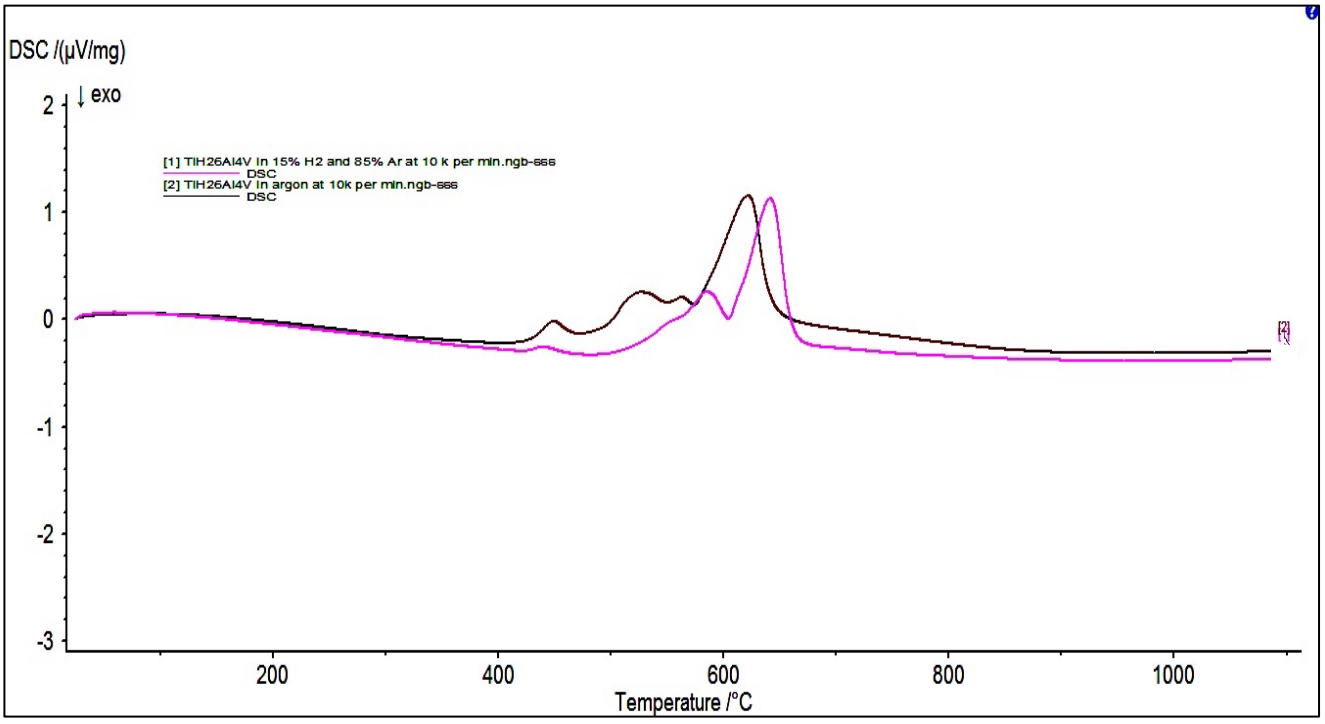

Figure 6.11: Comparative DSC curves of TiH2-6Al-4V in argon and in 15%H2/85%Ar

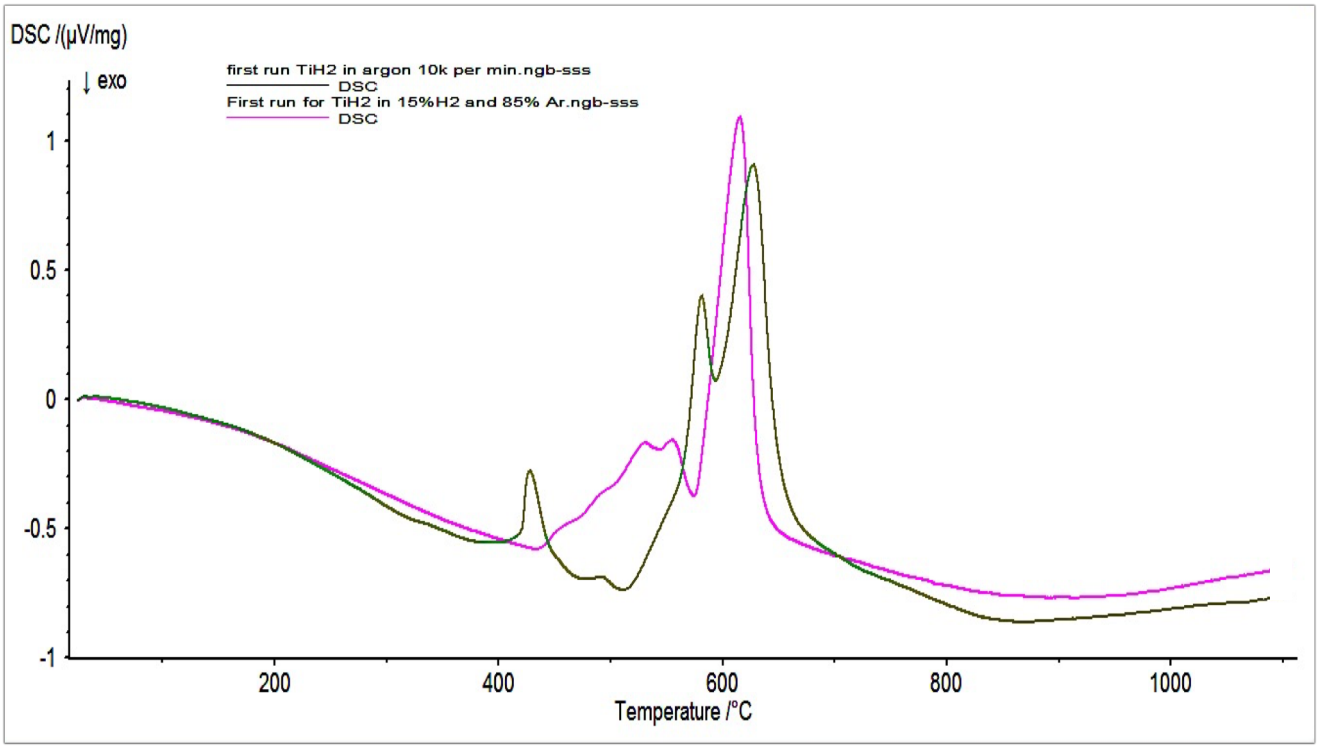

Figure 6.12 :Comparative DSC curves of TiH_2 in argon and in 15%H_2/85%Ar

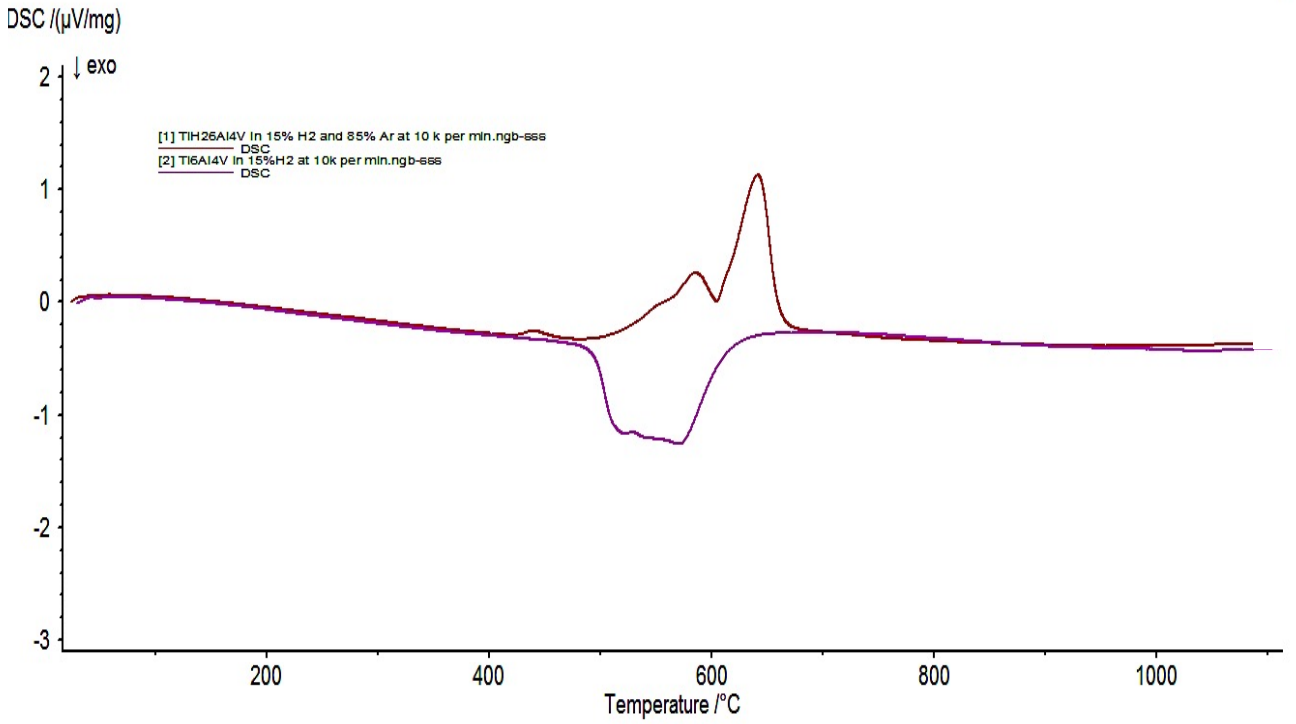

Figure 6.13: Comparative DSC curves of TiH_2-6Al-4V and Ti-6Al-4V in 15%H_2/85%Ar

The TGA and DSC curves of the various powder blends are significantly different in a partial hydrogen atmosphere as compared to an argon atmosphere. Figure 6.4 shows that for powder blends with no TiH_2 content (CP Ti and CP Ti-6Al-4V), hydrogen absorption, as expected, results in a mass increase from 470°C up to 610°C (Temperature G and H respectively from Figure 6.4). Hydrogenation of these powders begins at a temperature of 470°C up to a temperature of 610°C which is supported by the exothermic peaks on the DSC curves for CP Ti and CP Ti-6Al-4V.

Absorption of hydrogen is an exothermic reaction due to a phase transformation from α' phase to α phase and eventually to β phase and will therefore occur prior to any endothermic reactions such as dehydrogenation [38]. These results are supported by the DSC curves in Figure 6.5, which show exothermic peaks followed by endothermic peaks for powder blends containing both CP Ti and TiH_2.

For 100% CP Ti and Ti-6Al-4V, hydrogen is absorbed and dissolves in the CP Ti matrix to result in the possible formation of δ TiH_2. At higher temperatures, the hydrogen is retained in the microstructure and hence no dehydrogenation will take place. These are confirmed by the mass gain and exothermic peaks in Figure 6.4 and Figure 6.5 respectively at temperatures of 500 and 550°C (Temperature I and J). For the other powder blends containing more than 20% TiH_2, an exothermic followed by an endothermic step is observed on their respective DSC curves (the endothermic peaks are observed at higher temperatures, see Temperature K and L from Figure 6.5). The higher the level of TiH_2 in the powder blend, the higher is the enthalpy change associated with the decomposition of TiH_2.

Comparing the DSC and TGA results of the different powder blends in an argon and partial hydrogen atmosphere to determine whether there are any additional benefits in sintering in a partial hydrogen atmosphere to manufacture Ti-6Al-4V by the PM route is a key investigation. The results suggest that hydrogen is expected to be retained at slightly higher temperature if TiH_2-6Al-4V is sintered in a partial hydrogen atmosphere as compared to the same sample in an argon atmosphere (see Figure

6.11). However, the enthalpy change associated with dehydrogenation of TiH_2-6Al-4V remains the same irrespective of the atmosphere used. Whether or not the increase in dehydrogenation temperature is significant needs to be investigated further by means of sintering treatments. From a previous study that examines the behaviour of TiH_2 powder under stagnant argon atmosphere [46], it was reasonable to assume that such an environment more or less correspond to a partial hydrogen/ argon atmosphere. The reason being that under stagnant condition the argon gas does not flow which will decrease the rate of hydrogen liberation which also occurs in a partial hydrogen atmosphere. A study that examines the decomposition of TiH_2 under stagnant and flowing argon conditions shows that the phase transformation associated with dehydrogenation (endothermic peaks) occurs at a much higher temperature under stagnant conditions [46]. Therefore, it makes sense that hydrogenation can be retained at slightly higher temperature in a partial hydrogen atmosphere. These deductions are supported by Figure 6.11 and Figure 6.12. Further, the phase transformations that take place under stagnant (or partial) argon atmosphere are different when compared to a flowing argon atmosphere. The phase transformation that takes place under flowing argon conditions and stagnant conditions for TiH_2 are denoted by Sequence 1 and 2 respectively [46]. It is expected that the phase transformation that takes place under stagnant argon conditions is very similar to the phase transformation that take place in a partial hydrogen atmosphere.

Sequence 1 (flowing argon):

$$\begin{cases} \text{heating}: \ \delta \xrightarrow{432\,^\circ\text{C}} \delta+\alpha \xrightarrow{514\,^\circ\text{C}} \delta+\alpha+\beta \xrightarrow{536\,^\circ\text{C}} \alpha+\beta \xrightarrow{702\,^\circ\text{C}} \alpha \\ \text{cooling}: \ \text{no phase transformation } (\alpha \text{ remains}) \end{cases}$$

Sequence 2 (Stagnant argon):

$$\begin{cases} \text{heating}: \ \delta \xrightarrow{448\,^\circ\text{C}} \delta+\alpha \xrightarrow{578\,^\circ\text{C}} \delta+\alpha+\beta \xrightarrow{620\,^\circ\text{C}} \alpha+\beta \xrightarrow{744\,^\circ\text{C}} \beta \\ \text{cooling}: \ \beta \xrightarrow{568\,^\circ\text{C}} \beta+\alpha \xrightarrow{264\,^\circ\text{C}} \beta+\alpha+\delta \xrightarrow{157\,^\circ\text{C}} \alpha+\delta \end{cases}$$

The main difference between these two sequences is the phase transformation that takes place during the cooling phase under stagnant conditions which can be equivalent to a partial hydrogen atmosphere. Additionally, the temperatures at which the first three phase transformations occurs is higher under stagnant (partial hydrogen/ argon atmosphere) conditions. These results are again supported by the

DSC results obtained in Figure 6.5. Hence, the assumption made that the stagnant argon atmosphere can be equivalent to a partial hydrogen/argon atmosphere is valid. Moreover, under partial hydrogen/argon atmosphere the structure is fully β after temperature equivalent to or higher than 744°C whereas in a flowing argon atmosphere the phase present after 702°C is α. It can be thus expected that sintering under argon is most likely going to stabilise the α phase and correspondingly sintering under a partial hydrogen atmosphere will stabilise the β phase. With the introduction of MA with TiH_2, the sintering atmosphere is expected to play a vital role. It is expected that sintering TiH_2-6Al-4V in a partial hydrogen atmosphere will allow vanadium (a β stabiliser) to diffuse at a faster rate since the latter stabilises the β phase. Hence, a TiH_2-6Al-4V powder blend compact sintered in a flowing argon atmosphere is expected to promote faster diffusion of aluminium (an α stabiliser) thus stabilising the α phase. Thus, sintering trials of these TiH2-6Al-4V powder blend compacts should be conducted in both atmospheres in order to assess and confirm whether the sequence of events described in this paragraph is in fact true. Additionally, the role than TiH_2 can play during sintering can also be investigated.

It is important to note as well that the Ti-H phase diagram is based on the fact that the highest pure solid under consistent one bar pure atmosphere is used which in turn will not allow the coexistence of α and β phase. However, the use of commercial powders can very often imply that impurities such as oxide layers are present and since oxygen is an α stabiliser, the α phase will form prior to the β phase. These impurities as well as fluctuations in experimental conditions can lead to the coexistence of the α and β phase. Hence, the reaction that takes place at 432°C is also valid for commercial TiH_2 powders which is confirmed for the DSC curves of 100% TiH_2 in Figure 6.2 but not in Figure 6.5. This adds to the benefits of using a partial hydrogen atmosphere which is thus expected to limit the formation of the α phase even if the TiH_2 powders are slightly oxidised (reducing abilities of TiH_2 that prevents oxidation).

The DSC and TGA results suggest that sintering in a partial hydrogen atmosphere will most likely be beneficial to a higher extent for CP Ti as compared to TiH_2. Additionally,

the TiH_2 used for this dissertation is smaller in size and hence sintering of finer particles is also expected to result in higher sintered densities. Hence, as discussed in Chapter 5, the level of TiH_2 that will enable reasonable green densities while maintaining good sintering properties is most likely to be a 60% CP Ti/ 40% TiH_2 powder blend. Since most sintering studies are conducted under vacuum, it would have been vital to conduct TGA and DSC of the powder blends under vacuum. However, the vibrations associated with the turbo pump prevented a smooth TGA and DSC curves to be obtained. Consequently, any mass change or exothermic or endothermic peaks were hard to distinguish with the fluctuations in mass readings that were associated with the vibrations. It is to be noted that for the other DSC/TGA analysis, the turbo pump used to remove the air (oxygen) was turned off for at least 45 minutes and the argon and partial hydrogen atmosphere were flowing at constant speed prior to the start of each test. Hence, no vibrations associated with the turbo affected the readings of the mass balance in the TGA/DSC equipment.

Chapter 7: Sintering

Based on the powder analysis, compaction study and the TGA and DSC analysis, a subset of the powder blends and a fixed compaction pressure were chosen for the sintering trials. Table 7.1 summarises the composition, number of samples as well as compaction pressure of the selected powder blends.

Table 7.1: Description of selected samples for sintering trials

Chemical composition	Compaction pressure (MPa)	Number of samples for sintering trials
100 CP Ti	500	27
80% CP Ti 20% TiH_2	500	27
60% CP Ti 40% TiH_2	500	27
CP Ti-6Al-4V	500	27
TiH_2-6Al-4V	500	27

Nine of the samples were sintered in a 15% H_2/85% argon atmosphere and another nine were sintered in argon at 1050°C for eight hours (dwell time) at a heating rate of 5K/min. Only three samples from each powder blend for each sintering treatments were used for the density measurements. The remaining were used for microstructural analysis. Additional Ti-6Al-4V and TiH_2-6Al-4V green compacts were kept for additionally sintering treatments.

7.1 Sintered density

Table 7.2 shows the relative sintered densities for the five selected sets of samples in an argon atmosphere.

Table 7.2: Sintered density of samples in argon atmosphere at 1050°C

Sample composition	Relative sintered density (%)	Relative green density (%)	Percentage increase from green to sintered state (%)
100% CP Ti	92.8±0.1	87.4±0.1	5.4
80% CP Ti/20% TiH_2	82.8±0.1	77.9±0.1	4.9

60% CP Ti/40% TiH_2	80.1±0.1	76.2±0.1	3.9
CP Ti-6Al-4V	90.8±0.1	86.4±0.1	4.4
TiH_2-6Al-4V	81.9±0.1	79.3±0.1	2.6

Table 7.2 confirms that with increasing TiH_2 content, the increase in sintered density is lower which does not favour the use of TiH_2 in an argon atmosphere. It is expected, based on the current literature [31][34][40], that TiH_2 should improve the sintered density under vacuum and thus it can be said that the sintering atmosphere plays a critical role in the densification mechanism of the samples. It is very likely, since dehydrogenation of TiH_2 takes place from 430-620°C, that the hydrogen evolved is trapped temporarily within the partially sintered samples. The presence of a positive sintering atmosphere will not enable hydrogen released to easily diffuse out as compared to a negative sintering atmosphere such as vacuum. Hence, the trapped hydrogen can hinder densification to take place rapidly particularly at temperatures lower than 1200°C. Diffusion rate generally increases with increasing temperatures and hence the diffusion rates of Ti, TiH_2, aluminium and vanadium (from the MA) is expected to be higher at 1200°C as compared to 1050°C [33][34]. At 1200°C it is less likely that the amount of hydrogen trapped is sufficient to hinder or delay densification since sufficient energy is given to allow shrinkage causing the hydrogen to be easily released. These are discussed in depth later in this chapter.

The particle size of the TiH_2 powder being significantly lower than that of the CP Ti is also expected to result in higher sintered density. Based on the particle size, the sintered densities were expected to be higher when compared to the sintered compacts with no TiH_2 content since small particles implies higher contact surface area which will result in less energy required for diffusion. While in the current literature, the densities of TiH_2 based compacts are higher when compared to CP Ti [31][33][40], the temperature and atmosphere under which sintering were conducted are different. Based on a study conducted on the sintering mechanism (discussed in Chapter 2) [47], the major shrinkage take places from 1040°C. Hence, at 1050°C, it is very likely that the densification and shrinkage of samples containing TiH_2 were not complete. However, a dwell time of eight hours used for this dissertation was

expected to allow densification and further shrinkage to take place. Further investigations on the sintering mechanism for each powder blends are required.

It is highly likely that the sintering parameters could have played a role in the unexpected results. While the samples made from 60% CP Ti/40% TiH_2 and 80% CP Ti/20% TiH_2 have lower sintered density, the biggest anomaly in the change in density was noted in the TiH_2-6Al-4V samples. In TiH_2-6Al-4V, the diffusion of the MA is expected to occur differently as compared to CP Ti-6Al-4V. In TiH_2-6Al-4V, vanadium is expected to diffuse first since TiH_2 is a β-stabiliser whereas in CP Ti-6Al-4V, aluminium should diffuse first (temperatures below 910°C). The possible sequence of events that could occur based on the MA particle diffusion being different for TiH_2-6Al-4V and CP-ti-6Al-4V is discussed further in Section 7.3 of this chapter since microstructural analysis was also deemed necessary to investigate whether the density results correlates to the microstructural analysis obtained for the respective samples. More experiments were conducted to ensure that the results were reproducible and to determine any difference in sintered density when similar samples were sintered under a partial hydrogen atmosphere as well as under vacuum.

Table 7.3 shows the relative sintered densities for the five selected sets of samples in a partial hydrogen atmosphere.

Table 7.3: Density results of samples sintered in a 15% H_2/85% Ar atmosphere at 1050°C

Sample composition	Relative sintered density (%)	Relative green density (%)	Percentage increase from green to sintered state (%)
100% CP Ti	91.2±0.1	87.4±0.1	3.8
80% CP Ti/20% TiH_2	85.2±0.1	77.9±0.1	7.3
60% CP Ti/40% TiH_2	89.9±0.1	76.2±0.1	13.7
CP Ti-6Al-4V	93.2±0.1	86.4±0.1	6.8
TiH_2-6Al-4V	71.3±0.1	79.3±0.1	-8.0

TiH_2-6Al-4V (second set)	71.5±0.1	79.3±0.1	-7.8

Table 7.3 shows a considerable improvement in the sintered densities for samples containing both CP Ti and TiH_2.The densities were calculated as per method described in ASTM B962 The presence of a partial hydrogen atmosphere assists in improving the sintered density but this is likely due to the dissolution of hydrogen in the CP Ti matrix. As observed in the TGA and DSC studies, hydrogen is not retained after 620°C in TiH_2 (see Figures 6.1, 6.2, 6.4 and 6.5). Hence, based on the density results from Table 7.3 and the TGA and DSC results of powder blends samples tested in the same atmosphere (partial hydrogen atmosphere), it can be said that even though hydrogen (from the TiH_2) is not retained, the positive impacts of hydrogen absorption and dissolution in the CP Ti matrix is sufficient enough to result in good densification being achieved at 1050°C. Hydrogen, when absorbed in the CP Ti matrix, results in the phase transformation from α to β occurring at a much lower temperature [47]. The phase transformation is associated with shrinkage which improves the sintered density. In addition, the reducing ability of hydrogen also prevents the formation of any surface oxides present in the CP Ti and hence improves diffusion contact between particles.

Based on the unexpected decrease from the green to sintered densities of the TiH_2-6Al-4V samples in a partial hydrogen atmosphere, additional TiH_2-6Al-4V and CP Ti-6Al-4V samples were sintered under vacuum at 1050°C for eight hours and at 1200°C for four hours. The sintering trials under vacuum at 1200°C for four hours were conducted in past research [27][41][42] and hence it was deemed vital to also establish whether similar relative sintered densities could be obtained for the TiH_2-6Al-4V and CP Ti-6Al-4V samples prepared for this dissertation. Additionally, sintering trials were also conducted for CP Ti-6Al-4V and TiH_2-6Al-4V at 1200°C in a 15%H_2/85% Ar atmosphere to establish whether the sintering temperature could be the cause for the low relative sintered densities of TiH_2-6Al-4V. Table 7.4 shows the results of the relative sintered densities for the additional sintering trials.

Table 7.4 : Density results of additional sets of sintering trials

Sample composition and sintering conditions	Relative sintered density (%)	Relative green density (%)	Percentage increase from green to sintered state (%)
CP Ti-6Al-4V at 1050°C for 8 hrs under vacuum	93.8±0.1	86.4±0.1	7.4
TiH_2-6Al-4V at 1050°C for 8 hrs under vacuum	95.0±0.1	79.3±0.1	15.7
CP Ti-6Al-4V at 1200°C for 4 hrs under vacuum	97.6±0.1	86.4±0.1	11.2
TiH_2-6Al-4V at 1200°C for 4 hrs under vacuum	98.5±0.1	79.3±0.1	19.2
CP Ti-6Al-4V at 1200°C for 4 hrs in 15%H_2/85%Ar	97.1±0.1	86.4±0.1	10.7
TiH_2-6Al-4V at 1200°C for 4 hrs in 15%H_2/85%Ar	97.7±0.1	79.3±0.1	18.4

Figure 7.1 graphically shows a comparative analysis of the relative green and sintered densities in various sintering atmospheres and times. The results of the additional sintering trials summarised in Table 7.4 confirm that the relative densities of CP Ti-6Al-4V and TiH_2-6Al-4V sintered at 1200°C under vacuum are similar to the results of past research conducted (relative sintering density >97%) [41]. In addition, the CP Ti-6Al-4V and TiH_2-6Al-4V sintered in a partial hydrogen atmosphere at 1200°C did result in a significant increase from green to sintered density. The temperature of 1200°C, irrespective of the sintering atmosphere does result in relative sintered densities to be higher than 97% which, are reasonable. At 1200°C, diffusion rates are higher for CP Ti, TiH_2, aluminium and vanadium (from the MA) and hence the sequence of events that is expected to take place at 1050°C can be completely different at 1200°C. This is discussed further in Section 7.3 of this chapter.

It is important to note here, that sintering in a partial hydrogen atmosphere does not result in the highest sintered densities. The results support that sintering under vacuum results in the best sintered densities at 1050°C and 1200°C.

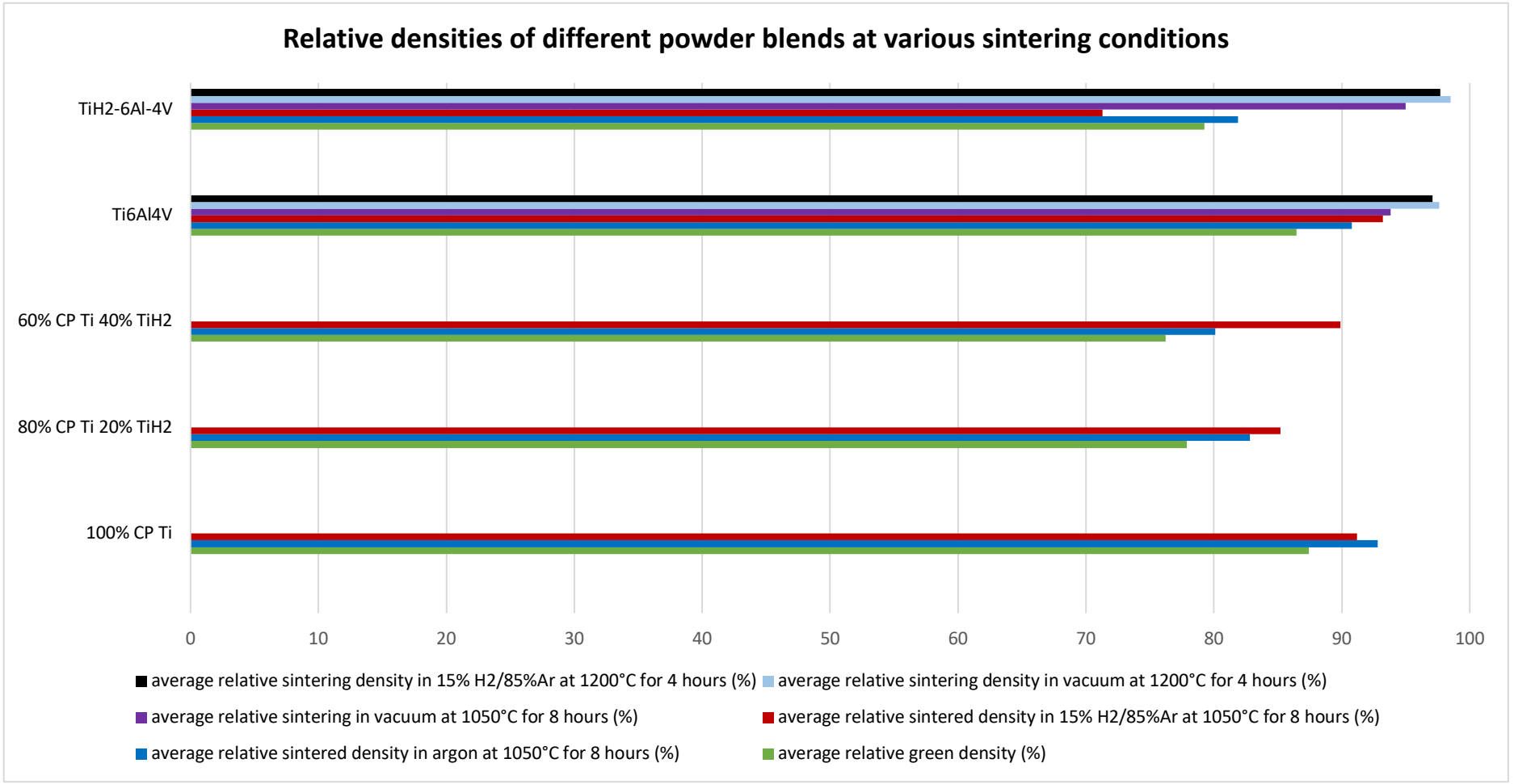

Figure 7.1 :Comparative density from green to sintered in different atmospheres

7.2 Microstructural analysis

Figures 7.2-7.5 show the microstructure of the various samples sintered under an argon atmosphere, under partial hydrogen and under vacuum at 1050°C for eight hours and at 1200°C under vacuum and partial hydrogen atmosphere for four hours respectively.

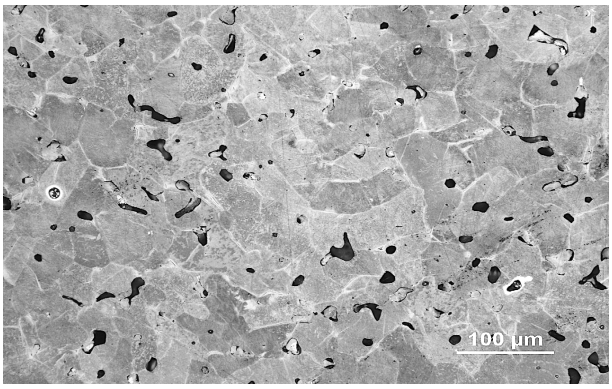

(a)

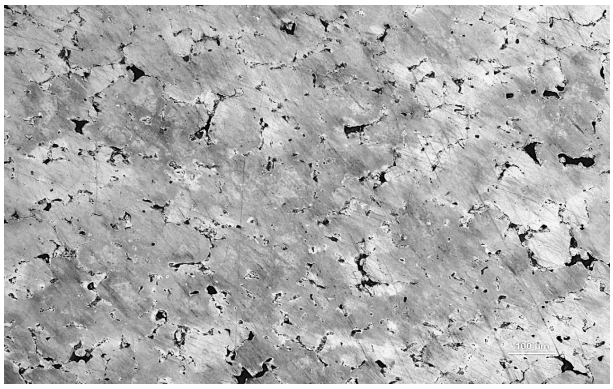

(b)

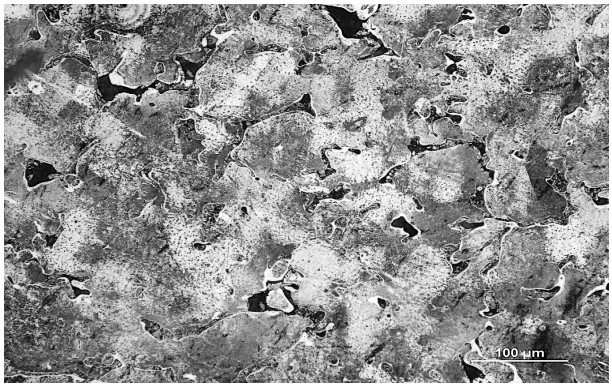

(c)

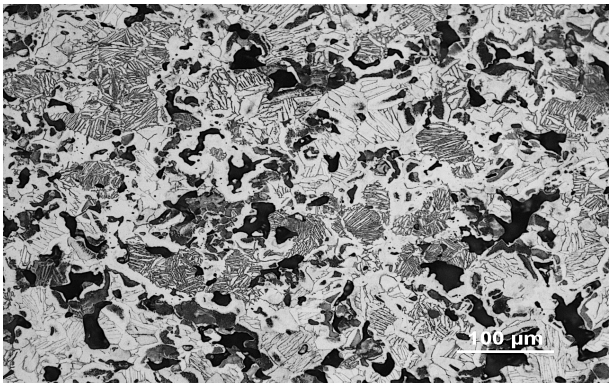

(d)

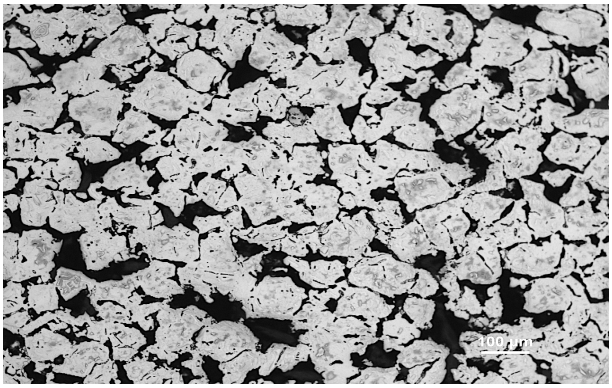

(e)

Figure 7.2: Microstructure of sintered 1050°C for 8 hours under argon (a) 100% CP Ti, (b) 80% CP Ti/20%TiH_2, (c) 0% CP Ti/40%TiH_2, (d) CP Ti-6Al-4V (e) TiH_2-6Al-4V

The microstructure of the 100% CP Ti corresponds to an α-equiaxed microstructure. The CP Ti-6Al-4V sample sintered in argon has a Widmanstätten structure showing the presence of α and β phases as expected.

Figure 7.3 show the representative microstructures of the five different set of samples sintered at 1050°C for eight hours in a partial hydrogen atmosphere (15%H_2/85% Ar).

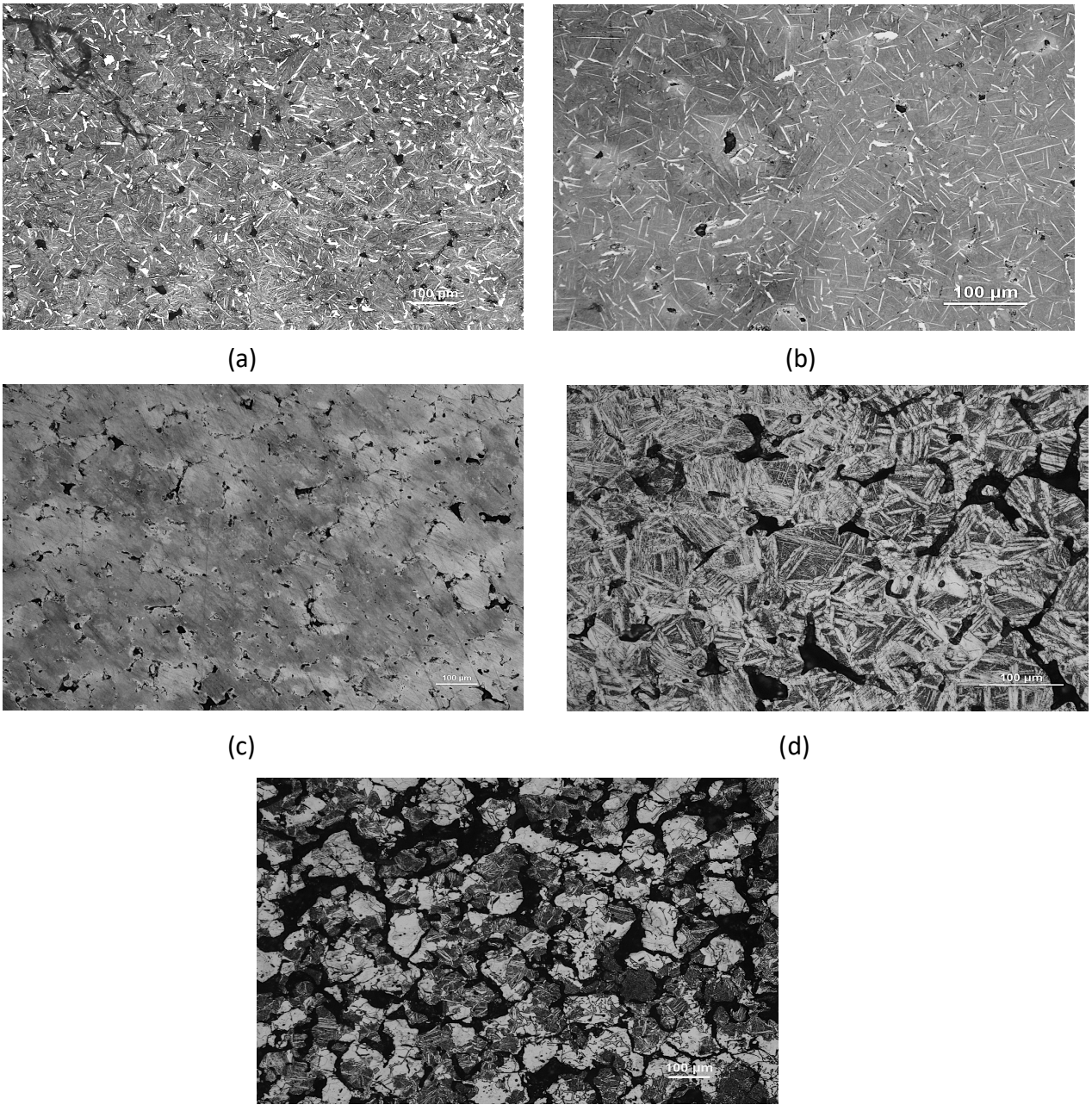

(a) (b)

(c) (d)

(e)

Figure 7.3: Microstructure of sintered 1050°C for 8 hours under 15%H_2/85% Ar (a) 100% CP Ti, (b) 80% CP Ti/20%TiH_2, (c) 0% CP Ti/40%TiH_2, (d) CP Ti-6Al-4V (e) TiH_2-6Al-4V

The microstructure of the 100% CP Ti, 80% CP Ti/20% TiH_2 and 60% Ti/40% TiH_2 have similar microstructures where the most noticeable feature is the presence of needle like structure suggesting the presence of the δ TiH_2 phase. This confirms that hydrogen dissolved in the CP Ti matrix. The microstructure confirms that sintering in a partial hydrogen atmosphere does improve the relative sintered density of these three samples since less pores are observed. Hydrogen (being a β stabiliser) lowers the β-transus temperature to promote densification at a lower temperature. Thus at 1050°C, the densification was higher for the CP Ti/ TiH_2 blends sintered in hydrogen as compared to those sintered in argon. Thus, there are positive attributes in sintering in hydrogen which occurs as a result of hydrogen dissolving in the CP Ti matrix. Hydrogen is only retained during sintering by dissolving in the CP Ti matrix and not due to the presence of TiH_2 in a positive pressure atmosphere.

The microstructure of CP Ti-6Al-4V does show an α Widmanstätten structure as expected.

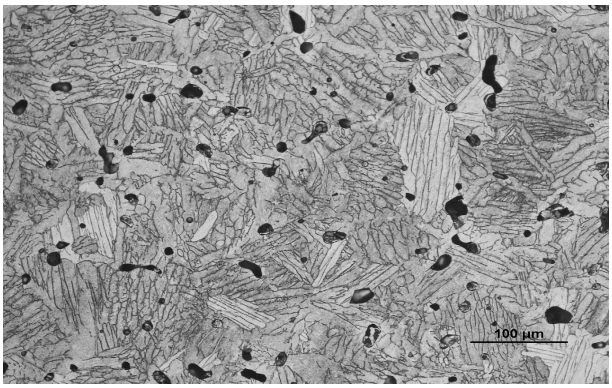

(a)

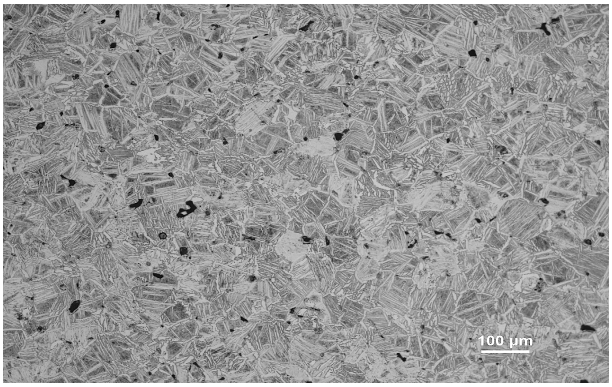

(b)

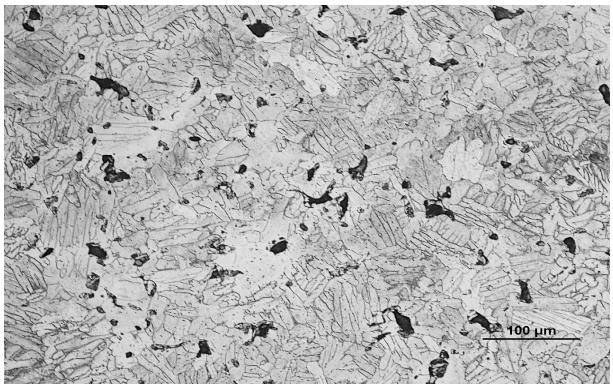

(c)

Figure 7.4 : Microstructure of sintered CP Ti-6Al-4V at (a) 1050°C for 8 hours under vacuum (b) 1200°C for 4 hours under vacuum (c) 1200°C for 4 hours under 15%H_2/85% Ar

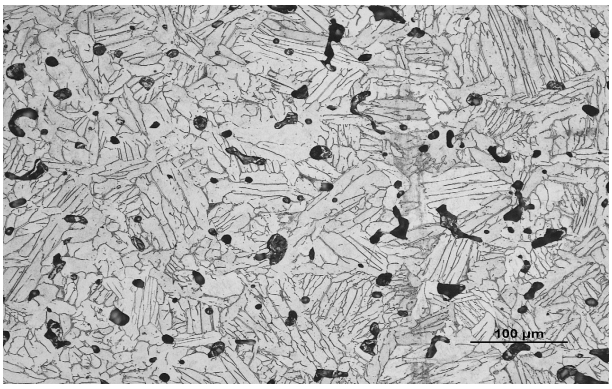

(a)

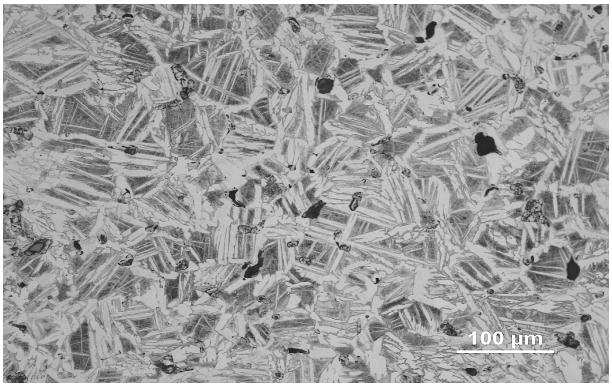

(b)

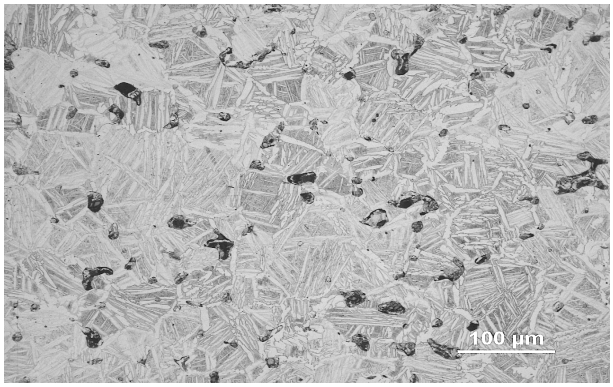

(c)

Figure 7.5: Microstructure of sintered TiH_2-6Al-4V at (a) 1050°C for 8 hours under vacuum(b) 1200°C for 4 hours under vacuum (c) 1200°C for 4 hours under 15%H_2/85% Ar

The density results are supported by the microstructural investigation conducted. The presence of TiH_2 should result in higher diffusion rate since the particle size is smaller (greater surface area for contact). The presence of hydrogen in TiH_2 also prevents the formation of surface oxides which again promote sintering by lowering the activation energy required for sintering.

The samples with the higher sintered densities are those sintering under vacuum at 1200°C for four hours. It is evident that the best sintering atmosphere for the CP Ti-6Al-4V and TiH_2-6Al-4V is vacuum. A higher sintering temperature results in better sintered densities for a shorter sintering time. The sintering of TiH_2-6Al-4V in partial hydrogen also supports the results in the current literature (>97%) [27][43] which confirms that the methodology used for the sintering treatments were correct. It is

evident from this additional set of sintering trials that sintering of TiH_2-6Al-4V at 1050°C may be different. Possible explanation for this anomaly is explained in depth in Section 7.3.

7.3 CP Ti-6Al-4V and TiH_2-6Al-4V in 15% H_2/85% Ar atmosphere at 1050°C

While the sintered density obtained for CP Ti-6Al-4V in partial hydrogen is expected (higher than the sintered density in argon), that of TiH_2-6Al-4V in the partial hydrogen atmosphere shows that the sintered density of the sample is lower than not only its corresponding sintered density in argon but also its green density. The results are supported by the microstructural analysis (see Figure 7.3). The possible sequence of events and phenomenon that is taking place during sintering of CP Ti-6Al-4V and TiH_2-6Al-4V compacts in a partial hydrogen atmosphere are explained in detail in this section.

During sintering of CP Ti-6Al-4V in a partial hydrogen atmosphere, the MA will diffuse into CP-Ti matrix but aluminium will diffuse much faster than vanadium and hence the α-phase is stabilised in preference to transformation to the β-phase. However, because hydrogen stabilises the β-phase in TiH_2, the MA diffuses into the Ti (H) matrix during sintering but as opposed to CP Ti it is expected that vanadium will diffuse faster in preference to aluminium because the β-phase already exists. Thus, the preferable vanadium diffusion (which will deplete the MA of vanadium) will result in aluminium enrichment in the decomposing MA particle. Consequently, the aluminium can melt and thus lead to melt-related porosity developments which eventually leads to lower density realisation for the partially sintered TiH_2-6Al-4V compact. To better explain this sequence of events schematic drawings in Figure 7.6 are demonstrated. In both figures, the thickness of each arrow is directly proportional to the diffusion rate of the element. The green arrow is for vanadium diffusion in β-TiH_2, the black arrow is for Ti diffusion into the MA particle and the orange arrow is for aluminium diffusion in β-TiH_2 [41].

Onset of sintering: Stage 1

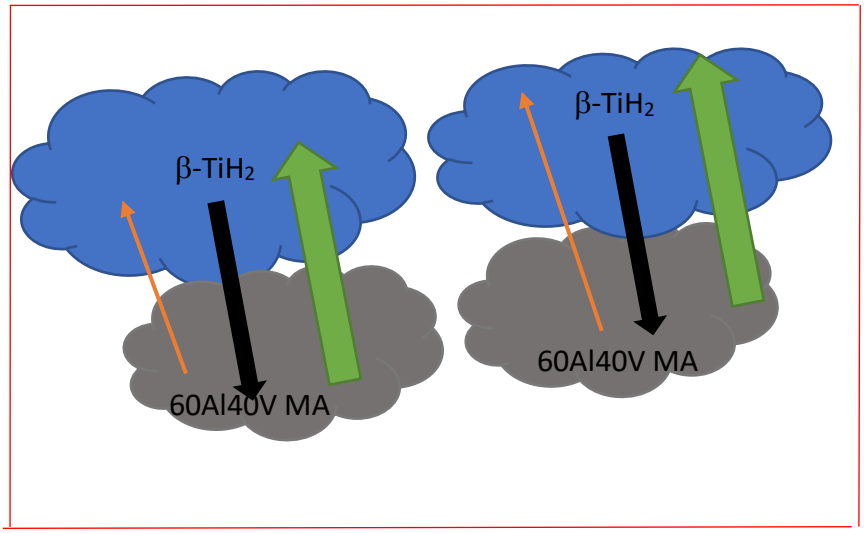

As diffusion takes place: Stage 2; fragmentation of MA particles causing gas between primary Ti particles and MA to increase

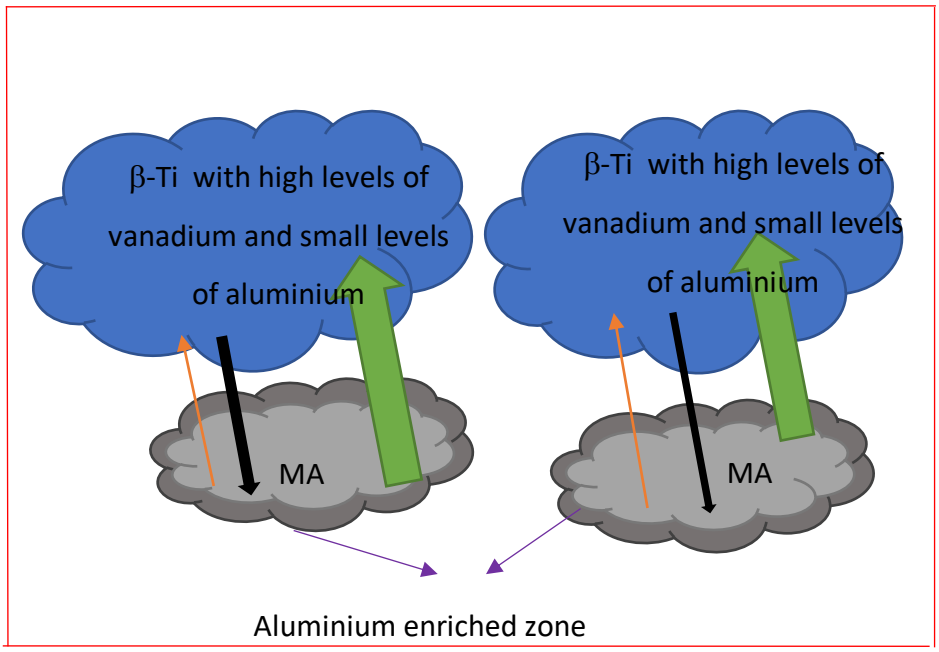

Sintering from 660°C: Stage 3 (gaps formed during volume expansion can no longer be healed as no more diffusion is taking place)

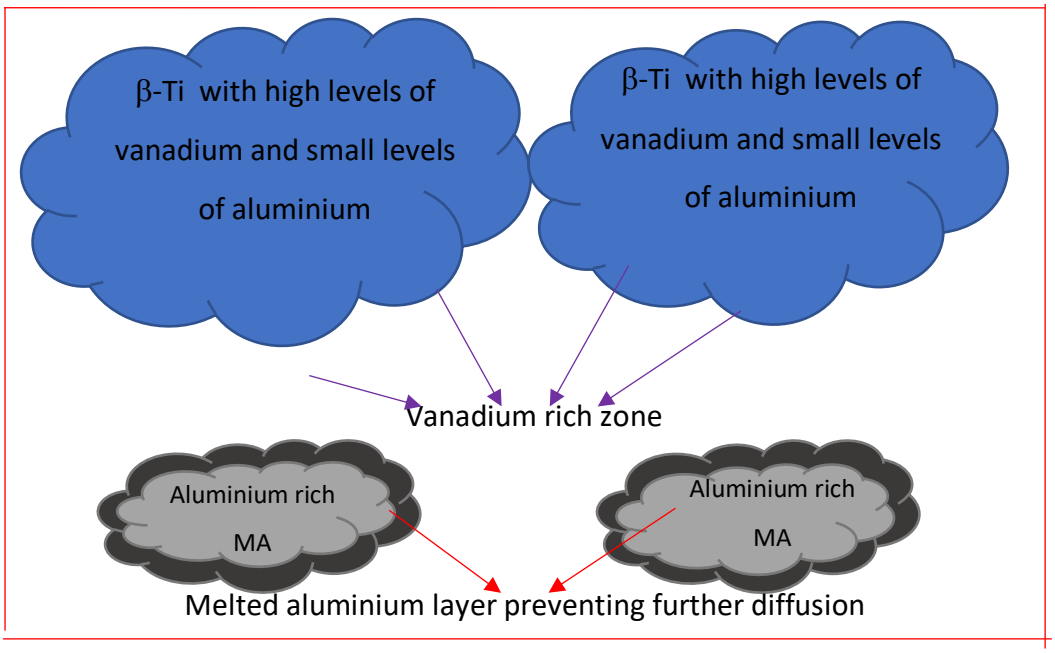

Figure 7.6: Schematic drawing of the sequence of events during sintering of TiH_2-6Al-4V at 1050°C in 15%H_2/85%Ar atmosphere

The sequence of events described in Figure 7.6, Stage 1-3, are as follows:

1) Stage 1: TiH_2 and Ti(H) is a β-stabiliser and should promote diffusion of vanadium (also a β-stabiliser). Hence, the diffusion rate of vanadium is the highest. Small levels of aluminium will also diffuse but are insignificant as compared to the levels of vanadium. TiH_2 also diffuses slightly into the MA particles but at a lower diffusion rate.
2) Stage 2: As vanadium diffuses in TiH_2 now in the β-Ti phase, the titanium matrix further stabilisers the β phase which, further hinders aluminium diffusion into the titanium matrix. Thus, the resulting MA particles are enriched in aluminium specifically at the contact interface where diffusion takes place.
3) Stage 3: As from 660°C, aluminium melts and thus the enriched aluminium zones form a melted layer around the edges of the MA particles, which prevents further diffusion from taking place. Thus, the pores formed from

Stage 1 and 2 as a result of diffusion, can no longer be closed or healed since diffusion of aluminium cannot take place.

To investigate whether or not this sequence of events described in Figure 7.6 is taking place during sintering, a few element maps were generated using the SEM on the TiH_2-6Al-4V and CP Ti-6Al-4V compacts made from heating 150mg of each powder blend in the DSC/TGA heating furnace at a rate of 10K/min up to a temperature of 1000°C under 15%H_2/85%Ar atmosphere for 2 hours. Several other samples sintered at 1050°C for longer periods were also investigated. However, the long sintering treatment would not provide any indication of the initial diffusion of TiH_2-6Al-4V and CP Ti-6Al-4V sample. Figures 7.7 and 7.8 show representative element maps for both samples.

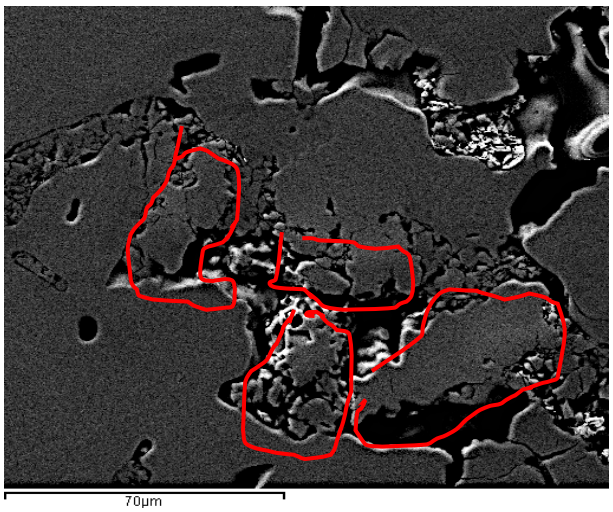

SEM image of selected area

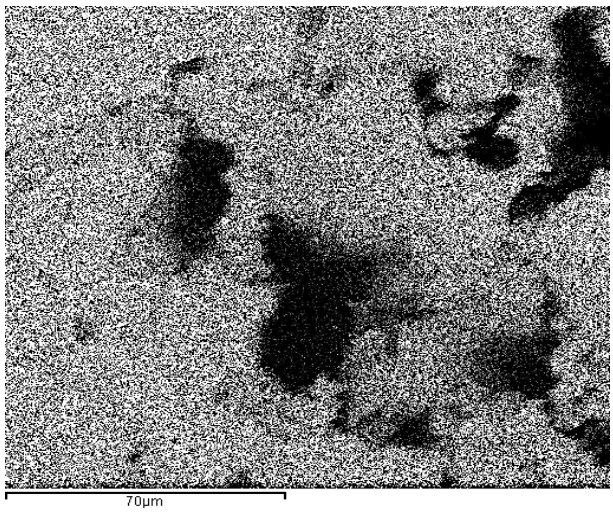

Titanium element map

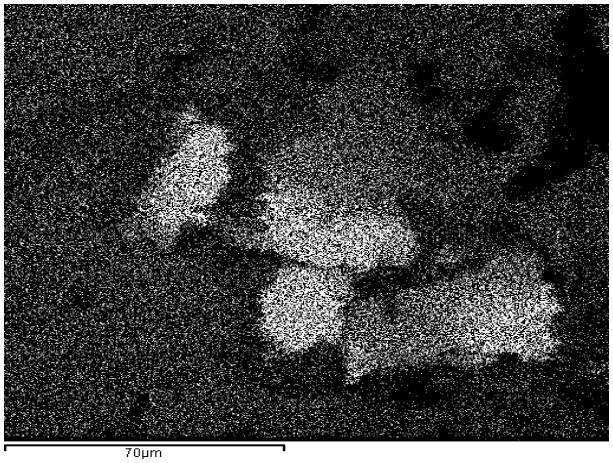

Vanadium element map

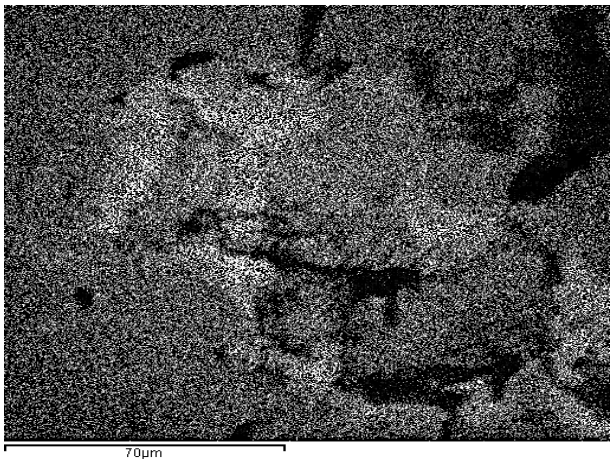

Aluminium element map

Figure 7.7: Elemental mapping of CP Ti-6Al-4V partially sintered at 1000°C (decomposing MA particle circled in red)

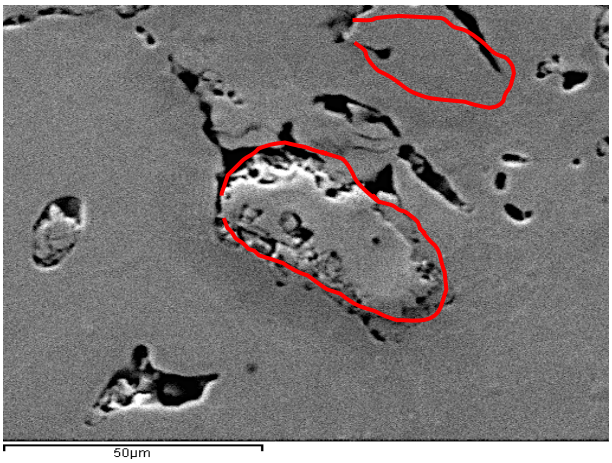

SEM image of selected area

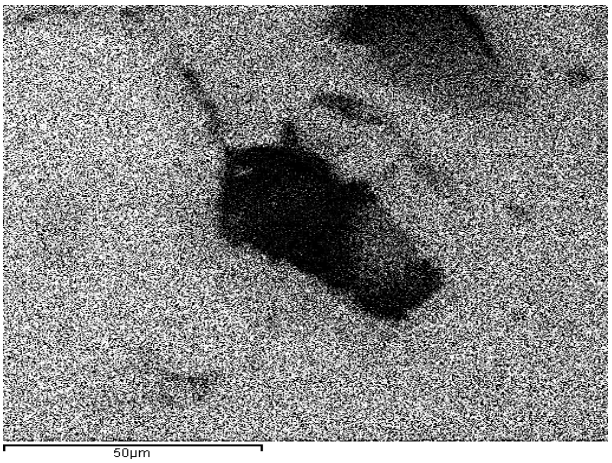

Titanium element map

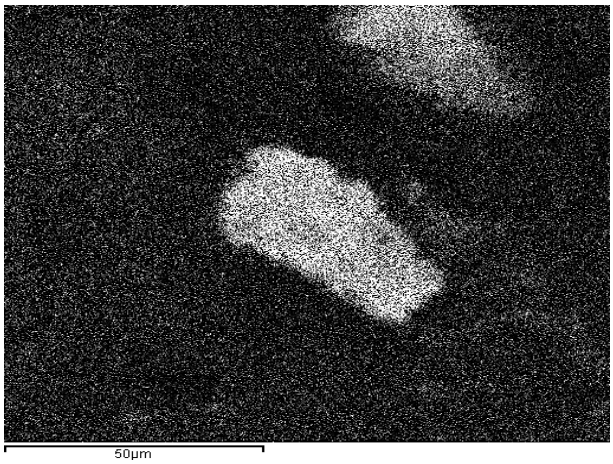

Vanadium element map

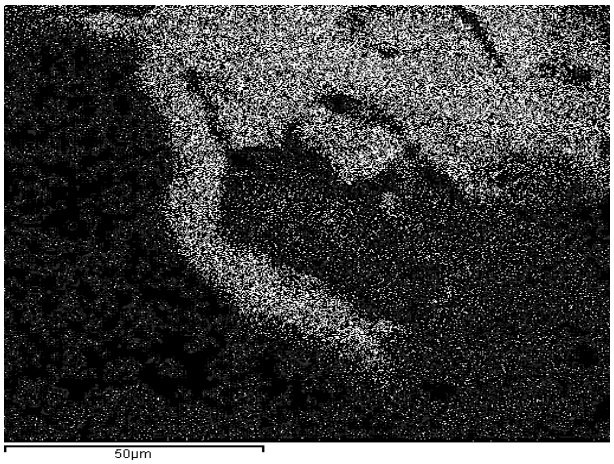

Aluminium element map

Figure 7.8: Elemental mapping of TiH_2-6Al-4V partially sintered at 1000°C (decomposing MA particle circled in red)

In both Figures 7.7 and 7.8 it is vital to emphasise that the element maps are the results of the X-rays maps from the image generated by the SEM. The brightness of the pixels in the X-ray maps indicates the relative concentration of the particular element. Figure 7.7 shows that for partially sintered CP Ti-6Al-4V, aluminium enrichment takes place in the outer shell of the CP-Ti particles which supports the description provided at the beginning of this section. However, the sequence of events described by Figure 7.6 for TiH_2-6Al-4V is not supported by the elemental mapping provided in Figure 7.8.

The latter exhibits the same characteristics as for the CP-Ti-6Al-4V sample during heating. This can now be explained by not referring to the diffusion path according to the Ti-H phase diagram (see Figure 6.3) but rather according to the shell model in a previous study described in Chapter 2 [46]. In this case, the α-phase formation in the shell will support the preferable aluminium diffusion which would suggest that CP-Ti-6Al-4V and TiH_2-6Al-4V should behave in a similar manner during sintering and hence should realise similar densities. Additionally, one would expect the TiH_2-6Al-4V sample to have greater density because of the reducing action of the liberated hydrogen but this is not the case. The significantly lower sintered density of TiH_2-6Al-4V is very likely due to the liberation of H_2O (gas) which can result in open porosity during sintering. Hydrogen from TiH_2 can be trapped during sintering especially when it takes place in a stagnant or partial hydrogen atmosphere. The formation of H_2O (g) takes place if the hydrogen from TiH_2 reacts with the surface oxide. This can be the case during sintering since the hydrogen concentrations are high enough on the oxide surface due to the difference in diffusion rate between the TiH_2 particles and that of its oxide layer. The reaction that takes place is shown in Equation 7. 1.

Equation 7. 1 $TiO_2 + 4H = Ti + 2H_2O$ (g)

The sintering behaviour of CP Ti and that of TiH_2 are compared in Figure 7.9 which allows one to obtained and idea of the sintering mechanism that takes in compacts made from CP Ti and TiH_2 powder blends with MA.

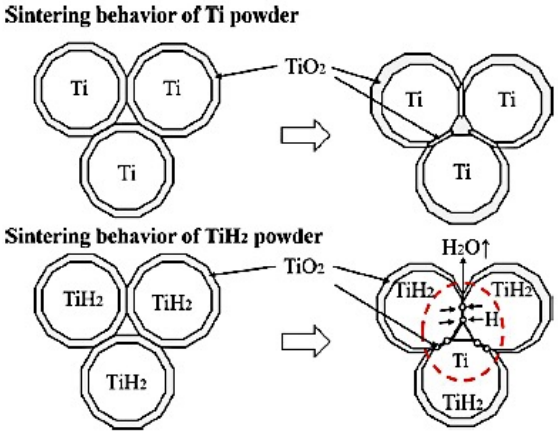

Figure 7.9: Sintering behaviour of CP Ti and TiH_2

The release of H_2O (g) as seen in Figure 7.9 will result in the formation of pores which are not necessarily overcome especially at lower sintering temperatures. At higher temperatures hydrogen diffusion rate is higher and hence H_2O (g) release occurs at a faster rate since the hydrogen is less likely to be trapped. Hence, sintering at 1200°C is less likely to result in H_2O (g) formation as a result of faster diffusion rate of hydrogen. Additionally, for sintering at 1050°C under vacuum (a negative pressure atmosphere) the rate of formation of the H_2O (g) formed is expected to be higher. Under vacuum hydrogen easily diffuses out as compared to a positive pressure sintering atmosphere such as argon or partial hydrogen. The difference in partial pressure between the TiH_2-6Al-4V sample under vacuum is higher as compared to the same sample under argon or partial hydrogen atmosphere. The higher the difference in partial pressure, the higher is the diffusion rate of hydrogen from the sample to the sintering atmosphere. Since trapped hydrogen can hinder densification sintering under vacuum is expected to result in better densification (better sintering densities and corresponding microstructures with less pores) as compared to the corresponding samples sintered in argon or partial hydrogen atmosphere.

Additionally, the Kirkendall effect [43] can also affect the sintered densities. This is illustrated in Figure 7.10. The green, orange and black arrows correspond to vanadium, aluminium and β-TiH_2 diffusion rate. The thicker the arrow the faster is the diffusion rate.

Stage 1: Difference in diffusion rate of TiH_2 and MA powder particles

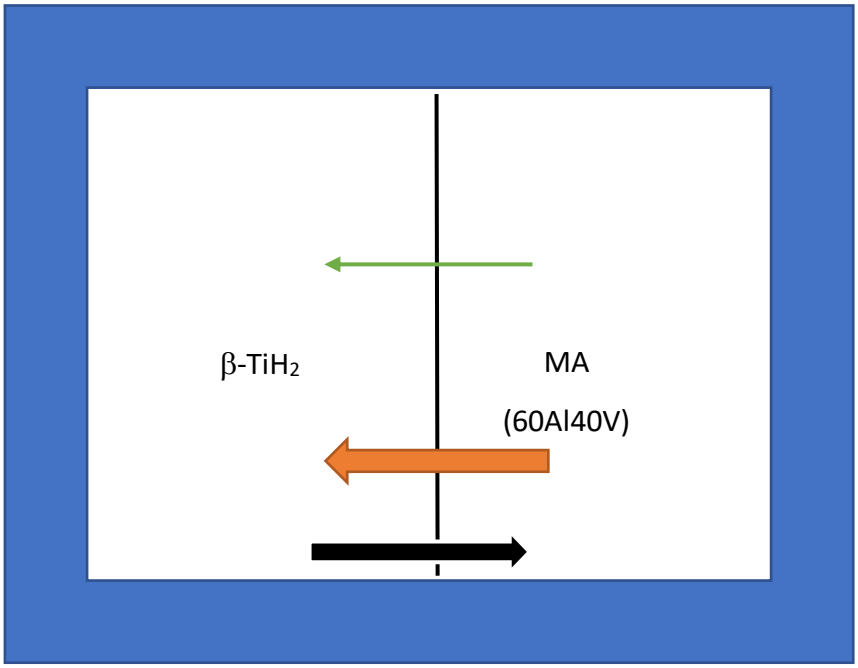

Stage 2: Diffusion rate is higher for vanadium hence motion of the boundary layer shift resulting in a formation of pore between the TiH_2 particles and the MA powder particle

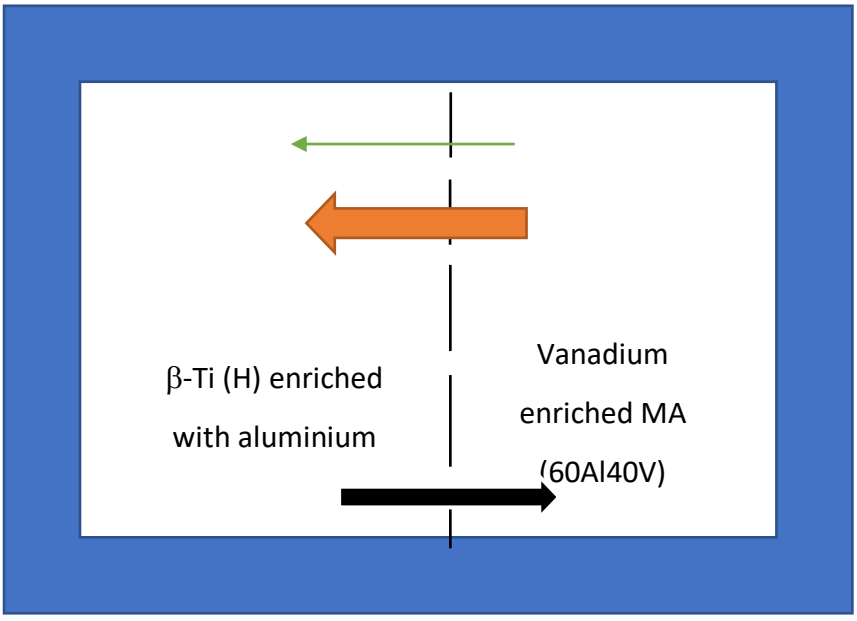

Figure 7.10: Kirkendall effect during sintering of TiH_2-6Al-4V

In addition to the production and liberation of H_2O (g) illustrated in Figure 7.9 the occurrence of the Kirkendall effect can also affect the sintered density of TiH_2-6Al-4V. Kirkendall effect takes place since the diffusion rate of vanadium, TiH_2 and aluminium are different at 1050°C in a partial hydrogen atmosphere. This difference in diffusion results in the motion of the boundary layer as depicted in Stage 2 of Figure 7.10. Thus, as a result of the Kirkendall effect, pores are formed. This residual porosity and consequent swelling as a result of phase transformation, induced by the Kirkendall effect, will result in incomplete densification which implies a low sintered density. The unexpected lower sintered density of TiH_2-6Al-4V in partial hydrogen at 1050°C is mainly due to the formation and liberation of H_2O (g) illustrated in Figure 7.9. However, the swelling effects associated with the Kirkendall effect illustrated in Figure 7.10 are secondary contributing factors that resulted in the low sintered density of TiH_2-6Al-4V in partial hydrogen at 1050°C. At higher temperatures, the diffusion rate is very likely to be significantly higher and thus sintering takes place faster preventing the swelling and pores formation in the sample [43].

Chapter 8: Conclusions

The aim of this research was to investigate the effects of using hydrogen as a temporary alloying element in possibly lowering the sintering temperature while resulting in reasonable green and sintered densities of commercially pure titanium (CP Ti), titanium hydride (TiH_2) and Ti-6Al-4V compacts produced by the PM route. From the research and experiments conducted, it can be concluded that most of the expected outcomes outlined in Section 1.6 were supported by the results gathered. However, decrease in sintered density for TiH_2-6Al-4V in a partial hydrogen atmosphere as compared to the green density was not expected. Through extensive research and further sintering and elemental mapping analyses, the possible explanations for this unexpected decrease, not documented in the literature, was described and illustrated.

From all the experiments and research conducted, the following were concluded:

1) The larger the powder particle size, the higher is the green density. The powders' particle size outweighs its chemical composition and mechanical properties.

2) The green strength of the pressed compacts increases with higher levels of CP Ti (ductile powder) due to the latter's ability to plastically deform and form stronger bonds. This is not the case for TiH_2 (brittle powder) which fractures upon compaction and hence does not result in any bond formation resulting in a lower green strength.

3) Pressed compacts with more than 40wt% of TiH_2 do not result in significant decrease in green density or strength.

4) The presence of a partial hydrogen atmosphere does not significantly delay the temperature range at which dehydrogenation occurs for the various powder blends containing TiH_2. However, sintering in a partial hydrogen atmosphere

is beneficial for CP Ti and its blends with either TiH_2 or MA. Hydrogen diffuses into the CP Ti matrix to result in β-Ti (the desired phase) to form at a lower temperature which promotes faster sintering and shrinkage resulting in reasonable densities being achieved at 1050**°**C.

5) The benefits of sintering in a partial hydrogen atmosphere only improves the density (when compared with the equivalent samples sintered in argon) if the powder blends contain TiH_2 except for TiH_2-6Al-4V sintered at 1050**°**C under a partial hydrogen atmosphere.

6) While it was expected that the low sintered density obtained for TiH_2-6Al-4V is due to vanadium diffusing first in the TiH_2 (β-phase) during sintering (leaving melted aluminium related porosity issues), this was disproved by the elemental mapping analysis conducted in Chapter 7. Additionally, the core shell model discussed also supports that there is no apparent difference in the diffusion of MA in CP Ti and TiH_2. The cause for the very low sintered density of TiH_2-6Al-4V was primarily due to the formation of H_2O (gas). The presence of a partial hydrogen further hinders the diffuse rate of the H_2O gas generated since the pressure gradient is even lower (due to the presence of hydrogen in the sintering atmosphere) as compared to a flowing argon atmosphere. The latter being bigger as compared to hydrogen gas would leave larger residual pores when the H_2O(g) diffuses out. The residual porosity remains since the diffusion rate at 1050°C is low as 1040°C is the temperature at which rapid shrinkage begins and thus is very likely that complete shrinkage was not achieved at 1050°C. Additionally, the Kirkendall effects associated with different diffusion rate also promotes the formation of pores which hinders densification further.

7) The sintering temperature of 1050°C in a positive pressure atmosphere is not enough to allow maximum shrinkage of the CP Ti-6Al-4V and TiH_2-6Al-4V to take place to result in relative sintered densities greater than 97%.

8) At 1200°C, reasonable relative sintered densities (>97%) are obtained irrespective of the sintering atmosphere and time. Hence, it is clear that the diffusion rate is likely to be highly dependent on the sintering temperature.

9) While it can be argued that reasonable relative sintered densities are obtained in a partial hydrogen atmosphere, the equivalent densities are still higher under vacuum. Vacuum being a negative atmosphere results in the pressure difference between the sample and the sintering atmosphere to be higher. Therefore, the release and diffusion of H_2 and H_2O (g) from the TiH_2-6Al-4V will take place at a much higher rate which in turn promote shrinkage resulting in better densification even at 1050°C.

Chapter 9: Future work

To conclusively determine the effects of hydrogen as a temporary alloying element on the PM manufacturing route of Ti-6Al-4V, the following should be investigated:

1) Use the same particle size for CP Ti and TiH_2 to press and sinter samples over the same conditions used during the compaction and sintering study of this dissertation. Hence, the role that the powders' chemical composition and mechanical properties have on the green density and strength as well as the sintered density can be independently evaluated.

2) Conduct the compaction study at compaction pressures higher than 500MPa to determine the maximum compaction pressure than can be used for the various CP-Ti/TiH_2 powder blends with and without MA powder.

3) Conduct TGA and DSC of the powder blends under vacuum to potentially explain why the sintered densities of TiH_2-6Al-4V and Ti-6Al-4V under vacuum are significantly higher compared to the same samples tested in argon and partial hydrogen atmospheres at 1050°C.

4) Vary the sintering times and temperatures on the various powder blends to determine the effects that time and temperature will play for compacts made from each powder blend.

5) Sinter all the other CP Ti/ TiH_2 powder blends under vacuum at 1050°C and 1200°C.

6) Sinter TiH_2-6Al-4V in a partial hydrogen atmosphere at 1100°C. and 1150°C for different times to determine whether a sintering temperature lower than 1200°C can result in acceptable relative sintered density.

7) Conduct more element mapping on the samples from 4) and 6) to determine the time and temperature at which vanadium diffusion begins in the various samples.

Chapter 10: References

[1] F.H Froes et al. *Cost Affordable Titanium*, TMS, Warrandale, Pa. (2004).

[2] F.H Froes et al. *Titanium Technology: Present Status and Future Trends,* TDA, Dayton, Ohio, 1985.

[3] D. Eylon et al., Titanium and Titanium Alloy Castings, *Properties and Selection: Nonferrous Alloys and Special-Purpose Materials*, Vol 2, *ASM Handbook*, ASM International, 1990, p 634–646.

[4] G.R. Yoder et al, On the Effect of Colony Size on Fatigue Crack Growth in Widmänstatten Structure Alpha + Beta Alloys, *Metall. Trans. A,* Vol 10A, 1979, p 1808–1810.

[5] F.H (Sam) Froes, "Titanium powder Metallurgy A review-Part 2, Royal Belgian Institute of Marine Engineers.

[6] The Metal Casting. Com, 2017, Available from URL: http://www.themetalcasting.com/powder-metallurgy.html [Accessed on 27th of April 2017].

[7] M. Qian et al. Titanium Powder Metallurgy: Science, Technology and Applications. Elsevier Inc, First Edition 2015.

[8] FH Froes et al. *The technologies of titanium powder metallurgy*. JOM Journal of the Minerals, Metals and Materials Society, 2004; 56(11):46–48.

[9]R. German. Powder Metallurgy Science second edition. Princeton, 1994.

[10] N. Clinning, *Thermomechanical Processing of Blended Elemental Powder Ti-6Al-4V*, 2012 pp25-27.

[11] F. Thümmler et al. A*n introduction to powder metallurgy*. Institute of Materials series on powder metallurgy. Institute of Materials, 1993.

[12] The library of Manufacturing, Powder Processes Powder Metallurgy. Available from URL: http://thelibraryofmanufacturing.com/powder_processes.html, [Accessed on 28th of March 2015].

[13]Google. Available URL: https://www.google.co.za/search?q=various+particle+size&rlz=1C5CHFA_enZA728ZA728&source=lnms&tbm=isch&sa=X&ved=0ahUKEwjmwOS6ns_TAhXLLMAKHQyDDs8Q_AUICigB&biw=1050&bih=729#tbm=isch&q=schematic+drawing+of++sieve+to+determine+particle+size&imgrc=f3IN1Qtwwka6kM: [Accessed 28/03/2017]

[14] Guden et al. *Effect of Compression Pressure and Particles Shape effects on the Porosity and compression and final mechanical properties of Sintered Ti6Al4V Powder Compacts for Hard Tissue Implantation,* 2007.

[15] D. Blaine et al. *Influence of Powder Particle Size Distribution on the Press-and-Sinter Titanium,* October 2014.

[16] B.A Kolachev et al.*Hydride Systems: Handbook [in Russian], Metallurgiya,* Moscow, 1992.

[17] Z.Fang. *Sintering of Advanced Materials,* 2010, pp335-338.

[18] D.H Savvakin et al. *Role of Hydrogen in the Process of Sintering of Titanium Powder,* Materials Science, Ukrainian Original Vol. 47 No.5, 2011.

[19] R. Machaka et al. Metall. *Mater. Trans. A*, 2015,vol. 46A, pp. 2194–2200.

[20] JE Smugeresky et al. *New titanium alloys for blended elemental powder processing*. Powder Technology, 1981; 30(1):87–94.

[21] R. Ellis *The optimisation of a highly effective, homogenising metal powder mixer*, Stellenbosch: Department of Mechanical and Mechatronical Engineering, Stellenbosch University.

[22] Compaction Process Related Keywords. Available from URL: https://www.google.co.za/search?q=powder+compaction&rlz=1C5CHFA_enZA728ZA728&source=lnms&tbm=isch&sa=X&ved=0ahUKEwiM0LK8zsvTAhUBDsAKHczsApEQ_AUIBigB&biw=1050&bih=726#imgrc=X_UvbQppT9U0JM:, [Accessed 28/03/2015].

[23] E. Park 2007, *Chapter 3 Solid State Sintering fundamentals, Slide share. Accessible from URL:* https://www.slideshare.net/support.xhht/solid-state-sintering-fundamentals-242041. [Accessed on 30th of March 2015].

[24] D.F et al. *Advances in the sintering of titanium powders*: In PM Lightweight and Porous Materials, 2004.

[25] C. Leyens et al. *Titanium and titanium alloys*. Wiley Online Library, 2003.

[26] G. Greetham, Powder metallurgy – component manufacture by uniaxial pressing, Materials Information Service. 2001.

[27] Z. Fang et al. *Hydrogen Sintering of Titanium to Produce High Density Fine Grain Titanium Alloys;* Advance Engineering Materials: 2011.

[28] W. R. Kerr: *The effect of hydrogen as a temporary alloying element on the microstructure and tensile properties of Ti-6Al-4V*, Metall. Mater. Trans. A, 1985, 16(6), 1077-1087.

[29] J. Williams, *Effect of Hydrogen on Behavior of Materials*, (Eds.: A. W. Thompson, I. M. Bernstein), AIME, New York, NY, 1976, p. 367.

[30] Baynakov. Y et al. *Titanium and Hydrogen.* Foreign Technology Division, 1965.

[31] Liu et al. *Kinetics Study on Non-isothermal dehydrogenation of TiH_2.* International journal of hydrogen of energy, 2009.

[32] Froes et al. *Titanium Powder Metallurgy.* Science Technology and Applications, 2015 pp 458-462.

[33] Ellis. A et al. *Teaching General Chemistry: A Materials Science Companion* (3rd ed.). Washington, DC: American Chemical Society, 1995.

[34] Froes et al. *Titanium Powder Metallurgy.* Science Technology and Applications, 2015 pp 294-300.

[35] J. Waisman et al. *Diffusion of Hydrogen in Titanium Alloys Due to Composition, Temperature, and Stress Gradients.* Metallurgical Transactions, Vol. 4,1973, p. 291.

[36] J. Qazi et al. *Phase transformations in Ti-6Al-4V-x H alloys*, Metall. Mater. Trans. A, 2001, 32(10), 2453-2463.

[37] L. Matthews et al. *Embrittlement of the Ti-6Al-4V alloy by hydrogen dosing at elevated temperatures*, SAIMM, 2010, 111, 155-156.

[38] M. Ivasishin et al. *Low-cost PM titanium materials for automotive applications*, presented at TMS-2005 134th Annual Meeting & Exhibition, San Francisco, CA, USA, 2005.

[39] V. Duz et al. *Novative Powder Metallurgy Process for Producing Low Cost Titanium and Titanium and Titanium Alloy Components*, presented at Titanium 2008 24th Annual ITA.

[40] O. Savvakin et al. *Role of Hydrogen in the Process of Sintering of Titanium Powders;* 2011.

[41] O.M Ivasishin et al. *Diffusion During Powder Metallurgy Synthesis of Titanium Alloys*. Defect and Diffusion Forum Vol, 2008, pp 177-185.

[42] Oh. J et al. *Sintering Properties of Ti-6Al-4V Alloys Prepared Using Ti-TiH_2 powders.* 2012.

[43] O.M Ivasishin et al. (2002), 'Synthesis of alloy Ti-6Al-4V with residual porosity by a powder metallurgy method', powder metallurgy and metal ceramics, vol.41, pp382-390.

[44] C.Wang et al. *Sintering Densification of Titanium Hydride,* Materials and Manufacturing Processes 2017, Vol.32, No 5,517-522.

[45]M.Ma et al. *Phase transformations of titanium hydride in thermal desorption process with different heating rate.* International Journal if Hydrogen Energy 40 (2015) 8926-8934.

[46] C. Jimenez et al. *Decomposition of TiH_2 studied in situ by synchrotron X-ray and neutron diffraction.* Acta Materialia 59 (2011) 6318-6330.

[47] X. Xu et al. *Sintering Mechanism of Blended Ti6Al4V Powder from Diffusion Path Analysis.* 2014.

[48] Jones. R. Particle Size Analysis by Laser Diffraction: ISO 13320, standard operating procedures, and Mie Theory, American Laboratory (2003).

[49] McCave, et al. "Evaluation of a Laser-Diffraction-Size Analyzer For Use With Natural Sediments". *Journal of sedimentary Research"* October 2013.

[50] American Society for Testing Materials (ASTM) international B962-13 (2014) (*Standard Test Methods for Density of Compacted or Sintered Powder Metallurgy (PM) Products Using Archimedes' Principle*[1].

[51] American Society for Testing Materials (ASTM) international B312-09 (2014). *Standard Test Method for Green* Strength *of Specimens Compacted from Metal Powders*[1].

Chapter 11: Appendices

Appendix A summarises the detailed procedures of various tests conducted based on ASTM standards B962-13 and B312-09.

11.1 Standard Procedure to measure green of specimens compacted from metal powders (ASTM B962-13)

INTERNATIONAL

Standard Test Methods for Density of Compacted or Sintered Powder Metallurgy (PM) Products Using Archimedes' Principle[1]

This standard is issued under the fixed designation B962; the number immediately following the designation indicates the year of original adoption or, in the case of revision, the year of last revision. A number in parentheses indicates the year of last reapproval. A superscript epsilon (ε) indicates an editorial change since the last revision or reapproval.

This standard has been approved for use by agencies of the U.S. Department of Defense.

1. Scope*

1.1 This standard describes a method for measuring the density of powder metallurgy products that usually have surface-connected porosity.

1.2 The density of impermeable PM materials, those materials that do not gain mass when immersed in water, may be determined using Test Method B311.

1.3 The current method is applicable to green compacts, sintered parts, and green and sintered test specimens.

1.4 With the exception of the values for density and the mass used to determine density, for which the use of the gram per cubic centimetre (g/cm^3) and gram (g) units is the long-standing industry practice, the values in inch-pound units are to be regarded as standard. The values given in parentheses are mathematical conversions to SI units that are provided for information only and are not considered standard.

1.5 *This standard does not purport to address all of the safety concerns, if any, associated with its use. It is the responsibility of the user of this standard to establish appropriate safety and health practices and determine the applicability of regulatory limitations prior to use.*

2. Referenced Documents

2.1 *ASTM Standards:*[2]

B243 Terminology of Powder Metallurgy

B311 Test Method for Density of Powder Metallurgy (PM) Materials Containing Less Than Two Percent Porosity

3. Terminology

3.1 Definitions of powder metallurgy (PM) terms can be found in Terminology B243. Additional descriptive material is available in the Related Material section of Vol. 02.05 of the *Annual Book of ASTM Standards*.

3.2 *Definitions of Terms Specific to This Standard:*

3.2.1 *green density (D_g)*—the mass per unit volume of an unsintered PM part or test specimen.

3.2.2 *impregnated density (D_i)*—the mass per unit volume of a sintered PM part or test specimen, impregnated with oil.

3.2.3 *sintered density (D_s)*—the mass per unit volume of a sintered, non oil-impregnated PM part or test specimen.

4. Summary of Test Method

4.1 The test specimen is first weighed in air. It is then oil impregnated or some other treatment is used to seal the surface-connected porosity and the specimen is reweighed. The test specimen is then weighed when immersed in water and its density calculated based on Archimedes' principle.

5. Significance and Use

5.1 The volume of a complex shaped PM part cannot be measured accurately using micrometers or calipers. Since density is mass per unit volume, a precise method for measuring the volume is needed. Archimedes' principle may be used to calculate the volume of water displaced by an immersed object. For this to be applicable to PM materials that contain surface connected porosity, the surface pores are sealed by oil impregnation or some other means.

5.2 The green density of compacted parts or test pieces is normally determined to assist during press set-up, or for quality control purposes. It is also used for determining the compressibility of base powders, mixed powders, and premixes.

5.3 The sintered density of sintered PM parts and sintered PM test specimens is used as a quality control measure.

[1] These test methods are under the jurisdiction of ASTM Committee B09 on Metal Powders and Metal Powder Products and are the direct responsibility of Subcommittee B09.04 on Bearings.

Current edition approved April 1, 2013. Published June 2013. Originally approved in 2008. Last previous edition approved in 2008 as B962 – 08. DOI: 10.1520/B0962-13.

[2] For referenced ASTM standards, visit the ASTM website, www.astm.org, or contact ASTM Customer Service at service@astm.org. For *Annual Book of ASTM Standards* volume information, refer to the standard's Document Summary page on the ASTM website.

***A Summary of Changes section appears at the end of this standard**

5.4 The impregnated density of sintered bearings is normally measured for quality control purposes as bearings are generally supplied and used oil-impregnated.

6. Interferences

6.1 A gain in mass when a test specimen is immersed in water is an indication that the specimen contains surface-connected porosity. Unsealed surface porosity will absorb water and cause the calculated density values to be higher than the true value.

6.2 Test specimens that contain surface-connected porosity shall be oil impregnated or have the surface-connected porosity sealed by some other means prior to their immersion in water.

7. Apparatus

7.1 *Analytical Balance*—Precision single-pan balance that will permit readings within 0.01% of the test specimen mass. See Table 1.

7.2 *Water Container*—A glass beaker or other suitable transparent container should be used to contain the water.

NOTE 1—A transparent container makes it easier to see air bubbles adhering to the test specimen and specimen support when immersed in water.

NOTE 2—For the most precise density determination, the water container should be of a size that the level of the water does not rise more than 0.10 in. (2.5 mm) when the test specimen is lowered into the water.

7.3 *Water*—Distilled or deionized water to which 0.05 to 0.1 volume percent of a wetting agent has been added to reduce the effects of surface tension.

NOTE 3—Degassing the water by evacuation, boiling, or ultrasonic agitation helps to prevent air bubbles from collecting on the test specimen and support when immersed in water.

7.4 *Test Specimen Support for Weighing in Water*—Two typical arrangements are shown in Fig. 1. The suspension wire may be twisted around the test specimen or the test specimen may be supported in a wire basket that is attached to the suspension wire. For either arrangement, a single corrosion-resistant wire—for example, austenitic stainless steel, copper, or nichrome—shall be used for the basket and suspension wire. The maximum recommended diameter of suspension wire to be used for various mass ranges is summarized in Table 2.

NOTE 4—For the most precise density determinations, it is important that the mass and volume of all supporting wires immersed in water be minimized.

7.5 *Oil for Oil-Impregnation*—Oil with a viscosity of 20 to 65 cSt or 100 to 300 SSU (20×10^{-6} to 65×10^{-6} m^2/s) at 100 °F (38 °C) has been found to be suitable.

7.5.1 In the case of oil-impregnated bearings, make an effort to match the oil that was originally used to impregnate them.

TABLE 1 Balance Sensitivity

Mass, g	Balance Sensitivity, g
less than 10	0.0001
10 to less than 100	0.001
100 to less than 1000	0.01
1000 to less than 10 000	0.1

7.6 *Vacuum Impregnation Apparatus*—Equipment to impregnate the part or test specimen with oil.

7.7 *Thermometer*—A thermometer with an accuracy of 1.0 °F (0.5 °C) to measure the temperature of the water.

8. Preparation of Test Specimens

8.1 The mass of the test specimen shall be a minimum of 1.0 g. For small parts, several parts may be combined to reach the minimum mass.

8.2 Thoroughly clean all surfaces of the test specimen to remove any adhering foreign materials such as dirt or oxide scale. Take care with cut specimens to avoid rough surfaces to which an air bubble may adhere. A 100-grit sanding or abrasive grinding is recommended to remove all rough surfaces.

9. Procedure

9.1 The part or test specimen, the analytical balance and surrounding air shall be at a uniform temperature when weighing is performed.

9.2 For the most precise density determinations, duplicate weighings should be made for all mass measurements. Adjust the analytical balance to zero prior to each weighing. Average the mass determinations before calculating the density.

9.3 For improved repeatability and reproducibility, verify the analytical balance periodically with a standard mass that is approximately equal to the part or test specimen mass.

9.4 This standard contains three separate test methods; determination of green density, determination of sintered density, and determination of impregnated density. Each is detailed in the following sections.

Determination of Green Density

9.5 This procedure is used to determine the green density of PM parts and test specimens.

9.5.1 Determine the mass of the green part or test specimen. This is mass A. This and all subsequent weighings shall be to the precision stated in Table 1.

9.5.2 Oil impregnate the green part or test specimen as follows:

Preferred Procedure

9.5.3 Immerse the part or test specimen in oil at room temperature.

9.5.4 Reduce the pressure over the sample to 1 psi (7 kPa) or less for 30 minutes, then increase the pressure back to atmospheric pressure and keep the sample immersed for at least 30 minutes.

9.5.5 Remove excess oil by wiping gently with an absorbent, lint-free material. Take care not to extract oil absorbed within the part or test specimen.

9.5.6 Do not place or store parts on porous surfaces such as paper, cloth, or cardboard as these will absorb oil.

9.5.7 Proceed to 9.5.13.

Alternative Procedure

9.5.8 Immerse the part or test specimen in oil at a temperature of 180 ± 10 °F (82 ± 5 °C) for at least 4 hours.

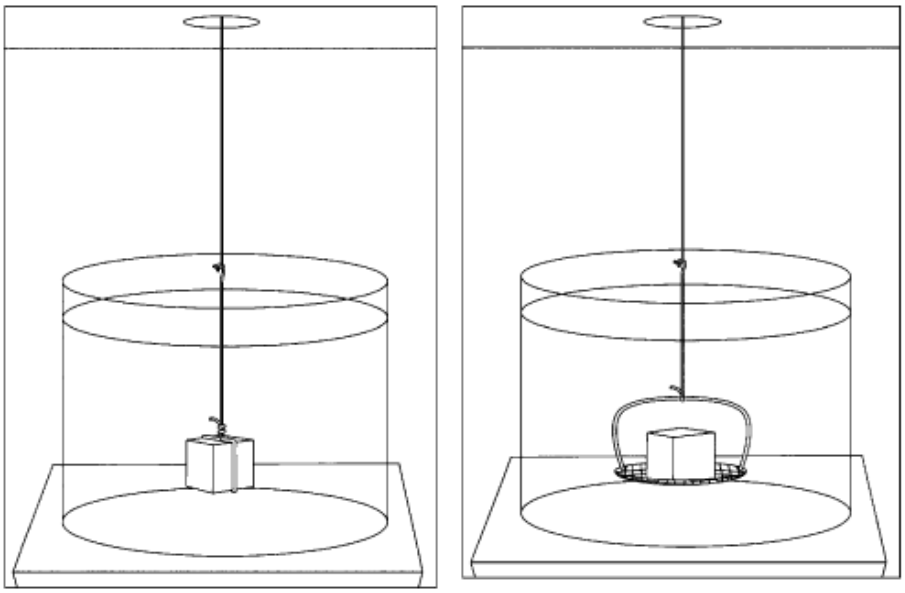

a. Twisted wire arrangement b. Basket support arrangement

FIG. 1 Methods for Holding the Test Specimen When Weighing in Water

TABLE 2 Maximum Recommended Wire Diameters

Mass, g	Wire Diameter, in. (mm)
less than 50	0.005 (0.12)
50 to less than 200	0.010 (0.25)
200 to less than 600	0.015 (0.40)
600 and greater	0.020 (0.50)

9.5.9 Cool by immersing in a bath of the same oil held at room temperature and keep in this oil for at least 30 minutes.

9.5.10 Remove excess oil by wiping gently with an absorbent, lint-free material. Take care not to extract oil absorbed within the part or test specimen.

9.5.11 Do not place or store parts on porous surfaces such as paper, cloth, or cardboard as these will absorb oil.

9.5.12 Proceed to 9.5.13.

NOTE 5—It may not be necessary to oil impregnate the green part with oil. There may be enough admixed lubricant present in the surface-connected pores to prevent the absorption of water. If the test specimen gains mass when immersed in water it is an indication that the specimen contains surface-connected porosity and that it needs to be sealed by oil impregnation or some other means.

9.5.13 Determine the mass of the oil-impregnated green part or test specimen to the precision stated in Table 1. This is mass B.

9.5.14 Support the container of water over the pan of the balance using a suitable bridge as shown in Fig. 2a. Take care to ensure that the bridge does not restrict the free movement of the balance pan. The container of water may also be supported below the balance for weighing larger specimens if the balance has a lower beam hook for this purpose. See Fig. 2b. If this arrangement is used, it is important to shield the weighing system, including the wire, from the effect of air drafts.

9.5.15 Suspend the test specimen support along with the part or test specimen from the beam hook of the balance. The water should cover any wire twists and the specimen support basket by at least ¼ in. (6 mm) to minimize the effect of surface tension forces on the weighing.

9.5.16 The test specimen support and test specimen shall hang freely from the balance beam hook, be free of air bubbles when immersed in the water, and be at the same temperature as the water and the balance.

9.5.17 The surface of the water shall be free of dust particles.

9.5.18 Weigh the part/test specimen and specimen support immersed in water. This is mass C.

9.5.19 Remove the part/test specimen from the support.

9.5.20 Weigh the test specimen support immersed in water at the same depth as before. This is mass E. The suspension support shall be free of air bubbles and the suspension wire shall not be immersed below its normal hanging depth, as a change in depth will change the measured mass.

NOTE 6—Some balances are capable of being tared. This automatically removes the necessity of reweighing the specimen support every time. In

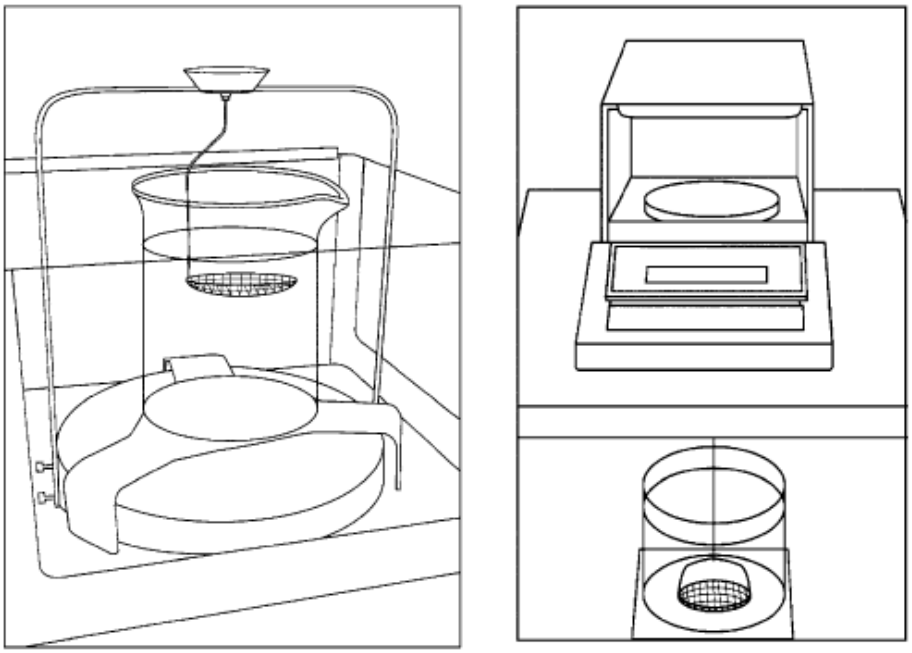

a. Beaker support above balance pan

b. Weighing arrangement below the balance pan

FIG. 2 Methods for Weighing in Water

this case, tare the specimen support alone, immersed in water to the same depth as with the specimen, before weighing the specimen support and part/test specimen immersed in water. The mass of the specimen support and specimen immersed in water is mass F, which replaces mass C minus mass E.

9.5.21 Measure the temperature of the water to the nearest 2 °F (1 °C) and record its density ρ_w, at that temperature, from Table 3.

9.5.22 Calculate the green density of a part or test piece from the following formula:

$$\text{Green Density, } D_g = \frac{A\rho_w}{B-(C-E)} \quad (1)$$

or

$$\text{Green Density, } D_g = \frac{A\rho_w}{B-F} \quad (2)$$

TABLE 3 Effect of Temperature on the Density of Air-Free Water[A]

Temperature		Density
°F	(°C)	g/cm³
59.0	(15)	0.9991
60.8	(16)	0.9989
62.6	(17)	0.9988
64.4	(18)	0.9986
66.2	(19)	0.9984
68.0	(20)	0.9982
69.8	(21)	0.9980
71.6	(22)	0.9978
73.4	(23)	0.9975
75.2	(24)	0.9973
77.0	(25)	0.9970
78.8	(26)	0.9968
80.6	(27)	0.9965
82.4	(28)	0.9962
84.2	(29)	0.9959
86.0	(30)	0.9956

[A] *Metrological Handbook 145*, "Quality Assurance for Measurements," National Institute of Standards and Technology, 1990, pp. 9-10.

where:

A = the mass of the green part or test piece in air, g,
B = the mass of the oil-impregnated green part or test piece, g,
C = the mass of the oil-impregnated part/test specimen and specimen support immersed in water, g,
E = the mass of the oil-impregnated part/test specimen support immersed in water, g,
F = the mass of the oil-impregnated part/test specimen in water with the mass of the specimen support tared, g, and
ρ_w = the density of the water, g/cm^3.

If the green part did not need to be oil impregnated then use the following formula:

$$\text{Green Density, } D_g = \frac{A\rho_w}{C-E} \quad (3)$$

Determination of Sintered Density

9.6 This procedure is used to determine the sintered density of PM parts and test pieces.

9.6.1 Determine the mass of the sintered part or test specimen to the precision stated in Table 1. This is mass A. This and all subsequent weighings shall be to the precision stated in Table 1.

NOTE 7—Oil impregnated specimens or specimens that contain any oil are to be free of lubricant for determining mass A. Remove the oil in a Soxhlet apparatus using a suitable solvent, such as petroleum ether. After extraction, residual solvent shall be removed by heating specimens at 250 °F (120 °C) for 1 hour. Alternate extraction and drying shall be continued until the dry mass, A, is constant to 0.05%.

NOTE 8—A practical and fast method of oil removal is to heat the specimen in a protective atmosphere in the temperature range of 800 to 1200 °F (425 to 650 °C). This method, which results in values in close agreement with those obtained using the Soxhlet apparatus, may be used if agreed upon by both parties. This method also is applicable to sintered aluminum materials if the temperature does not exceed 1000 °F (540 °C).

9.6.2 In order to seal the surface-connected porosity the parts/test pieces are oil impregnated or the pores are filled with a suitable material. If using oil impregnation, oil impregnate the part or test specimen using one of the procedures described in sections 9.5.2 – 9.5.12.

9.6.3 Determine the mass of the oil-impregnated part or test specimen to the precision stated in Table 1. This is mass B.

9.6.4 Support the container of water over the pan of the balance using a suitable bridge as shown in Fig. 2a. Take care to ensure that the bridge does not restrict the free movement of the balance pan. The container of water may also be supported below the balance for weighing larger specimens if the balance has a lower beam hook for this purpose. See Fig. 2b. If this arrangement is used, it is important to shield the weighing system, including the wire, from the effect of air drafts.

9.6.5 Suspend the test specimen support along with the part or test specimen from the beam hook of the balance. The water should cover any wire twists and the specimen support basket by at least ¼ in. (6 mm) to minimize the effect of surface tension forces on the weighing.

9.6.6 The test specimen support and test specimen shall hang freely from the balance beam hook, be free of air bubbles when immersed in the water, and be at the same temperature as the water and the balance.

9.6.7 The surface of the water shall be free of dust particles.

9.6.8 Weigh the part/test specimen and specimen support immersed in water. This is mass C.

9.6.9 Remove the part/test specimen from the support.

9.6.10 Weigh the test specimen support immersed in water at the same depth as before. This is mass E. Take care to ensure that the suspension support is free of air bubbles and that the suspension wire is not immersed below its normal hanging depth, as a change in depth will change the measured mass.

NOTE 9—Some balances are capable of being tared. This automatically removes the necessity of reweighing the specimen support every time. In this case, tare the specimen support alone, immersed in water to the same depth as with the specimen, before weighing the specimen support and part/test specimen immersed in water. The mass of the specimen support and specimen immersed in water is mass F, which replaces mass C minus mass E.

9.6.11 Measure the temperature of the water to the nearest 2 °F (1 °C) and record its density ρ_w, at that temperature, from Table 3.

9.6.12 Calculate the sintered density from the following formula:

$$\text{Sintered Density, } D_s = \frac{A\rho_w}{B-(C-E)} \quad (4)$$

or

$$\text{Sintered Density, } D_s = \frac{A\rho_w}{B-F} \quad (5)$$

where:

A = the mass of the sintered part or test piece in air, g,
B = the mass of the oil-impregnated part or test piece, g,
C = the mass of the oil-impregnated part/test specimen and specimen support immersed in water, g,
E = the mass of the oil-impregnated part/test specimen support immersed in water, g,
F = the mass of the oil-impregnated part/test specimen in water with the mass of the specimen support tared, g, and
ρ_w = the density of the water, g/cm^3.

Determination of Impregnated Density

9.7 This procedure is used to determine the density of oil-impregnated PM bearings or parts/test pieces.

9.7.1 Oil impregnate the specimen using one of the procedures described in sections 9.5.2 – 9.5.12 to ensure that the bearing, part, or test piece is fully oil impregnated.

9.7.2 Determine the mass of the oil-impregnated green part or test specimen to the precision stated in Table 1. This is mass B.

9.7.3 Support the container of water over the pan of the balance using a suitable bridge as shown in Fig. 2a. Take care to ensure that the bridge does not restrict the free movement of the balance pan. The container of water may also be supported below the balance for weighing larger specimens if the balance has a lower beam hook for this purpose. See Fig. 2b. If this arrangement is used, it is important to shield the weighing system, including the wire, from the effect of air drafts.

9.7.4 Suspend the test specimen support along with the part or test specimen from the beam hook of the balance. The water should cover any wire twists and the specimen support basket by at least ¼ in. (6 mm) to minimize the effect of surface tension forces on the weighing.

9.7.5 The test specimen support and test specimen shall hang freely from the balance beam hook, be free of air bubbles when immersed in the water, and be at the same temperature as the water and the balance.

9.7.6 The surface of the water shall be free of dust particles.

9.7.7 Weigh the part/test specimen and specimen support immersed in water. This is mass C.

9.7.8 Remove the part/test specimen from the support.

9.7.9 Weigh the test specimen support immersed in water at the same depth as before. This is mass E. Take care to ensure that the suspension support is free of air bubbles and that the suspension wire is not immersed below its normal hanging depth as a change in depth will change the measured mass.

NOTE 10—Some balances are capable of being tared. This automatically removes the necessity of reweighing the specimen support every time. In this case, tare the specimen support alone, immersed in water to the same depth as with the specimen, before weighing the specimen support and part/test specimen immersed in water. The mass of the specimen support and specimen immersed in water is mass F, which replaces mass C minus mass E.

9.7.10 Measure the temperature of the water to the nearest 2 °F (1 °C) and record its density ρ_w, at that temperature, from Table 3.

9.7.11 Calculate the impregnated density of an oil-impregnated part or test piece from the following formula:

$$\text{Impregnated Density, } D_i = \frac{B\rho_w}{B-(C-E)} \quad (6)$$

or

$$\text{Impregnated Density, } D_i = \frac{B\rho_w}{B-F} \quad (7)$$

where:

B = the mass of the oil-impregnated part or test piece, g,
C = the mass of the oil-impregnated part/test specimen and specimen support immersed in water, g,
E = the mass of the oil-impregnated part/test specimen support immersed in water, g,
F = the mass of the oil-impregnated part/test specimen in water with the mass of the specimen support tared, g, and
ρ_w = the density of the water, g/cm^3.

10. Report

10.1 Report the green density, sintered density, or the impregnated density rounded to the nearest 0.01 g/cm^3.

10.2 For the green density measurement report if the green part/test specimen was impregnated and which method was used.

11. Precision and Bias

11.1 The results of an interlaboratory study to determine the precision of this test method are available in an ASTM Research Report.[3] The study involved six laboratories and covered identical samples of both iron and copper-based sintered parts.

11.2 For ferrous and copper-based sintered parts, the repeatability interval, r, is 0.05 g/cm^3 for sintered or impregnated density. Duplicate results from the same laboratory should not be considered suspect at the 95% confidence level unless they differ by more than r.

11.3 There are no data available for the repeatability of this test method for green density. An interlaboratory study to determine repeatability is planned within the next five years.

11.4 For ferrous and copper-based sintered parts, the reproducibility interval, R, is 0.06 g/cm^3 for sintered or impregnated density. The results from two laboratories should not be considered suspect at the 95% confidence level unless they differ by more than R.

11.5 There are no data available for the reproducibility of this test method for green density. An interlaboratory study to determine reproducibility is planned within the next five years.

11.6 There is no estimate of bias because there is no accepted porous reference material.

11.7 *Measurement Uncertainty*—The precision of this test method shall be considered by those performing the test when reporting the results.

12. Keywords

12.1 density; green density; impregnated density; PM products; powder metallurgy products; sintered density

[3] Supporting data have been filed at ASTM International Headquarters and may be obtained by requesting Research Report RR:B09-1008. Contact ASTM Customer Service at service@astm.org.

SUMMARY OF CHANGES

Committee B09.04 has identified the location of selected changes to this standard since the last issue (B962 – 08) that may impact the use of this standard. (Approved April 1, 2013.)

(1) Changed the statement on units in Section 1.4 to make this an inch-pound standard.

(2) Added a new note following Section 9.6.1 to indicate that oil impregnated specimens or specimens that contain any oil are to be free of oil before determining mass A. The note provides instructions for removing the oil.

(3) Added a new note following the new note referred to above in which an alternative method is provided for the removal of the oil.

11.2 Standard Procedure to green strength of specimens compacted from metal powders (adapted from ASTM standard B312-09)

Designation: B312 – 09

Standard Test Method for Green Strength of Specimens Compacted from Metal Powders[1]

This standard is issued under the fixed designation B312; the number immediately following the designation indicates the year of original adoption or, in the case of revision, the year of last revision. A number in parentheses indicates the year of last reapproval. A superscript epsilon (ε) indicates an editorial change since the last revision or reapproval.

1. Scope*

1.1 This standard covers a test method that may be used to measure the transverse rupture strength of a compacted but unsintered (green) test specimen produced from lubricated or unlubricated metal powders or powder mixtures.

1.2 Green strength is measured by a quantitative laboratory procedure in which the fracture strength is calculated from the force required to break an unsintered test specimen supported as a simple beam while subjected to a uniformly increasing three-point transverse load under controlled conditions.

1.3 This test method is a companion standard to Test Method B528 that covers the measurement of the transverse rupture strength of sintered PM test specimens.

1.4 With the exception of density values, for which the g/cm^3 unit is the industry standard, and mass measurements used to calculate density, the values stated in inch-pound units are to be regarded as the standard. The SI equivalents shown in parentheses have been converted in accordance with IEEE/ASTM SI 10, may be approximate and are only included for information.

1.5 *This standard does not purport to address all of the safety concerns, if any, associated with its use. It is the responsibility of the user of this standard to establish appropriate safety and health practices and determine the applicability of regulatory limitations prior to use.*

2. Referenced Documents

2.1 *ASTM Standards:*[2]

B215 Practices for Sampling Metal Powders
B243 Terminology of Powder Metallurgy
B528 Test Method for Transverse Rupture Strength of Powder Metallurgy (PM) Specimens
B925 Practices for Production and Preparation of Powder Metallurgy (PM) Test Specimens
B962 Test Methods for Density of Compacted or Sintered Powder Metallurgy (PM) Products Using Archimedes' Principle
E691 Practice for Conducting an Interlaboratory Study to Determine the Precision of a Test Method
IEEE/ASTM SI 10 American National Standard for Metric Practice

3. Terminology

3.1 *Definitions*—the definitions of powder metallurgy (PM) terms used in this test method can be found in Terminology B243. Additional descriptive PM information is available in the Related Material section of Vol 02.05 of the *Annual Book of ASTM Standards*.

4. Summary of Test Method

4.1 Three rectangular test specimens are compacted to a predetermined green density from test portions of the metal powder or powder mixture that is to be tested.

4.2 Each unsintered bar is placed, in turn, in a test fixture and subjected to a uniformly increasing transverse load under controlled conditions until fracture occurs.

4.3 The green strength or maximum flexural stress of each specimen is determined by calculation using the stress equation for a simply supported beam with a concentrated mid-point load.

4.4 The green strength of the material being tested is reported as the arithmetic mean of the results of three individual tests at the measured green density rounded to the nearest 100 psi (0.5 MPa).

5. Significance and Use

5.1 The green strength value determined under the conditions specified by this test method is influenced by the characteristics of the powder, how it compacts under the specified conditions (i.e., the particle to particle bonding that exists following compacting), and the lubrication system used.

[1] This test method is under the jurisdiction of ASTM Committee B09 on Metal Powders and Metal Powder Products and is the direct responsibility of Subcommittee B09.02 on Base Metal Powders.

Current edition approved May 1, 2009. Published July 2009. Originally approved in 1956. Last previous edition approved in 2002 as B312 – 96 (2002). DOI: 10.1520/B0312-09.

[2] For referenced ASTM standards, visit the ASTM website, www.astm.org, or contact ASTM Customer Service at service@astm.org. For *Annual Book of ASTM Standards* volume information, refer to the standard's Document Summary page on the ASTM website.

*A Summary of Changes section appears at the end of this standard

5.2 Knowledge of the green strength value is useful to the production, characterization and utilization of metal powders in the manufacture of PM structural parts and bearings.

5.3 The test for green strength of a compacted metal powder can be used to:

5.3.1 Relate the resistance of a pressed compact to breakage or damage due to handling.

5.3.2 Compare the quality of a metal powder or powder mixture from lot to lot.

5.3.3 Determine the effect of the addition of a lubricant or other powders to a base powder.

5.3.4 Evaluate powder mixing or blending variables.

5.4 Factors that are known to influence the green strength of a metal powder are particle shape, particle size distribution and compressibility of the metal powder.

5.5 The amount and type of lubricant or other additives and the mixing procedures have a strong effect on the green strength of specimens produced from metal powder mixtures.

6. Apparatus

6.1 *Analytical Balance*—a laboratory instrument with a capacity of at least 100 g suitable for determining the mass of both the test portion of powder and the green test specimen to an accuracy of 0.001 g.

6.2 *PM Tool Set*—a compacting die and punches capable of producing the test specimens; an example of which is shown in Practices B925 as *Laboratory Tooling –Transverse Rupture Test Specimen*.

6.3 *Universal Testing Machine or PM Compacting Press*—a press with the ability to hold the PM tooling and apply the force necessary to compact the test specimens to the target green density.

6.4 *Outside Micrometers or Calipers*—instruments capable of measuring from 0.000 to 1.250 in. (0.00 to 31.75 mm) with an accuracy of 0.001 in. (0.03 mm).

6.5 Either of the following sets of testing apparatus:

6.5.1 *Transverse Rupture Test Fixture and Compression Testing Machine*—a fixture (Fig. 1) for locating the test specimen and a press capable of applying a breaking load at a controlled rate of approximately 20 lbf/min (~90 N/min), and on which the force can be read to the nearest 0.1 lbf (0.5 N), or

6.5.2 *Constant Loading Beam Device, Metal Shot and Scale*—– a lever-arm laboratory device (Fig. 2), designed to collect a controlled flow of metal shot that will produce a force with a loading rate of approximately 20 lbf/min (~90 N/min) on a pre-positioned test specimen until fracture occurs, and a scale with a capacity of at least 25 lb (10 kg) to determine the mass to the nearest 0.01 lb (0.005 kg) of the shot that was required.

7. Test Specimen

7.1 The recommended test specimen is an unsintered, (green), rectangular compact having dimensions of 0.500 in. (12.70 mm) wide by 1.250 in. (31.75 mm) long as specified in Practices B925 as *Transverse Rupture Strength Test Specimen*.

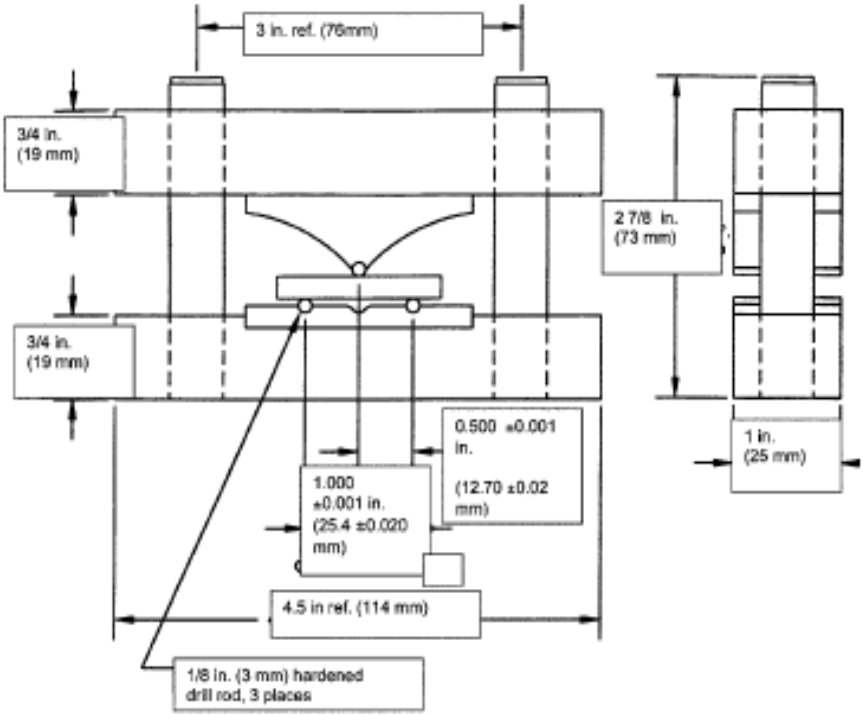

FIG. 1 Example of Constant Loading Beam Device

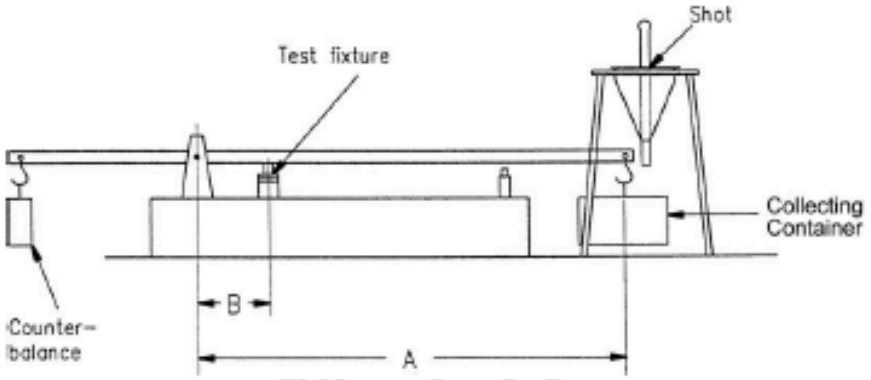

FIG. 2 Transverse Rupture Test Fixture

7.2 Either the *thin* test specimen with a thickness 0.250 ± 0.005 in. (6.35 ± 0.13 mm) or the *thick* test specimen having a thickness of 0.500 ± 0.005 in. (12.70 ± 0.13 mm) may be used as agreed to by the concerned parties.

7.3 The top and bottom faces of the green compact shall be parallel within 0.001 in. (0.03 mm).

7.4 The green density shall be within ± 0.05 g/cm^3 of the target green density that has been agreed to between the concerned parties.

8. Procedure

8.1 *Lubrication Method*—The lubrication system to be used when compacting the test specimen shall be a matter of agreement between the concerned parties. Compactibility and green density will vary with the method chosen as well as the care with which it is applied and affect the green strength value.

8.1.1 Lubricated metal powder mixtures should be tested in the as-received condition.

8.1.2 Unlubricated metal powder or powder mixtures may be compacted with the aid of die-wall lubrication or an admixed powder lubricant.

8.1.2.1 If die-wall-lubrication is chosen, it shall be applied prior to the compacting of each test specimen following the procedures in Practices B925.

8.1.2.2 If an admixed lubricant is to be used; the type, grade, percentage and mixing procedure shall be agreed upon between the concerned parties or shall closely follow accepted PM practice.

8.2 *Powder Sampling*—Using Eq 1, calculate the mass of metal powder that will be needed to produce one test specimen from the nominal dimensions and desired thickness at the target green density.

$$M = \frac{D_G \times W \times T \times L}{0.061} \quad (1)$$

where:

M = mass of powder needed, g,
D_G = target green density, g/cm^3,
W = width of test specimen, in.,
T = thickness of test specimen, in.,
L = length of test specimen, in., and
0.061 = conversion factor, in^3 to cm^3

8.2.1 Following the recommendations in Practices B215, take a gross sample of powder from the lot that is to be tested of sufficient quantity to produce a minimum of three test specimens.

8.2.2 From this gross sample, remove three test portions of powder that can be used to produce three test specimens of the desired thickness at the target green density. Each test portion shall be within 0.02 g of the powder mass that was calculated.

8.3 *Compacting Procedure*—Set-up the PM Tooling in the compacting press or the universal testing machine. Then, using the force that is necessary to produce the desired thickness at the target green density, compact three test specimens from the three test portions of powder following the compacting procedure in Practices B925.

8.3.1 Determine the mass of each test specimen to the nearest 0.001 g, measure the specimen dimensions to the nearest 0.001 in. (0.03 mm), number and identify the top of each specimen.

8.3.2 Calculate the green density of each test specimen using Eq 2. Record these values to the nearest 0.01 g/cm^3.

$$D_G = 0.061 \frac{M}{W \times T \times L} \quad (2)$$

where:

D_G = green density of the test specimen, g/cm^3,
0.061 = conversion factor, in^3 to cm^3 ,
M = mass of the test specimen, g,
W = width of test specimen, in.,
T = thickness of test specimen, in., and
L = length of test specimen, in.

NOTE 1—Do not use Test Method B962 to measure the green density of the test specimens because of the possible effect of absorbed water on the green strength value.

8.4 *Testing Procedure*—Select a set of three green test specimens that are within ± 0.05 g/cm^3 of the target green density, and break each bar in turn using either the Transverse Rupture Test Fixture, or the Constant Loading Beam Device.

USING THE TRANSVERSE RUPTURE STRENGTH TEST FIXTURE

8.4.1 Place the *Transverse Rupture Test Fixture*, Fig. 1, between the platens of the compression testing machine with the movable upper portion securely attached, (if possible), to the upper platen.

8.4.1.1 Locate each of the measured test specimens, in turn, centered lengthwise on the supporting rods of the test fixture with the top face uppermost.

8.4.1.2 Apply a uniformly increasing compressive load at a rate of approximately 20 lbf/min (~90 N/min), until fracture occurs. Record the force at fracture directly from the read-out on the testing machine for each test specimen as the breaking force, P, in lbf (or N) to the nearest 0.1 lbf (0.5 N) for use in future calculations.

8.4.1.3 If the upper portion of the test fixture is not attached to the upper press platen, then the force in lbf (N), exerted by the mass of the upper portion of the test fixture shall be determined and added to the read-out to determine the true breaking force.

USING THE CONSTANT LOADING BEAM DEVICE

8.4.2 Set up the Constant Loading Beam Device, Fig. 2, on a sturdy laboratory table or bench and balance the lever arm with the empty collecting container hanging in place on the hook.

8.4.2.1 Open the valve and adjust the flow rate of the shot to approximately 20 lb/min (~9 kg/min). Record the setting, empty and rehang the collecting container.

8.4.2.2 Locate each of the measured test specimens, in turn, centered lengthwise on the supporting rods of the test fixture with the top face uppermost.

8.4.2.3 Open the valve to the predetermined setting and allow metal shot to flow into the collecting container until fracture occurs.

8.4.2.4 Stop the flow, empty the container and determine the mass of the shot, S, to the nearest 0.01 lb (0.005 kg).

8.4.2.5 Calculate the breaking force, P, to the nearest 0.01 lbf (0.5 N) using the following equation:

$$P = \frac{A \times F}{B} \quad (3)$$

where:

P = force required to break the test specimen, lbf (N),
A = length of lever arm A, in. (mm) see Fig. 2,
B = length of lever arm B, in. (mm) see Fig. 2, and
F = force on the lever arm caused by the mass of the metal shot, lbf (N).

When using in-lb units, F in lbf = S in lb.

When using SI units, F in N = 9.8 times S in kg.

where:

S = mass of the metal shot, lb (kg)

9. Calculations

9.1 Using the breaking force values, P, obtained from the stress equation in sec. 8.4.1.2, 8.4.1.3 or 8.4.2.5, calculate the green strength values for each of the test specimens as follows:

$$GS = \frac{3 \times P \times L}{2 \times T^2 \times W} \quad (4)$$

where:

GS = green strength, psi (MPa),
P = Breaking force required to rupture, lbf (N)
L = length of span between supports of test fixture, in. (mm), (see Fig. 1) to the nearest 0.001 in. (0.03 mm)

W = width of specimen, in. (mm), and
T = thickness of specimen, in. (mm.)

10. Report

10.1 The general reporting format shall be : *Green Strength of a (nominal thickness) test specimen at (the measured) green density.*

10.1.1 The green strength shall be reported in psi (or MPa) as the arithmetic mean of three individual test results rounded to the nearest 100 psi (or 0.5 MPa).

10.1.2 The thickness of the test specimen that was used shall be included in the report as a nominal value.

10.1.3 The green density shall be reported as the average of the three test specimens to the nearest 0.01 g/cm^3.

10.2 An alternative reporting method may be to graph the green strength as a function of green density using the results obtained at a minimum of three data points.

10.3 The following information may also be reported to help interpret the test results:

10.3.1 Testing apparatus used, either the *Transverse Rupture Test Fixture or The Constant Loading Beam Device.*

10.3.2 Powder type, brand, grade and lot identification number.

10.3.3 Composition of the powder mixture if other than a base powder.

10.3.4 Lubrication system as well as type, brand and amount.

10.3.5 Apparent density, flow rate and sieve analysis of the powder and the test methods used to determine these properties.

10.3.6 Compacting pressure used to achieve the target green density.

11. Precision and Bias[3]

11.1 The precision of this test method has been determined from an interlaboratory study, (ILS) conducted on two ferrous materials by the Metal Powder Industries Federation in 2005 in which 32 laboratories participated. Practice E691 was used to perform a statistical analysis of the data at the 95% confidence level.

[3] The precision for this test method was developed by the Metal Powder Industries Federation (MPIF), 105 College Road East, Princeton, NJ 08540 USA and is used herein with their permission, The ILS data and results are available in MPIF Research Report-R-15-05.

TABLE 1 Precision of Green Strength Measurements Using the Test Fixture and Compression Testing Machine

Material	Nominal thickness, in. (mm)	Number of Laboratories	Mean strength, psi[A]	Repeatability r psi	Reproducibility, R, psi
water atomized pre-alloyed powder + 0.5% wax lubricant (green density = 6.8 g/cm³)	0.250 (6.35)	32	1301	246	452
	0.500 (12.70)	32	1685	436	540
	0.250 (6.35)	32	4079	727	1941
sponge iron + 0.5% wax lubricant (green density = 7.2 g/cm³)	0.500 (12.70)	32	5432	648	1814

[A] Strength values listed are the arithmetic averages of the test data and have not been rounded

TABLE 2 Precision of Green Strength Measurements for the Lower Green Strength Materials Using the Constant Loading Beam Device with Metal Shot

Material	Nominal thickness, in. (mm)	Number of Laboratories	Mean strength, psi[A]	Repeatability r psi	Reproducibility, R, psi
water atomized pre-alloyed powder + 0.5% wax lubricant (green density = 6.8 g/cm³)	0.250 (6.35)	9	1274	113	201
	0.500 (12.70)	9	1703	136	518

[A] Strength values listed are the arithmetic averages of the test data and have not been rounded

11.1.1 *Repeatability Values, r,* obtained when using the test fixture and compression testing machine are listed in Table 1 and in Table 2 when using the constant loading beam device with metal shot. On the basis of test error alone, duplicate tests in the same laboratory by the same operator on the same material should not differ more than the value listed.

11.1.2 *Reproducibility Values,R,* for the two methods are also listed in Table 1 and Table 2. For tests conducted in two laboratories, and on the basis of test error alone, the results should not differ by more than the value listed.

11.2 *Bias*—The bias of the green strength test can not be established because there is no standard available for comparison.

11.3 *Measurement Uncertainty*—The precision of this test method shall be considered by those performing the test when reporting the results.

12. Keywords

12.1 constant loading beam device; green strength; PM; powder metallurgy; transverse strength; unsintered compact

SUMMARY OF CHANGES

Committee B09 has identified the location of selected changes to this standard since the last issue (B312–96(2002)) that may impact the use of this standard.

(1) 1. Changed "for" to "of" and added "from " in the Title.
(2) All reference to B328 was removed from the document, and Test Methods B962 was added.
(3) Sec 6.2 – The scale required to weigh the metal shot added.
(4) Sec 7.2 – Added parallelism requirement to specimen to agree with MPIF 15.
(5) Sec 8 – The procedure for producing the test specimen removed and reference to B925 substituted and the rest of the procedure rewritten and rearranged.
(6) Table 1, used to determine the mass of powder needed to produce the test specimen was removed and replaced by Eq 1.
(7) Fig 1 – Drawing of die removed and reference to Practices B925 substituted.
(8) Fig 3 – Drawing of Test Fixture removed and drawing for TRS Fixture from Test Method B528 substituted and renumbered as Fig. 1.
(9) Fig 4 – Drawing of test specimen removed and reference to Practices B925 substituted.
(10) In 8.4.2.4 - Changed the requirement for weighing the shot from nearest 0.0022 lb to the nearest 0.01 lb to agree with MPIF 15.
(11) In the formulas, the 0.061 conversion factor was added to the list of symbols.
(12) The formula #4 was rewritten in terms of force exerted by the mass of the shot to correct the error in units present in the formula in Sec. 8.5 of B312-96
(13) Sec 10 - The reporting instructions, were rewritten and rearranged.
(14) Sec 11 - The P and B section was reproduced from MPIF #15 with their permission.
(15) A statement on Measurement Uncertainty was added in Section 11.3.